UC Berkeley
UC Berkeley Previously Published Works

Title

Spectroscopic, Magnetic, and Computational Investigations on a Series of Rhenium(III) Cyclopentadienide β–diketiminate Halide and Pseudohalide Complexes

Permalink

Journal

Organometallics, 41(22)

ISSN

0276-7333

Authors

Ouellette, Erik T
Estrada, Jorge Ivan Amaro
Lussier, Daniel J
et al.

Publication Date

2022-11-28

DOI

10.1021/acs.organomet.1c00516

Copyright Information

Peer reviewed

Spectroscopic, Magnetic, and Computational Investigations on a Series of Rhenium(III) Cyclopentadienide β-diketiminate Halide and Pseudohalide Complexes

Erik T. Ouellette,[†,§] Jorge Ivan Amaro Estrada,[‡] Daniel J. Lussier,[†] Khetpakorn Chakarawet,[†] Trevor D. Lohrey,[†,§] Laurent Maron,[‡] Robert G. Bergman,[†] John Arnold[†,§,*]

†Department of Chemistry, University of California, Berkeley, California 94720, USA
§Chemical Sciences Division, Lawrence Berkeley National Laboratory, Berkeley, California 94720, USA
‡LPCNO, Université de Toulouse, INSA Toulouse, 135 Avenue de Rangueil, 31077 Toulouse, France

*Email: arnold@berkeley.edu

Abstract

The low-valent rhenium(I) salt Na[Re(η^5-Cp)(BDI)] (BDI = N,N′-bis(2,6-diisopropylphenyl)-3,5-dimethyl-β-diketiminate) was shown to react with various halide and chalcogenolate reagents, leading to the isolation of a series of rhenium(III)–halide and –pseudohalide complexes: Re(X)(η^5-Cp)(BDI) (**1-X**, X = F, Cl, Br, I; **2**, X = OTf) and Re(ER)(η^5-Cp)(BDI) (**3-ER**, ER = SBn, SeBn, TePh). The ^{1}H NMR spectra of these complexes displayed sharp resonances shifted several ppm from typical diamagnetic regions, as well as distinct chemical shift trends down both the halide (with the exception of F) and chalcogenolate series, with both Cp and BDI backbone peaks moving downfield with increasing atomic number. Subsequent magnetic susceptibility measurements of the rhenium(III) halides **1-Cl**, **1-Br**, and **1-I** indicated that these complexes display temperature-independent paramagnetism (TIP), with χ_{TIP} values of 7.41(44) $\times 10^{-4}$ to 1.50(51)$\times 10^{-3}$ cm^3 mol^{-1}. Multireference complete active space self-consistent field (CASSCF) computations incorporating spin-orbit state mixing revealed small energy separations (1.7–3.0 kcal/mol) between thermally isolated ground states and first excited spin-orbit states for the rhenium halides, confirming that low-lying excited states are responsible for the observed TIP behavior.

Introduction

Monometallic rhenium(III) coordination complexes have a variety of applications, including acting as structural models for radiopharmaceutical development,[1–5] utility in studying the electronic, magnetic, and photophysical properties of new or exotic ligands,[6–9] and the binding and functionalization of dinitrogen.[10–15] Within this subset of compounds, numerous octahedral or pseudo-octahedral rhenium(III) complexes have displayed substantial temperature-independent paramagnetism (TIP).[1,6,7,15–21] TIP is a physical phenomenon in which the magnetic susceptibility of a compound does not arise strictly from electron spins of a magnetic ground state according to Curie law, but is instead caused by the coupling of an isolated ground state with thermally inaccessible low-lying magnetic excited states through a Zeeman perturbation.[22] Many inorganic complexes exhibit negligible TIP effects; however, metal centers that possess large spin-orbit coupling (SOC), such as rhenium, may enable the presence of low-lying excited states available for effective Zeeman coupling and thus lead to TIP effects worthy of further study.[22] While work has been done to quantify and investigate TIP in a number of rhenium(III) complexes, there has yet

to be published a detailed investigation into how systematically varying ligand identity in such complexes affects structural, spectroscopic, and magnetic properties.

Recently, our group reported the highly reactive, low-valent rhenium(I) salt Na[Re(η^5-Cp)(BDI)],[23] which has been used to access unusual multimetallic species[23–25] along with a low-coordinate paramagnetic rhenium(II) complex,[26,27] and to reductively bind and functionalize dinitrogen.[12,27] Given its synthetic versatility and high reduction potential, we reasoned Na[Re(η^5-Cp)(BDI)] could further be used to access rhenium(III) chemistry. Here we report the synthesis and structures of rhenium(III) halide and pseudohalide complexes, as well as corresponding spectroscopic characterizations, magnetic susceptibility measurements, and computational investigations to correlate electronic structure in these complexes with observed TIP behavior.

Results and Discussion

Synthesis and Structure of Rhenium(III)–Halide and –Chalcogenolate Complexes

Addition of a dark purple solution of Na[Re(η^5-Cp)(BDI)] to a stirred suspension of one equivalent of $CuCl_2$ in THF led to a rapid color change to orange. Upon workup, we isolated the rhenium(III) monochloride complex Re(Cl)(η^5-Cp)(BDI) (**1-Cl**) as red crystals in 89% yield (Scheme 1). Reaction of Na[Re(η^5-Cp)(BDI)] with $CoCl_2$ also led to formation of **1-Cl**, in contrast to reactions with $MnCl_2$ and $ZnCl_2$ which led to formation of the rhenium(II) species Re(η^5-Cp)(BDI) and tetrametallic complex [ZnRe(η^5-Cp)(BDI)]$_2$, respectively.[23,26] Similarly, the reaction of Na[Re(η^5-Cp)(BDI)] with $CuBr_2$ or two equivalents of CuI led, upon workup, to isolation of Re(Br)(η^5-Cp)(BDI) (**1-Br**) and Re(I)(η^5-Cp)(BDI) (**1-I**), respectively, as red crystalline solids, both in 82% yield. Surprisingly, reactions with CuF_2 were unsuccessful in yielding the desired fluoride product, Re(F)(η^5-Cp)(BDI) (**1-F**). As an alternative route to **1-F**, we first synthesized Re(OTf)(η^5-Cp)(BDI) (**2**) in 64% yield by the reaction of Na[Re(η^5-Cp)(BDI)] with two equivalents of silver(I) triflate. Subsequently, salt metathesis of **2** with excess tetramethylammonium fluoride led to the isolation of **1-F** in 89% yield.

Due to their electronic similarities to halides (monoanionic, X-type ligands with π-donor ability that show common trends in behavior down a column), we targeted the synthesis of a series of chalcogenolates.[28,29] To this end, we prepared the rhenium(III)–thiolate, Re(SCH$_2$Ph)(η^5-Cp)(BDI) (**3-SBn**) in 61% yield by reaction of Na[Re(η^5-Cp)(BDI)] with one equivalent of dibenzyl disulfide (Scheme 1).[*] Similarly, we employed dibenzyl diselenide and diphenyl ditelluride to produce the analogous chalcogenolate products Re(SeCH$_2$Ph)(η^5-Cp)(BDI) (**3-SeBn**) and Re(TePh)(η^5-Cp)(BDI) (**3-TePh**) in 63% and 83% yield, respectively. While **3-SBn** and **3-SeBn** were isolated as brick red crystals, **3-TePh** formed dark green crystals.

---

[*] We suggest that dibenzyl disulfide formally acts as two equivalents of "•SBn" in this reaction, enabling the net two-electron oxidation of the rhenium(I) center while presumably forming one equivalent of NaSBn as a byproduct.
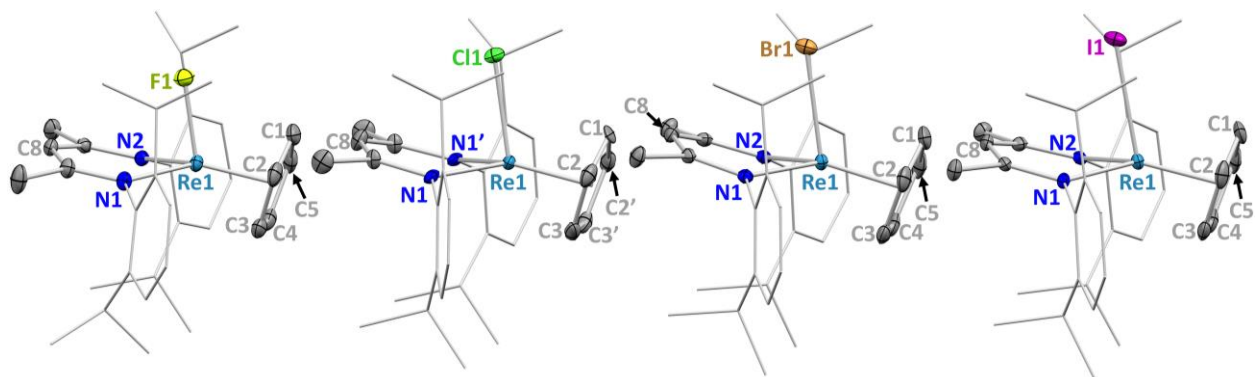
Scheme 1. Synthesis of rhenium(III)–halide complexes **1**-**X** (X = F, Cl, Br, I), triflate complex **2**, and chalcogenolates **3-ER** (ER = SBn, SeBn, TePh).

The solid-state structures of **1-X** (X = F, Cl, Br, I), **2**, and **3-ER** (ER = SBn, SeBn, TePh) were determined by X-ray crystallography (Figures 1, 2, and S23). The complexes all adopt half-sandwich, or pseudo-piano stool, geometries in which the two BDI nitrogen atoms and the halide/chalcogenolate ligand act as "legs" opposite a Cp "seat." The Re–X distances in **1-X** range from 1.979(2) Å for **1-F** to 2.7287(3) Å for **1-I**, increasing as expected down the halide series, and are generally consistent with those of other rhenium half-sandwich halide complexes (Table 1).[30–39] The Re–O1 distance of **2** is measured at 2.173(2) Å, and the structure itself is isomorphic to the reported chromium analogue.[40] The Re–E distances in **3-ER** range from 2.3274(8) to 2.6852(2) Å, and increase as anticipated down the chalcogenolate series, much like in the **1-X** series. The Re–N distances for **1-X** range from 2.028(7)–2.053(7) Å, similar to the 2.031(3) Å distances in the starting material, Na[Re(η^5-Cp)(BDI)]. In **3-ER**, however, Re–N bond lengths fall into a greater range, from 2.015(3)–2.085(3) Å, and displayed larger variability between Re–N1 and Re–N2 distances within each complex relative to those measured for **1-X**. Among all complexes, Re–Cp(centroid) distances range from 1.901(2)–1.920(4) Å (Table S3); however, the Re–C1 distances are consistently the longest Re–C(Cp) contacts at 2.314(4)–2.350(3) Å, while the Re–C3 and Re–C4 distances are notably shorter at 2.164(3)–2.199(3) Å. While not indicative of complete ring slippage, this does suggest that the η^5-cyclopentadienyl rings are tilted slightly away from the halide/chalcogenolate ligand. Although there is some precedent for this phenomenon in four-legged piano-stool complexes[41,42] and in half-sandwich complexes containing strong trans-influencing ligands,[43–45] this degree of tilting seems to be greater in magnitude than in other three-legged rhenium piano-stool complexes.[46–52] That said, we have observed similar Cp tilting in other complexes that utilize the same Cp and BDI ligand set.[12,23,25,26]

Figure 1. X-ray crystal structures of **1-X** (X = F, Cl, Br, I) shown with 50% probability ellipsoids. The BDI aryl groups are shown in wireframe, and hydrogen atoms are omitted for clarity. Atoms generated by mirror symmetry in **1-Cl** are represented with a prime symbol.
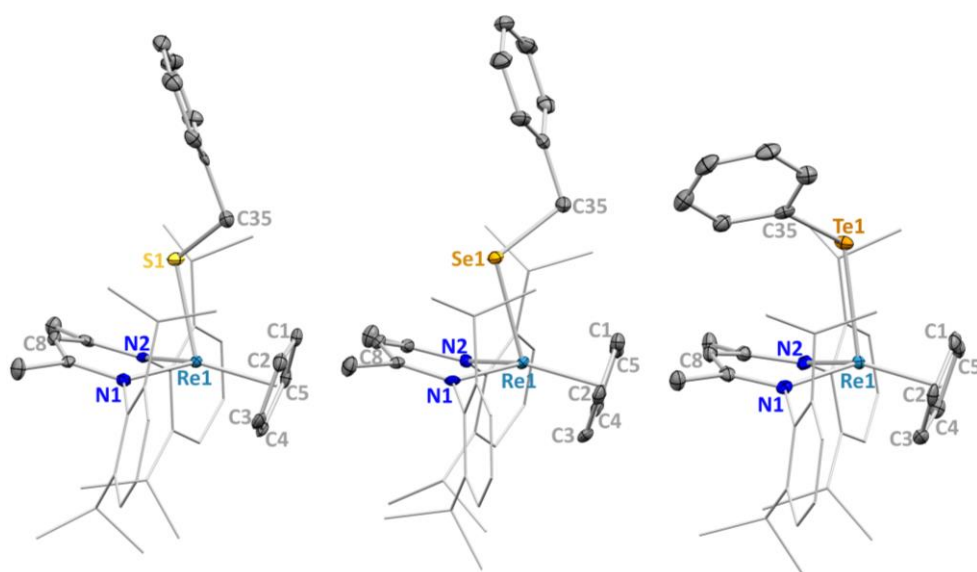

Figure 2. X-ray crystal structures of **3-ER** (ER = SBn, SeBn, TePh) shown with 50% probability ellipsoids. The BDI aryl groups are shown in wireframe, and hydrogen atoms are omitted for clarity.

Table 1. Selected distances (Å) and angles (deg) for **1-X** (X = F, Cl, Br, I), **2**, and **3-ER** (ER = SBn, SeBn, TePh).

complex	Re–Cp(cent)	Re–X[a]	Re–N	Cp(cent)–Re–X[a]
1-F	1.901(2)	1.979(2)	2.035(2), 2.036(2)	110.91(5)
1-Cl[b]	1.920(4), 1.914(4)	2.396(3), 2.376(3)	2.053(7), 2.028(7)	113.2(2), 111.4(2)
1-Br	1.906(2)	2.5408(2)	2.033(2), 2.039(2)	113.53(4)
1-I	1.906(2)	2.7287(3)	2.035(3), 2.030(3)	113.77(6)
2	1.905(2)	2.173(2)	2.042(3), 2.027(3)	123.49(8)
3-SBn	1.905(2)	2.3274(8)	2.017(3), 2.085(3)	117.70(6)
3-SeBn	1.900(2)	2.5119(3)	2.069(3), 2.015(3)	118.02(6)
3-TePh	1.914(2)	2.6852(2)	2.074(3), 2.030(3)	111.61(6)

NMR Spectroscopy

The ^{1}H NMR spectrum of **1-X** displayed chemical shifts outside of the typical diamagnetic region (Figure 3). While all the signals in C_6D_6 were sharp, the Cp signals were shifted downfield to $\delta = 13.6$–15.1 ppm, and the backbone proton of the BDI ligand (bound to C8) was shifted upfield to $\delta = 0.1$–1.0 ppm. For reference, the ^{1}H NMR spectra of four similar rhenium(III)–Cp–BDI complexes[†] in C_6D_6 contain Cp proton chemical shifts at $\delta = 4.6$–6.8 ppm, with shifts for the BDI backbone at $\delta = 6.1$–6.5 ppm.[12,23,26,53] Chemical shifts for the remaining protons in **1-X** are closer to those in corresponding positions in these comparable rhenium(III)–Cp–BDI complexes. These results indicate the presence of paramagnetic contributions to the chemical shifts in **1-X** with an anisotropic component to the shifts (considering the Cp and BDI backbone protons are located on opposite sides of the rhenium metal center) and shift in opposite directions in the ^{1}H NMR spectra. Intriguingly, variable-temperature (VT) ^{1}H NMR experiments on **1-Cl** did not show a strict dependence of the Cp or BDI backbone proton chemical shifts on $(1/T)^n$ for any value of n, as would be expected for typical paramagnetic species containing unpaired electron spins in the ground state (Figures S20-21).[54] Furthermore, no signal was observed in the continuous-wave X-band EPR spectrum of **1-Cl** in frozen toluene at 10 K, additional evidence that **1-Cl**, as well as the rest of the **1-X** series, exhibit non-Curie paramagnetism. The presence of shifted, yet sharp, NMR spectral peaks has been reported for several other rhenium(III) complexes, typically with octahedral or pseudo-octahedral geometries,[1,6,7,16–20,55] and has been attributed to the presence of TIP.

Interestingly, the ^{1}H NMR data for the halide series **1-X** revealed trends in chemical shifts among the **1-X** series, highlighted by both the Cp and BDI backbone shifts moving downfield with increasing atomic number (Figure 3). However, the fluoride complex **1-F** was inconsistent with these trends, as its Cp shift of $\delta = 14.43$ ppm falls between those in **1-Cl** ($\delta = 13.65$ ppm) and **1-Br** ($\delta = 14.49$ ppm), while its BDI backbone shift ($\delta = 0.54$ ppm) lies downfield of both **1-Cl** ($\delta = 0.06$ ppm) and **1-Br** ($\delta = 0.11$ ppm). In addition, the BDI methyl groups shift upfield with increasing atomic number for **1-X**, though the upfield jump from **1-F** to **1-Cl** is quite significant compared to the upfield trend observed between the remaining halides.

[†]Re(H)(η^5-Cp)(BDI), Re(H)(η^5-$C_5H_4SiMe_3$)(BDI), Re(Me)(η^5-Cp), and Re(η^5:η^1-C_5H_4-C(C_6H_5)$_2$(o-C_6H_4))(BDI).
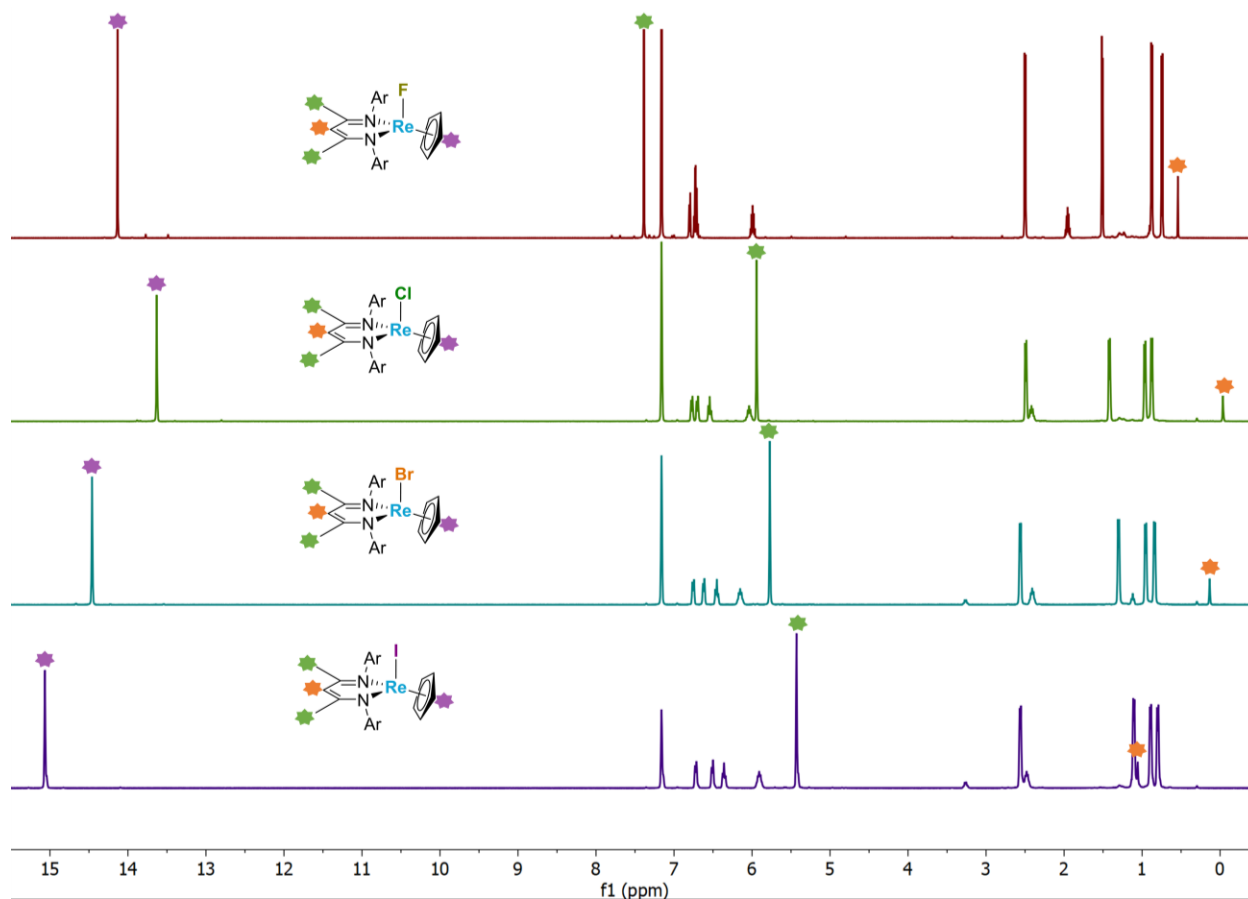
Figure 3. ^{1}H NMR spectra of **1-X** in C_6D_6 (293 K, 600 MHz) displaying trends in chemical shifts with increasing atomic number of bound halide. The Cp and BDI backbone proton peaks move downfield for **1-X** (X = Cl, Br, I). BDI methyl group peaks move upfield for **1-X** (X = F, Cl, Br, I), with the largest upfield jump between **1-F** and **1-Cl**.

As for the pseudohalides, triflate complex **2** showed characteristic paramagnetic chemical shifts, with its Cp protons shifted to δ = 14.14 ppm and a BDI backbone shift found quite far upfield at δ = –3.61 ppm (Figure S10). The ^{1}H NMR spectra of chalcogenolates **3-ER** also revealed paramagnetically shifted peaks and displayed similar overall trends as in the halide series **1-X**: both the Cp and BDI backbone proton shifts move downfield with increasing atomic number (Figure S22). But while we see a similar trend, the overall magnitude of the shifts outside of the diamagnetic region is smaller for **3-ER**, with Cp shifts of δ = 8.6–9.0 ppm compared to δ = 13.6–15.1 ppm for **1-X**. We also note that the furthest downfield chemical shifts in the chalcogenolate series now correspond to the methylene protons of **3-SBn** and **3-SeBn**. Considering the near-identical geometry of the solid-state structures of **1-X**, **2**, and **3-ER**, we suspected that the trend in paramagnetic shifting of the ^{1}H NMR peaks may be related to ligand strength or π-donation ability across the halide and chalcogenolate series. We hoped to gain further understanding of these trends by characterizing the magnitude of TIP in these complexes.

Magnetic Studies

We started by measuring magnetic susceptibility using the Evans NMR method and obtained an effective magnetic moment of 1.0 μ_B for both **1-Cl** and **1-I**, suggesting any differences in magnetic moment

between these two complexes are likely small and indistinguishable via this technique. In any case, 1.0 μ_B is far lower than the spin-only value of 2.83 μ_B that might be expected for a rhenium(III) d^4 triplet electronic state with $S = 1$. Despite a large orbital contribution to the magnetic moment for this third-row metal, the observed magnetic susceptibility is still considerably lower than the expected spin-only value. This result, together with the observation of sharp NMR signals and the relatively small magnitude of the paramagnetic chemical shifts, suggests that these species cannot be described as having an isolated ground state triplet, or other spin-unpaired, configuration.

Variable-temperature magnetic susceptibility measurements were collected using a SQUID magnetometer on microcrystalline samples of **1-X**. Under a 7 T applied field, the $\chi_M T$ products of 0.221, 0.444, and 0.289 cm^3 K mol^{-1} were obtained for **1-Cl**, **1-Br**, and **1-I**, respectively, at 300 K. These values correspond to effective magnetic moments of 1.33, 1.88, and 1.52 μ_B, respectively. Upon decreasing the temperature, the $\chi_M T$ products decrease linearly with temperature and approach zero. This behavior is characteristic of TIP, arising from a second order Zeeman perturbation in which the ground state couples with low-lying magnetic excited states through the Zeeman operator.[22,56] At 2 K, the $\chi_M T$ products of **1-Cl**, **1-Br**, and **1-I** are 0.001, 0.003, and 0.002 cm^3 K mol^{-1}, respectively, indicating that the ground state of these complexes are diamagnetic. Fitting to the susceptibility data gives χ_{TIP}(**1-Cl**) = 7.41(44) × 10^{-4} cm^3 mol^{-1}, χ_{TIP}(**1-Br**) = 1.50(51) × 10^{-3} cm^3 mol^{-1}, and χ_{TIP}(**1-I**) = 9(3) × 10^{-4} cm^3 mol^{-1} (Figure S24), values similar to several other reported rhenium(III) systems.[1,6–8,16–20] Susceptibility data measured at 1 T for **1-Cl**, **1-Br**, and **1-I** feature slight to moderate reduction of the χ_{TIP} (Figures S25–S27, Table S4), which indicates that the magnetic field facilitates mixing of the excited state wavefunction, presumably by stabilizing the excited state via Zeeman interaction with respect to the ground state. While the susceptibility data is consistent with TIP in **1-X**, baseline contributions to the susceptibility data are on a similar order to the overall susceptibility, precluding us from making definitive conclusions on the relative magnitude of TIP amongst the samples in this halide series. Instead, we turned to computations to investigate the unique Zeeman perturbations experienced by complexes **1-X** (X = Cl, Br, I) and to unravel the distinct coupling schemes between each complexes' ground and low-lying electronic states.

Computational Studies

Computational investigations were carried out on **1-X** (X = F, Cl, Br, I) following a multiconfigurational strategy initially proposed by Booth et al. to study Cp$^*_2$Yb(bipy) complexes.[57] The geometries of the four halides were optimized at the DFT level (B3PW91) for two different spin states (singlet and triplet). In all cases, while the triplet was found to be slightly more stable than the singlet (0.8 kcal/mol for **1-F**, 1.9 kcal/mol for **1-Cl**, 1.1 kcal/mol for **1-Br** and 1.3 kcal/mol for **1-I**), we note that this energy difference lies within the precision of the method. More interestingly, the geometrical parameters found for the singlet are in slightly better agreement with the experimental ones (see Figures S33–S36).

These early computational results, in addition to the presence of TIP in the susceptibility measurements, indicated that the electronic structure of complexes **1-X** in the ground state are peculiar and worthy of more detailed investigation. To this end, CASSCF calculations were performed on **1-X** in their singlet geometries in which six electrons were distributed into five molecular orbitals (MO's). The MO's employed were carefully chosen in the four cases (see ESI) and are derived from Restricted Open Shell Hartree-Fock (ROHF) calculations of **1-X** in either the quintet (X = F) or triplet (X = Cl, Br, I) state. For **1-F**, the ground state was found to be a singlet spin state (mainly single reference) with an open-shell singlet lying 11.1 kcal/mol higher in energy and the first triplet spin state 14.1 kcal/mol above the ground state. The situation is different for **1-Cl**, **1-Br**, and **1-I**: here the ground state was predicted to be a triplet with a very low-lying singlet spin state (Figure 4, *E(CASSCF)*). In fact, the singlet is almost degenerate with the triplet (ΔE = 0.5 kcal/mol) in **1-Cl** and **1-Br**, whereas the singlet was found slightly higher in energy (ΔE

= 3.2 kcal/mol) for **1-I**. Interestingly, an important difference was observed in the nature of the excited states between **1-Cl** and **1-Br**. In the case of **1-Cl**, the second excited state is another singlet (10.6 kcal/mol higher in energy relative to the ground state) followed by a triplet state (13.1 kcal/mol), whereas for **1-Br** these excited states are both singlets (7.1 and 19.6 kcal/mol). Complex **1-I** agrees with **1-Cl** in that the second and third excited states are a singlet (9.2 kcal/mol) and triplet (18.2 kcal/mol), respectively. The nature of these excited states is crucial once spin-orbit coupling is considered because they impact the interactions and overall stabilization of the ground state.

We incorporated the spin-orbit coupling of the ground and excited states using configuration interaction with perturbation including spin-orbit coupling (CIPSO) methods developed by Teichteil et al.[58,59] In this approach, different electronic spin-orbit states were computed using a minimal representation and their energies were corrected to the one found by our CASSCF calculations through defining an effective Hamiltonian (Figure 4, *E(CIPSO)*). Twenty buffer states were included to ensure a better representation of the low-lying spin-orbit states.
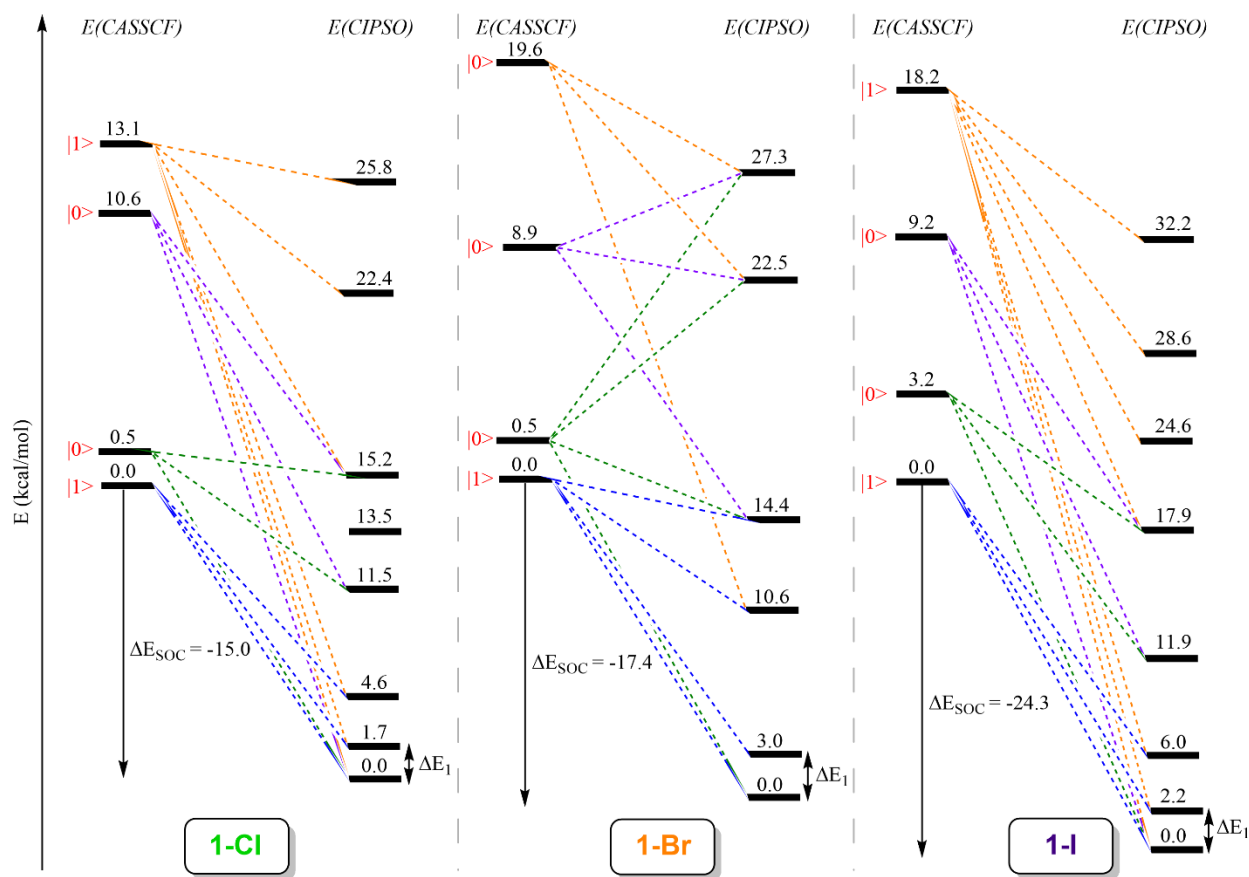
Figure 4. State-energy diagram of **1-X** (X = Cl, Br, I) depicting select calculated ground and low-lying electronic states before (*E(CASSCF)*) and after (*E(CIPSO)*) considering orbital mixing and energy stabilization due to spin-orbit coupling (SOC). Spin quantum number ($|S>$) labels are shown in red, and dashed lines represent pre–SOC states (*left*) that contribute meaningfully to resulting spin-orbit states (*right*). Small energy differences (1.7–3.0 kcal/mol) between ground and first excited spin-orbit states (ΔE_1) lead to the observed TIP behavior in these complexes.

8

As may be expected, the spin-orbit coupling stabilization of the ground state (ΔE_{SOC}) increases with increasing halide mass (Cl < Br < I), with a substantial stabilization of 24.3 kcal/mol for the heaviest compound, **1-I**. As for the resulting spin-orbit states, we observed that there are several very low-lying excited states for these complexes, with first excited states (ΔE_1) found only 1.7 (**1-Cl**), 2.2 (**1-I**), or 3.0 (**1-Br**) kcal/mol higher in energy relative to the respective ground states. Given the $\chi_{TIP} \propto 1/\Delta E_1$ relationship derived from the Van Vleck equation, these very low-lying excited states are likely responsible for the observed TIP behavior, i.e., large measured χ_{TIP} values and paramagnetically shifted ^{1}H NMR resonances.

Concluding Remarks

We isolated a number of rhenium(III)–halide and –pseudohalide complexes, expanding on the synthetic utility of the low-valent rhenium(I) salt Na[Re(η^5-Cp)(BDI)] while also providing an opportunity to compare structural, electronic, and magnetic properties among a series of rhenium(III) species. Structural analysis of **1-X** (X = F, Cl, Br, I), **2**, and **3-ER** (ER = SBn, SeBn, TePh) revealed consistent half-sandwich geometries. More importantly, the ^{1}H NMR spectra of these complexes displayed unusually sharp paramagnetically shifted resonances and distinct chemical shift trends down both the halide (with the exception of **1-F**) and pseudohalide series. Further investigations into electronic factors that contribute to these chemical shifts were conducted on **1-X**. Magnetic susceptibility measurements revealed the presence of large values of TIP in these rhenium(III) complexes, likely caused by second order coupling of a thermally isolated ground state and low-lying excited states through a Zeeman perturbation. Susceptibility studies measured χ_{TIP} values of $7.41(44) \times 10^{-4}$ to $1.50(51) \times 10^{-3}$ cm^3 mol^{-1}. Multireference computations incorporating spin-orbit coupling effects confirmed the presence of low-lying excited states, with small calculated ΔE_1 values leading to TIP behavior. While energy stabilization of the ground state through SOC (ΔE_{SOC}) was calculated to increase as the halide ligands become heavier, this trend did not correlate directly with TIP effects. Instead, the spin nature of the ground and excited states is likely more important in influencing the overall magnitude of TIP in a complex. Considering the observation of notable TIP effects in a number of other heavy octahedral d^4 and square planar d^6 metal complexes, we believe the results herein may help to inform the role ligand identity plays on determining the nature and magnitude of spin-orbit coupling of electronic states, and thus the resulting extent of TIP. Further investigations into the electronic structure and reactivity of rhenium cyclopentadienide β-diketiminate complexes are ongoing.

Supporting Information
Experimental procedures, NMR data, crystallographic data, magnetic data, UV-Vis data, and computational details

Cartesian coordinates of optimized structures **1a**, **1b**, and **1c**

Accession Codes
CCDC 2105396-2105403 contain the supplementary crystallographic data for this paper.

Author Information
Notes
The authors declare no competing financial interest.

Acknowledgements

References

(1)   Banerjee, S. R.; Wei, L.; Levadala, M. K.; Lazarova, N.; Golub, V. O.; O'Connor, C. J.; Stephenson, K. A.; Valliant, J. F.; Babich, J. W.; Zubieta, J. {REIIICl3} Core Complexes with Bifunctional Single Amino Acid Chelates. *Inorg. Chem.* **2002**, *41* (22), 5795–5802. https://doi.org/10.1021/ic020391d.

(2)   Machura, B.; Kruszynski, R.; Mroziński, J.; Kusz, J. Synthesis, Spectroscopic Characterization, X-Ray Structure and DFT Calculations of Rhenium(III) Complex with 1-Isoquinolinyl Phenyl Ketone. *Polyhedron* **2008**, *27* (6), 1739–1746. https://doi.org/10.1016/j.poly.2008.02.012.

(3)   Machura, B.; Kruszynski, R.; Kusz, J.; Kłak, J.; Mroziński, J. Novel Rhenium(III) Complexes with 5,6-Diphenyl-3-(2-Pyridyl)-1,2,4-Trazine: X-Ray Structures and DFT Calculations for [ReCl3(OPPh3)(Dppt)] and [ReCl3(PPh3)(Dppt)] Complexes. *Polyhedron* **2007**, *26* (15), 4427–4435. https://doi.org/10.1016/j.poly.2007.05.053.

(4)   Blower, P. Towards Molecular Imaging and Treatment of Disease with Radionuclides: The Role of Inorganic Chemistry. *J. Chem. Soc. Dalt. Trans.* **2006**, *60* (1414), 17051705–17111711. https://doi.org/10.1039/b516860k.

(5)   R. Dilworth, J.; J. Parrott, S. The Biomedical Chemistry of Technetium and Rhenium. *Chem. Soc. Rev.* **1998**, *27* (1), 43. https://doi.org/10.1039/a827043z.

(6)   Kalofolias, D. A.; Weselski, M.; Siczek, M.; Lis, T.; Tsipis, A. C.; Tangoulis, V.; Milios, C. J. Dinuclear and Mononuclear Rhenium Coordination Compounds upon Employment of a Schiff-Base Triol Ligand: Structural, Magnetic, and Computational Studies. *Inorg. Chem.* **2019**, *58* (13), 8596–8606. https://doi.org/10.1021/acs.inorgchem.9b00886.

(7)   Palion-Gazda, J.; Gryca, I.; Machura, B.; Lloret, F.; Julve, M. Synthesis, Crystal Structure and Magnetic Properties of the Complex [ReCl3(Tppz)]·MeCN. *RSC Adv.* **2015**, *5* (123), 101616–101622. https://doi.org/10.1039/c5ra21466a.

(8)   Machura, B.; Mroziński, J.; Kruszynski, R.; Kusz, J. Coordination Chemistry of Di-2-Pyridylketone. Synthesis, Spectroscopic Investigations, X-Ray Studies and DFT Calculations of Re(III) and Re(V) Complexes. *Polyhedron* **2009**, *28* (14), 2821–2830. https://doi.org/10.1016/j.poly.2009.06.048.

(9)   Pearson, C.; Beauchamp, A. L. 1H NMR Study of Monomeric Chloro-Rhenium(III) Complexes with Triarylphosphines and Nitriles. *Inorganica Chim. Acta* **1995**, *237* (1–2), 13–18. https://doi.org/10.1016/0020-1693(95)04657-U.

(10)   Bruch, Q. J.; Connor, G. P.; Chen, C. H.; Holland, P. L.; Mayer, J. M.; Hasanayn, F.; Miller, A. J. M. Dinitrogen Reduction to Ammonium at Rhenium Utilizing Light and Proton-Coupled Electron Transfer. *J. Am. Chem. Soc.* **2019**, *141* (51), 20198–20208. https://doi.org/10.1021/jacs.9b10031.

(11)   Schendzielorz, F.; Finger, M.; Abbenseth, J.; Würtele, C.; Krewald, V.; Schneider, S. Metal-Ligand Cooperative Synthesis of Benzonitrile by Electrochemical Reduction and Photolytic Splitting of Dinitrogen. *Angew. Chemie - Int. Ed.* **2019**, *58* (3), 830–834. https://doi.org/10.1002/anie.201812125.

(12)   Lohrey, T. D.; Bergman, R. G.; Arnold, J. Controlling Dinitrogen Functionalization at Rhenium through Alkali Metal Ion Pairing. *Dalt. Trans.* **2019**, *48* (48), 17936–17944. https://doi.org/10.1039/C9DT04489B.

(13)   Klopsch, I.; Finger, M.; Würtele, C.; Milde, B.; Werz, D. B.; Schneider, S. Dinitrogen Splitting and Functionalization in the Coordination Sphere of Rhenium. *J. Am. Chem. Soc.* **2014**, *136* (19), 6881–6883. https://doi.org/10.1021/ja502759d.

(14)   Lindley, B. M.; Van Alten, R. S.; Finger, M.; Schendzielorz, F.; Würtele, C.; Miller, A. J. M.; Siewert, I.; Schneider, S. Mechanism of Chemical and Electrochemical N 2 Splitting by a Rhenium Pincer Complex. *J. Am. Chem. Soc.* **2018**, *140* (25), 7922–7935. https://doi.org/10.1021/jacs.8b03755.

(15)   Weber, J. E.; Hasanayn, F.; Fataftah, M.; Mercado, B. Q.; Crabtree, R. H.; Holland, P. L. Electronic and Spin-State Effects on Dinitrogen Splitting to Nitrides in a Rhenium Pincer System. *Inorg. Chem.* **2021**, *60* (9), 6115–6124. https://doi.org/10.1021/acs.inorgchem.0c03778.

(16)   Chatt, J.; Leigh, G. J.; Mingos, D. M. P. Configurations of Some Complexes of Rhenium, Ruthenium, Osmium, Rhodium, Iridium, and Platinum Halides with Mono(Tertiary Phosphines) and Mono(Tertiary Arsines). *J. Chem. Soc. A Inorganic, Phys. Theor. Chem.* **1969**, No. 0, 1674–1680. https://doi.org/10.1039/J19690001674.

(17)   Rouschias, G.; Wilkinson, G. The Preparation and Reactions of Trihaolgeno(Alkanonitrile) Bis(Triphenylphosphine)Rhenium(III) Complexes. *J. Chem. Soc. A Inorganic, Phys. Theor. Chem.* **1967**, No. 0, 993–1000. https://doi.org/10.1039/J19670000993.

(18)   Earnshaw, A.; Figgis, B. N.; Lewis, J.; Peacock, R. D. 601. The Magnetic Properties of Some D4-Complexes. *J. Chem. Soc.* **1961**, No. 0, 3132–3138. https://doi.org/10.1039/jr9610003138.

(19)   Gunz, H. P.; Leigh, G. J. Magnetic Susceptibilities of Some Rhenium(III) and Osmium(IV) Halide Complexes; Preparation of Some New D4 Complexes. *J. Chem. Soc. A Inorganic, Phys. Theor. Chem.* **1971**, No. 0, 2229–2233. https://doi.org/10.1039/J19710002229.

(20)   MacHura, B.; Wolff, M.; Gryca, I.; Mroziński, J. Two Novel Rhenium Complexes Derived from [ReO(OMe)Cl2(Dpphen)] - Synthesis, Crystal Structure, Spectroscopic and Magnetic Properties. *Polyhedron* **2011**, *30* (2), 354–363. https://doi.org/10.1016/j.poly.2010.10.025.

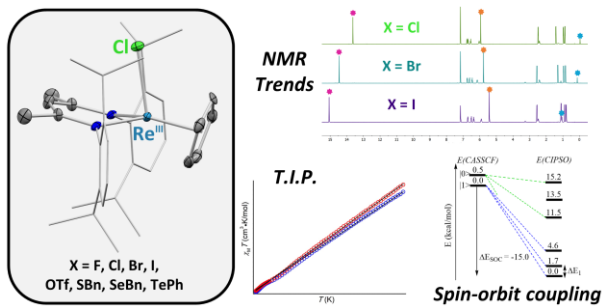(21)   Mitsopoulou, C. A.; Mahieu, N.; Motevalli, M.; Randall, E. W. Second-Order Paramagnetic

Rhenium(III) Complexes: Solid-State Structure and Assignment of the Carbon-13 Magnetic Resonance Spectra in Solution. *J. Chem. Soc. - Dalt. Trans.* **1996**, No. 24, 4563–4566. https://doi.org/10.1039/dt9960004563.

(22)   Kahn, O. Magnetization and Magnetic Susceptibility. In *Molecular Magnetism*; VCH Publishers: New York, 1993; pp 1–8.

(23)   Lohrey, T. D.; Maron, L.; Bergman, R. G.; Arnold, J. Heterotetrametallic Re-Zn-Zn-Re Complex Generated by an Anionic Rhenium(I) β-Diketiminate. *J. Am. Chem. Soc.* **2019**, *141* (2), 800–804. https://doi.org/10.1021/jacs.8b12494.

(24)   Boreen, M. A.; Lohrey, T. D.; Rao, G.; Britt, R. D.; Maron, L.; Arnold, J.; David Britt, R.; Maron, L.; Arnold, J. A Uranium Tri-Rhenium Triple Inverse Sandwich Compound. *J. Am. Chem. Soc.* **2019**, *141* (13), 5144–5148. https://doi.org/10.1021/jacs.9b01331.

(25)   Ouellette, E. T.; Carpentier, A.; Joseph Brackbill, I.; Lohrey, T. D.; Douair, I.; Maron, L.; Bergman, R. G.; Arnold, J. σ or π? Bonding Interactions in a Series of Rhenium Metallotetrylenes. *Dalt. Trans.* **2021**, *50* (6), 2083–2092. https://doi.org/10.1039/d1dt00129a.

(26)   Lohrey, T. D.; Rao, G.; Britt, R. D.; Bergman, R. G.; Arnold, J. H2 Activation and Direct Access to Terminal Nitride and Cyclo-P3 Complexes by an Acceptor-Free Rhenium(II) β-Diketiminate. *Inorg. Chem.* **2019**, *58* (19), 13492–13501. https://doi.org/10.1021/acs.inorgchem.9b02556.

(27)   Lohrey, T. D.; Rao, G.; Small, D. W.; Ouellette, E. T.; Bergman, R. G.; Britt, R. D.; Arnold, J. Electronic Structures of Rhenium(II) β-Diketiminates Probed by EPR Spectroscopy: Direct Comparison of an Acceptor-Free Complex to Its Dinitrogen, Isocyanide, and Carbon Monoxide Adducts. *J. Am. Chem. Soc.* **2020**, *142* (32), 13805–13813. https://doi.org/10.1021/jacs.0c04719.

(28)   Settineri, N. S.; Garner, M. E.; Arnold, J. A Thorium Chalcogenolate Series Generated by Atom Insertion into Thorium-Carbon Bonds. *J. Am. Chem. Soc.* **2017**, *139* (17), 6261–6269. https://doi.org/10.1021/jacs.7b02356.

(29)   Spencer, L. P.; Yang, P.; Scott, B. L.; Batista, E. R.; Boncella, J. M. Uranium(VI) Bis(Imido) Chalcogenate Complexes: Synthesis and Density Functional Theory Analysis. *Inorg. Chem.* **2009**, *48* (6), 2693–2700. https://doi.org/10.1021/ic802212m.

(30)   Nunn, C. M.; Cowley, A. H.; Lee, S. W.; Richmond, M. G. Reduction Pathways in Lateral and Diagonal (H5-C5Me5)Re(CO)2Br2. Synthesis, Structure, and Reactivity of [(H5-C5Me5)Re(CO)2Br−]. *Inorg. Chem.* **1990**, *29* (11), 2105–2112. https://doi.org/10.1021/ic00336a015.

(31)   Winter, C. H.; Veal, W. R.; Garner, C. M.; Arif, A. M.; Gladysz, J. A. Synthesis, Structure, and Reactivity of Stable Alkyl and Aryl Iodide Complexes of the Formula [(H5-C5H5)Re(NO)(PPh3)(IR)]+BF4−. *J. Am. Chem. Soc.* **1989**, *111* (13), 4766–4776. https://doi.org/10.1021/ja00195a033.

(32)   Ruwwe, J.; Martín-Alvarez, J. M.; Horn, C. R.; Bauer, E. B.; Szafert, S.; Lis, T.; Hampel, F.; Cagle, P. C.; Gladysz, J. A. Olefin Metatheses in Metal Coordination Spheres: Versatile New Strategies for the Construction of Novel Monohapto or Polyhapto Cyclic, Macrocyclic, Polymacrocyclic, and Bridging Ligands. *Chem. - A Eur. J.* **2001**, *7* (18), 3931–3950. https://doi.org/10.1002/1521-3765(20010917)7:18<3931::AID-CHEM3931>3.0.CO;2-Y.

(33)   Zobi, F.; Spingler, B.; Alberto, R. Syntheses, Structures and Reactivities of [CpTc(CO)3X] + and [CpRe(CO)3X]+. *Eur. J. Inorg. Chem.* **2008**, *2008* (27), 4205–4214. https://doi.org/10.1002/ejic.200800258.

(34)   Smith, J. M.; Cheng, L.; Coville, N. J.; Schulte, J.; Dimpe, P. S.; Adsetts, M. S.; Cook, L. M.; Boeyens, J. C. A.; Levendis, D. C. Solid-State Reactivity and Single-Crystal Structure Studies. The Case of Diag − Lat Isomerization in [Re(η 5 -C 5 H 4 Me)(CO)(P(OPh 3)Br 2] and [Re(η 5 - C 5 H 4 t Bu)(CO) 2 Br 2] . *Organometallics* **2000**, *19* (13), 2597–2602. https://doi.org/10.1021/om990959z.

(35)   Boeyens, J. C. A.; Cheng, L.; Coville, N. J.; Levendis, D. C.; McIntosh, K. The Importance of Inter-Molecular Forces in Crystal Structure Analysis: Solid State Study of the Diag-to-Lat Isomerization of (H5-C5H4Me)Re(CO)2Br2. *J. Chem. Crystallogr.* **1998**, *28* (3), 185–191. https://doi.org/10.1023/A:1022466126100.

(36)   Einstein, F. W.; Klahn-Oliva, A. H.; Sutton, D.; Tyers, K. G. Syntheses, X-Ray Structures, and Cis-Trans Isomerism of (Pentamethylcyclopentadienyl)Dicarbonylrhenium Dihalides, (η-CsMe5)Re(CO)2X2(X = Cl, Br, I). *Organometallics* **1986**, *5* (1), 53–59. https://doi.org/10.1021/om00132a009.

(37)   Apostolidis, C.; Kanellakopulos, B.; Maier, R.; Rebizant, J.; Ziegler, M. L. Bis(Cyclopentadienyl)Rhenium(III)Chlorid: Kristallstruktur, Eigenschaften Und Reaktivität; Darstellung Und Charakterisierung von Cp3Re Und Cp2ReH. *J. Organomet. Chem.* **1991**, *409* (1–2), 243–254. https://doi.org/10.1016/0022-328X(91)86150-O.

(38)   Zhu, B.; Huang, X.; Hao, X. Photochemical Reactions of [(η 5 -C 5 R 5)Re(CO) 3] (R = Me or H) with Aryl Halides in Benzene: Stoichiometric Formation of Biphenyl. *Eur. J. Inorg. Chem.* **2014**, *2014* (34), 5932–5939. https://doi.org/10.1002/ejic.201402793.

(39)   Hernández, J. G.; Macdonald, N. A. J.; Mottillo, C.; Butler, I. S.; Friščić, T. A Mechanochemical Strategy for Oxidative Addition: Remarkable Yields and Stereoselectivity in the Halogenation of Organometallic Re(I) Complexes. *Green Chem.* **2014**, *16* (3), 1087–1092. https://doi.org/10.1039/c3gc42104j.

(40)   Doherty, J. C.; Ballem, K. H. D.; Patrick, B. O.; Smith, K. M. Synthesis and Reactivity of Chromium Cyclopentadienyl β-Diketiminato Compounds. *Organometallics* **2004**, *23* (7), 1487–1489. https://doi.org/10.1021/om034065x.

(41)   Churchil, M. R.; Fennessey, J. P. Crystal and Molecular Structure Of A Perfluoropropyl Complex Of Molybdenum:π.π.-C5H5Mo(CO)3C3F7. *Inorg. Chem.* **1967**, *6* (6), 1213–1220. https://doi.org/10.1021/ic50052a032.

(42)   Kubáček, P.; Hoffmann, R.; Havlas, Z.; Kubácek, P.; Havlas, Z. Piano-Stool Complexes of the CpML4 Type. *Organometallics* **1982**, *1* (1), 180–188. https://doi.org/10.1021/om00061a029.

(43)   Okuda, J.; Herdtweck, E.; Herrmann, W. A. Synthesis and Structural Characterization of Trioxo(H5-Ethyltetramethylcyclopentadienyl)Rhenium, a Half-Sandwich Complex of Heptavalent Rhenium. *Inorg. Chem.* **1988**, *27* (7), 1254–1257. https://doi.org/10.1021/ic00280a032.

(44)   Herrmann, W. A.; Herdtweck, E.; Flöel, M.; Kulpe, J.; Küsthardt, U.; Okuda, J. Organometallic Oxides: The Example of Trioxo-(H5-Pentamethylcyclopentadienyl)Rhenium(VII). *Polyhedron* **1987**, *6* (6), 1165–1182. https://doi.org/10.1016/S0277-5387(00)80866-9.

(45)   Gibson, V. C.; Kee, T. P.; Clegg, W. Synthesis and Characterisation of Half-Sandwich Tantalum Compounds in Oxidation States (I)-(V): Tertiary Phosphine, Acetylene, Butadiene, Carbonyl, and Oxo Derivatives. X-Ray Crystal Structures of [Ta(C5Me5)Cl3(PMe3)] and [Ta(C5Me5)Cl2(CO)2(PMe3)]. *J. Chem. Soc. Dalt. Trans.* **1990**, *3* (11), 3199–3210. https://doi.org/10.1039/DT9900003199.

(46) Agbossou, F.; O'Connor, E. J.; Garner, C. M.; Méndez, N. Q.; Fernández, J. M.; Patton, A. T.; Ramsden, J. A.; Gladysz, J. A.; O'Connor, J. M.; Tajima, T.; Gable, K. P. Cyclopentadienyl Rhenium Complexes. *Inorg. Synth.* **2007**, *29*, 211–225. https://doi.org/10.1002/9780470132609.ch51.

(47) Méndez, N. Q.; Arif, A. M.; Gladysz, J. A. Synthesis, Structure, and Dynamic Behavior of Rhenium Sulfide and Sulfoxide Complexes of the Formula [(H5-C5H5)Re(NO)(L)(XRR′)]+X′−(X = S, SO). *Organometallics* **1991**, *10* (7), 2199–2209. https://doi.org/10.1021/om00053a024.

(48) Legoupy, S.; Crévisy, C.; Guillemin, J. C.; Grée, R.; Toupet, L. Regio- and Stereoselective Nucleophilic Substitutions of Chiral Allylic Alcohol Rhenium Complexes. *Chem. - A Eur. J.* **1998**, *4* (11), 2162–2172. https://doi.org/10.1002/(SICI)1521-3765(19981102)4:11<2162::AID-CHEM2162>3.0.CO;2-Y.

(49) Dembinski, R.; Lis, T.; Szafert, S.; Mayne, C. L.; Bartik, T.; Gladysz, J. A. Appreciably Bent Sp Carbon Chains: Synthesis, Structure, and Protonation of Organometallic 1,3,5-Triynes and 1,3,5,7-Tetraynes of the Formula (H5-C5Me5)Re(NO)(PPh 3)((C≡C)n-p-C6H4Me). *J. Organomet. Chem.* **1999**, *578* (1–2), 229–246. https://doi.org/10.1016/S0022-328X(98)01128-0.

(50) Kromm, K.; Hampel, F.; Gladysz, J. A. A New Family of Chelating Diphosphines with Transition-Metal and Carbon Stereocenters in the Backbone: A Second-Generation Rhenium-Containing System. *Organometallics* **2002**, *21* (20), 4264–4274. https://doi.org/10.1021/om020431l.

(51) Eichenseher, S.; Delacroix, O.; Kromm, K.; Hampel, F.; Gladysz, J. A. Rhenium-Containing Phosphorus Donor Ligands for Palladium-Catalyzed Suzuki Cross-Coupling Reactions: A New Strategy for High-Activity Systems. *Organometallics* **2005**, *24* (2), 245–255. https://doi.org/10.1021/om0492956.

(52) Seidel, S. N.; Prommesberger, M.; Eichenseher, S.; Meyer, O.; Hampel, F.; Gladysz, J. A. Syntheses and Structural Analyses of Chiral Rhenium Containing Amines of the Formula (H5-C5H5)Re(NO)(PPh3)((CH2)NNRR′) (n = 0, 1). *Inorganica Chim. Acta* **2010**, *363* (3), 533–548. https://doi.org/10.1016/j.ica.2009.03.047.

(53) Lohrey, T. D.; Bergman, R. G.; Arnold, J. Olefin-Supported Rhenium(III) Terminal Oxo Complexes Generated by Nucleophilic Addition to a Cyclopentadienyl Ligand. *Angew. Chemie - Int. Ed.* **2017**, *56* (45), 14241–14245. https://doi.org/10.1002/anie.201707957.

(54) Martin, B.; Autschbach, J. Temperature Dependence of Contact and Dipolar NMR Chemical Shifts in Paramagnetic Molecules. *J. Chem. Phys.* **2015**, *142* (5), 054108. https://doi.org/10.1063/1.4906318.

(55) Randall, E. W.; Shaw, D. Nuclear Magnetic Resonance Spectra of D4-Complexes of Rhenium(III) and Osmium(IV) with Phosphine and Arsine Ligands. *J. Chem. Soc. A Inorganic, Phys. Theor. Chem.* **1969**, No. 0, 2867–2872. https://doi.org/10.1039/J19690002867.

(56) Benelli, C.; Gatteschi, D. Magnetism of Ions. In *Introduction to Molecular Magnetism: From Transition Metals to Lanthanides*; Wiley-VCH Verlag GmbH & Co. KGaA: Weinheim, Germany, 2015; pp 69–82.

(57) Booth, C. H.; Walter, M. D.; Kazhdan, D.; Hu, Y. J.; Lukens, W. W.; Bauer, E. D.; Maron, L.; Eisenstein, O.; Andersen, R. A. Decamethylytterbocene Complexes of Bipyridines and Diazabutadienes: Multiconfigurational Ground States and Open-Shell Singlet Formation. *J. Am. Chem. Soc.* **2009**, *131* (18), 6480–6491. https://doi.org/10.1021/ja809624w.

(58)   Teichteil, C.; Spiegelmann, F. Ab Initio Molecular Calculations Including Spin-Orbit Coupling. II. Molecular Test on the InH Molecule and Application to the g States of the Ar2* Excimer. *Chem. Phys.* **1983**, *81* (3), 283–296. https://doi.org/10.1016/0301-0104(83)85322-1.

(59)   Teichteil, C.; Pelissier, M.; Spiegelmann, F. Ab Initio Molecular Calculations Including Spin-Orbit Coupling. I. Method and Atomic Tests. *Chem. Phys.* **1983**, *81* (3), 273–282. https://doi.org/10.1016/0301-0104(83)85321-X.

TOC graphic

Spectroscopic, Magnetic, and Computational Investigations on a Series of Rhenium(III) Cyclopentadienide β-diketiminate Halide and Pseudohalide Complexes

Erik T. Ouellette,[†,§] Jorge Ivan Amaro Estrada,[‡] Daniel J. Lussier,[†] Khetpakorn Chakarawet,[†] Trevor D. Lohrey,[†,§] Laurent Maron,[‡] Robert G. Bergman,[†] John Arnold[†,§,]*

[†]Department of Chemistry, University of California, Berkeley, California 94720, USA
[§]Chemical Sciences Division, Lawrence Berkeley National Laboratory, Berkeley, California 94720, USA
[‡]LPCNO, Universitéde Toulouse, INSA Toulouse, 135 Avenue de Rangueil, 31077 Toulouse, France

*Email: arnold@berkeley.edu

Supporting Information

Experimental Procedures

General Considerations: Unless otherwise stated, all reactions were performed under an inert atmosphere of nitrogen, either using standard Schlenk line techniques or in an MBraun inert atmosphere glove box. Glassware and Celite® were stored in an oven at ca. 150 °C for at least 3 hours prior to use. Molecular sieves (4 Å) were activated by heating to 200 °C overnight under vacuum prior to storage in a glovebox. NMR spectra were recorded on Bruker AV-700, AV-600, AV-500, AVB-400, AVQ-400 and AV-300 spectrometers. ^{1}H and ^{13}C{^{1}H} NMR chemical shifts (δ) were calibrated relative to residual solvent peaks and reported in parts per million (ppm). ^{19}F and ^{125}Te NMR chemical shifts were referenced to external standards (C_6F_6 and $(C_6H_5)_2Te_2$,[1] respectively). ^{1}H and ^{13}C NMR assignments were routinely confirmed by ^{1}H-^{13}C (HSQC) NMR experiments. FT-IR samples were prepared as Nujol mulls and data acquired between KBr disks using a Thermo Scientific Nicolet iS10 FT-IR spectrometer. Melting points were determined using sealed capillaries prepared under nitrogen on an OptiMelt automated melting point system. Elemental analyses were performed at the Microanalytical Facility at the College of Chemistry, University of California, Berkeley. UV/Vis measurements were performed on a Varian Cary® 50 UV-Vis Spectrophotometer with a 0.2 cm path length quartz cell and using a blank measurement before each run. Mass spectrometry experiments were performed by the QB3/Chemistry Mass Spectrometry Facility at the University of California, Berkeley

Materials: Diethyl ether, *n*-hexane, toluene, and THF were purified, dried and degassed using a Pheonix solvent drying system commercially available from JC Meyer Solvent Systems. Deuterated solvents were obtained from Cambridge Isotope Laboratories and dried by stirring over sodium/benzophenone (C_6D_6 and toluene-d_8) or calcium hydride (CDCl$_3$ and pyridine-d_5), degassed with three freeze-pump-thaw cycles, and stored over molecular sieves. Diphenyl ditelluride (($C_6H_5)_2Te_2$)[1] and Na[Re(μ^5-Cp)(BDI)][2] were prepared according to literature methods. All other chemicals were obtained from commercial sources and used as received.

Re(F)(η^5-Cp)(BDI) (1-F)

In a 20 mL glass scintillation vial, a solution of **2** (43 mg, 0.053 mmol) in 6 mL of Et$_2$O was added to a stirred suspension of tetramethylammonium fluoride ([Me$_4$N][F], 24 mg, 0.26 mmol) in 1.5 mL of Et$_2$O, and the mixture was stirred at room temperature overnight. Then, the mixture was filtered through Celite and volatiles were removed *in vacuo*. The residue was triturated with hexane (2 x 2 mL), extracted with hexane (10 mL), and the resulting solution was filtered through Celite, concentrated under reduced pressure, and stored at –40 °C overnight. Upon removal of the supernatant and drying *in vacuo*, dark red crystals of **1-F** (33 mg) were isolated. Total yield: 33 mg, 89 %. X-ray quality crystals of **1-F** were obtained from hexane at –40 °C. ^{1}H NMR (500 MHz, 293 K, C$_6$D$_6$) δ 14.13 (s, 5H, Cp), 7.39 (s, 6H, HC[*Me*C(NAr)]$_2$), 6.80 (dd, J = 7.0, 2.1 Hz, 2H, BDI Ar), 6.76–6.68 (m, 4H, BDI Ar), 5.99 (hept, J = 6.8 Hz, 2H, BDI C*H*(Me)$_2$), 2.50 (d, J = 6.7 Hz, 6H, BDI CH(*Me*)$_2$), 1.95 (hept, J = 6.7 Hz, 2H, BDI C*H*(Me)$_2$), 1.51 (d, J = 6.5 Hz, 6H, BDI CH(*Me*)$_2$), 0.88 (d, J = 6.9 Hz, 6H, BDI CH(*Me*)$_2$), 0.75 (d, J = 7.0 Hz, 6H, BDI CH(*Me*)$_2$), 0.54 (s, 1H, *H*C[MeC(NAr)]$_2$). ^{13}C NMR (151 MHz, 298 K, C$_6$D$_6$) δ 201.11, 159.02, 147.85, 146.74, 140.92 (H*C*[MeC(NAr)]$_2$), 126.57 (BDI Ar), 125.82 (BDI Ar), 125.68 (BDI Ar), 99.76 (Cp), 38.32 (BDI C*H*(Me)$_2$), 28.72 (BDI CH(*Me*)$_2$), 28.34 (BDI C*H*(Me)$_2$), 25.49 (BDI CH(*Me*)$_2$), 25.09 (BDI CH(*Me*)$_2$), 24.92 (BDI CH(*Me*)$_2$), 16.19 (HC[*Me*C(NAr)]$_2$). ^{19}F NMR (376 MHz, 298 K, C$_6$D$_6$) δ –100.86. IR: 1537 (m), 1319 (m), 1251 (w), 1170 (w), 1096 (w), 1057 (w), 984 (w), 823 (w), 797 (s), 761 (m). Anal. calcd.

for $C_{34}H_{46}FN_2Re$ (**1-F**): C, 59.36; H, 6.74; N, 4.07 %. Found: C, 59.39; H, 6.69; N, 3.93 %. M.p.: 132–137 ºC.

Re(Cl)(η^5-Cp)(BDI) (1-Cl)

In a 20 mL glass scintillation vial, Na[Re(η^5-Cp)(BDI)] (100 mg, 0.150 mmol) was dissolved in 3 mL THF, and the solution was added to a stirred suspension of $CuCl_2$ (20 mg, 0.15 mmol) in 2 mL of THF. The mixture was stirred for 20 minutes at room temperature before volatiles were removed *in vacuo*. The residue was triturated with hexane (2 mL), extracted with hexane (30 mL), and the resulting solution was filtered through Celite, concentrated under reduced pressure, and stored at –40 ºC overnight. Upon removal of the supernatant and drying *in vacuo*, red crystals of **1-Cl** (83 mg) were isolated. Concentration of the supernatant and storage at –40 ºC gave a second crop of **1-Cl** (9 mg). Total yield: 91 mg, 89 %. X-ray quality crystals of **1-Cl** were obtained from hexane at –40 ºC. ^{1}H NMR (600 MHz, 298 K, C_6D_6) δ 13.65 (s, 5H, Cp), 6.77 (dd, J = 7.7, 1.5 Hz, 2H, BDI Ar), 6.70 (dd, J = 7.8, 1.5 Hz, 2H, BDI Ar), 6.54 (t, J = 7.7 Hz, 2H, BDI Ar), 6.05 (hept, J = 6.8 Hz, 2H, BDI C*H*(Me)$_2$), 5.95 (s, 6H, HC[*Me*C(NAr)]$_2$), 2.49 (d, J = 6.7 Hz, 6H, BDI CH(*Me*)$_2$), 2.41 (hept, J = 6.7 Hz, 2H, BDI C*H*(Me)$_2$), 1.42 (d, J = 6.4 Hz, 6H, BDI CH(*Me*)$_2$), 0.97 (d, J = 6.9 Hz, 6H, BDI CH(*Me*)$_2$), 0.88 (d, J = 6.9 Hz, 6H, BDI CH(*Me*)$_2$), -0.06 (s, 1H, *H*C[MeC(NAr)]$_2$). ^{13}C NMR (151 MHz, 298 K, C_6D_6) δ 195.16, 164.61 (H*C*[MeC(NAr)]$_2$), 160.64, 149.63, 148.43, 126.24 (BDI Ar), 125.97 (BDI Ar), 98.48 (Cp), 35.44 (BDI *C*H(Me)$_2$), 27.86 (BDI CH(*Me*)$_2$), 27.05 (BDI *C*H(Me)$_2$), 25.99 (BDI CH(*Me*)$_2$), 24.77 (BDI CH(*Me*)$_2$), 24.53 (BDI CH(*Me*)$_2$), 20.88 (HC[*Me*C(NAr)]$_2$). IR: 1536 (w), 1333 (w), 1316 (w), 1249 (w), 1169 (w), 1100 (w), 1017 (w), 984 (w), 931 (w), 843 (w), 821 (w), 796 (m), 761 (m). Anal. calcd. for $C_{34}H_{46}ClN_2Re$ (**1-Cl**): C, 57.97; H, 6.58; N, 3.98 %. Found: C, 58.12; H, 6.51; N, 3.89 %. M.p.: 228–232 ºC. LRMS (EI) m/z: [M]$^+$ calcd. for $C_{34}H_{46}ClN_2Re$ (**1-Cl**): 704.29; Found: 704.

Re(Br)(η^5-Cp)(BDI) (1-Br)

In a 20 mL glass scintillation vial, Na[Re(η^5-Cp)(BDI)] (99 mg, 0.14 mmol) was dissolved in 3 mL THF, and the solution was added to a stirred solution of $CuBr_2$ (34 mg, 0.15 mmol) in 2 mL of THF. The mixture was stirred for 20 minutes at room temperature before volatiles were removed *in vacuo*. The residue was triturated with hexane (2 mL), extracted with Et_2O (20 mL), and the resulting solution was filtered through Celite, concentrated under reduced pressure, and stored at –40 ºC overnight. Upon removal of the supernatant and drying *in vacuo*, dark red crystals of **1-Br** (61 mg) were isolated. Concentration of the supernatant and storage at –40 ºC gave a second crop of **1-Br** (27 mg). Total yield: 88 mg, 82 %. X-ray quality crystals of **1-Br** were obtained from diethyl ether –40 ºC. ^{1}H NMR (600 MHz, 298 K, C_6D_6) δ 14.49 (s, 5H, Cp), 6.76 (dd, J = 7.7, 1.5 Hz, 2H, BDI Ar), 6.62 (dd, J = 7.8, 1.5 Hz, 2H, BDI Ar), 6.45 (t, J = 7.7 Hz, 2H, BDI Ar), 6.17 (hept, J = 6.9 Hz, 2H, BDI C*H*(Me)$_2$), 5.78 (s, 6H, HC[*Me*C(NAr)]$_2$), 2.57 (d, J = 6.7 Hz, 6H, BDI CH(*Me*)$_2$), 2.40 (hept, J = 6.7 Hz, 2H, BDI C*H*(Me)$_2$), 1.30 (d, J = 6.4 Hz, 6H, BDI CH(*Me*)$_2$), 0.96 (d, J = 6.9 Hz, 6H, BDI CH(*Me*)$_2$), 0.84 (d, J = 6.9 Hz, 6H, BDI CH(*Me*)$_2$), 0.11 (s, 1H, *H*C[MeC(NAr)]$_2$). ^{13}C NMR (151 MHz, 298 K, C_6D_6) δ 196.81, 169.92 (H*C*[MeC(NAr)]$_2$), 161.86, 150.72, 148.86, 126.34 (BDI Ar), 126.30 (BDI Ar), 125.99 (BDI Ar), 98.66 (Cp), 35.03 (BDI *C*H(Me)$_2$), 27.89 (BDI *C*H(Me)$_2$), 26.81 (BDI CH(*Me*)$_2$), 26.39 (BDI CH(*Me*)$_2$), 24.88 (BDI CH(*Me*)$_2$), 24.37 (BDI CH(*Me*)$_2$), 22.61 (HC[*Me*C(NAr)]$_2$). IR: 1532 (m), 1329 (w), 1313 (m), 1247 (m), 1176 (w), 1162 (w), 1111 (w), 1097 (m), 1059 (w), 1039 (w), 1018 (w), 993 (w), 983 (w), 935 (w), 916 (w), 851 (w), 825 (m), 793 (s), 759 (s). Anal. calcd. for $C_{34}H_{46}BrN_2Re$ (**1-Br**): C, 54.53; H, 6.19; N, 3.74 %. Found: C, 54.45; H, 6.27; N, 3.83 %. M.p.: 235–237 ºC.

Re(I)(η^5-Cp)(BDI) (1-I)

In a 20 mL glass scintillation vial, Na[Re(η^5-Cp)(BDI)] (99 mg, 0.14 mmol) was dissolved in 3 mL THF, and the solution was added to a stirred suspension of CuI (59 mg, 0.31 mmol) in 2 mL of THF. The mixture was stirred for 20 minutes at room temperature before volatiles were removed *in vacuo*. The residue was triturated with hexane (2 mL), extracted with Et$_2$O (30 mL), and the resulting solution was filtered through Celite, concentrated under reduced pressure, and stored at –40 ºC overnight. Upon removal of the supernatant and drying *in vacuo*, red crystals of **1-I** (80 mg) were isolated. Concentration of the supernatant and storage at –40 ºC gave a second crop of **1-I** (13 mg). Total yield: 93 mg, 82 %. X-ray quality crystals of **1-I** were obtained from diethyl ether at –40 ºC. ^{1}H NMR (600 MHz, 298 K, C$_6$D$_6$) δ 15.09 (s, 5H, Cp), 6.72 (dd, *J* = 7.7, 1.5 Hz, 2H, BDI Ar), 6.51 (dd, *J* = 7.9, 1.5 Hz, 2H, BDI Ar), 6.36 (t, *J* = 7.7 Hz, 2H, BDI Ar), 5.92 (hept, *J* = 6.8 Hz, 2H, BDI C*H*(Me)$_2$), 5.44 (s, 6H, HC[*Me*C(NAr)]$_2$), 2.57 (d, *J* = 6.6 Hz, 6H, BDI CH(*Me*)$_2$), 2.47 (hept, *J* = 6.7 Hz, 2H, BDI C*H*(Me)$_2$), 1.10 (d, *J* = 6.4 Hz, 6H, BDI CH(*Me*)$_2$), 1.04 (s, 1H, *H*C[MeC(NAr)]$_2$), 0.89 (d, *J* = 6.9 Hz, 6H, BDI CH(*Me*)$_2$), 0.80 (d, *J* = 6.9 Hz, 6H, BDI CH(*Me*)$_2$). ^{13}C NMR (151 MHz, 298 K, C$_6$D$_6$) δ 198.65, 171.25 (H*C*[MeC(NAr)]$_2$), 163.14, 151.61, 149.10, 126.46 (BDI Ar), 126.34 (BDI Ar), 125.98 (BDI Ar), 99.33 (Cp), 34.20 (BDI *C*H(Me)$_2$), 27.81 (BDI CH(*Me*)$_2$), 27.39 (BDI CH(*Me*)$_2$), 26.48 (BDI *C*H(Me)$_2$), 25.34 (HC[*Me*C(NAr)]$_2$), 25.00 (BDI CH(*Me*)$_2$), 24.12 (BDI CH(*Me*)$_2$). IR: 1532 (m), 1328 (w), 1313 (m), 1280 (w), 1251 (w), 1177 (m), 1161 (m), 1110 (w), 1098 (m), 1059 (w), 1039 (w), 1018 (w), 994 (w), 982 (w), 967 (w), 935 (m), 917 (w), 901 (w), 849 (w), 824 (m), 802 (m), 793 (s), 759 (s), 668 (w). Anal. calcd. for C$_{34}$H$_{46}$IN$_2$Re (**1-I**): C, 51.31; H, 5.83; N, 3.52 %. Found: C, 51.28; H, 5.81; N, 3.48 %. M.p.: 232–235 ºC.

Re(OTf)(η^5-Cp)(BDI) (2)

In a 20 mL glass scintillation vial inside an unlit glovebox, Na[Re(η^5-Cp)(BDI)] (48 mg, 0.069 mmol) was dissolved in 2 mL Et$_2$O, and the solution was slowly added to a stirred solution of silver(I) trifluoromethanesulfonate (AgOTf, 36 mg, 0.14 mmol) in 2 mL of Et$_2$O. The mixture was stirred for 2 hours at room temperature in the dark before volatiles were removed *in vacuo*. The residue was triturated with hexane (2 mL), extracted with hexane (15 mL), and the resulting solution was filtered through Celite, concentrated under reduced pressure, and stored at –40 ºC overnight. Upon removal of the supernatant and drying *in vacuo*, red crystals of **2** (28 mg) were isolated. Concentration of the supernatant and storage at –40 ºC gave a second crop of **2** (9 mg). Total yield: 36 mg, 64 %. X-ray quality crystals of **2** were obtained from hexane at –40 ºC. ^{1}H NMR (500 MHz, 293 K, C$_6$D$_6$) δ 14.14 (s, 5H, Cp), 7.03 (d, *J* = 7.5 Hz, 2H, BDI Ar), 6.88 (d, *J* = 7.6 Hz, 2H, BDI Ar), 6.81 (t, *J* = 7.6 Hz, 2H, BDI Ar), 6.05 (hept, *J* = 6.9 Hz, 2H, BDI C*H*(Me)$_2$), 5.49 (s, 6H, HC[*Me*C(NAr)]$_2$), 3.63 (hept, *J* = 6.6 Hz, 2H, BDI C*H*(Me)$_2$), 1.97 (d, *J* = 6.7 Hz, 6H, BDI CH(*Me*)$_2$), 1.56 (d, *J* = 6.6 Hz, 6H, BDI CH(*Me*)$_2$), 1.47 (d, *J* = 6.9 Hz, 6H, BDI CH(*Me*)$_2$), 1.25 (d, *J* = 6.7 Hz, 6H, BDI CH(*Me*)$_2$), –3.61 (s, 1H, *H*C[MeC(NAr)]$_2$). ^{13}C NMR (151 MHz, 298 K, C$_6$D$_6$) δ 192.09, 185.94 (H*C*[MeC(NAr)]$_2$), 153.54, 151.91, 149.09, 126.96 (BDI Ar), 126.89 (BDI Ar), 126.55 (BDI Ar), 90.74 (Cp), 32.17 (BDI *C*H(Me)$_2$), 31.20 (BDI *C*H(Me)$_2$), 26.60 (BDI CH(*Me*)$_2$), 26.36 (BDI CH(*Me*)$_2$), 25.80 (BDI CH(*Me*)$_2$), 25.26 (BDI CH(*Me*)$_2$), 19.38 (HC[*Me*C(NAr)]$_2$). ^{19}F NMR (376 MHz, 298 K, C$_6$D$_6$) δ –74.89. IR: 1538 (w), 1324 (w), 1230 (w), 1198 (m), 1179 (w), 1003 (s), 796 (w), 760 (w), 630 (m). Anal. calcd. for C$_{35}$H$_{46}$F$_3$N$_2$O$_3$ReS (**2**): C, 51.39; H, 5.67; N, 3.42 %. Found: C, 51.05; H, 5.95; N, 3.59 %. M.p.: 155–162 ºC (decomp.).

Re(SCH$_2$(C$_6$H$_5$))(η^5-Cp)(BDI) (3-SBn)

In a 20 mL glass scintillation vial, Na[Re(η^5-Cp)(BDI)] (51 mg, 0.074 mmol) was dissolved in 3 mL Et$_2$O, and the solution was added to a stirred solution of dibenzyl disulfide (S$_2$(CH$_2$(C$_6$H$_5$))$_2$, 19 mg, 0.077 mmol) in 2 mL of Et$_2$O. The mixture was stirred for 20 minutes at room temperature, during which time white-grey solids precipitated.. Volatiles were removed *in vacuo*, and the residue was extracted with toluene (9 mL) and filtered through Celite. The extracts were then concentrated under reduced pressure and stored at –40 ºC for two days. Upon removal of the supernatant and drying *in vacuo*, dark red/brown crystals of **3-SBn** (21 mg) were isolated. Concentration of the supernatant and storage at –40 ºC gave a second crop of **3-SBn** (15 mg). Total yield: 36 mg, 61 %. X-ray quality crystals of **3-SBn** were obtained from toluene at –40 ºC. ^{1}H NMR (600 MHz, 298 K, C$_6$D$_6$) δ 11.79 (s, 2H, SCH_2Ph), 7.59 (s, 5H, Cp), 7.54 (d, J = 7.2 Hz, 2H, Benzyl Ar), 7.16 (d, 2H, Benzyl Ar), 7.12 (dd, J = 7.5, 1.7 Hz, 2H, BDI Ar), 7.09 (t, J = 7.4 Hz, 1H, Benzyl Ar), 6.96 (dd, J = 7.7, 1.7 Hz, 2H, BDI Ar), 6.92 (t, J = 7.6 Hz, 2H, BDI Ar), 4.05 (hept, J = 6.9 Hz, 2H, BDI CH(Me)$_2$), 3.93 (s, 6H, HC[MeC(NAr)]$_2$), 3.45 (hept, J = 6.8 Hz, 2H, BDI CH(Me)$_2$), 1.77 (s, 1H, HC[MeC(NAr)]$_2$), 1.57 (d, J = 6.7 Hz, 6H, BDI CH(Me)$_2$), 1.32 (d, J = 6.6 Hz, 6H, BDI CH(Me)$_2$), 1.17 (d, J = 6.7 Hz, 6H, BDI CH(Me)$_2$), 0.95 (d, J = 6.8 Hz, 6H, BDI CH(Me)$_2$). ^{13}C NMR (151 MHz, 298 K, C$_6$D$_6$) δ 176.93, 157.98, 151.47, 147.04, 146.29, 136.36 (HC[MeC(NAr)]$_2$), 129.73 (Benzyl Ar), 128.89 (Benzyl Ar), 126.28 (Benzyl Ar), 126.12 (Ar), 125.99 (Ar), 125.04 (BDI Ar), 91.15 (Cp), 67.15 (SCH$_2$Ph), 30.92 (BDI CH(Me)$_2$), 28.08 (BDI CH(Me)$_2$), 27.43 (BDI CH(Me)$_2$), 26.66 (BDI CH(Me)$_2$), 25.01 (BDI CH(Me)$_2$), 24.90 (BDI CH(Me)$_2$), 22.59 (HC[MeC(NAr)]$_2$). IR: 1548 (m), 1316 (m), 1273 (w), 1243 (m), 1192 (w), 1157 (m), 1098 (m), 1057 (w), 1040 (w), 981 (w), 932 (w), 905 (w), 855 (w), 834 (w), 816 (s), 794 (s), 766 (m), 759 (m), 698 (s). Anal. calcd. for C$_{41}$H$_{53}$N$_2$ReS (**3-SBn**): C, 62.17; H, 6.74; N, 3.54 %. Found: C, 62.24; H, 6.53; N, 3.38 %. M.p.: 178–182 ºC.

Re(SeCH$_2$(C$_6$H$_5$))(η^5-Cp)(BDI) (3-SeBn)

In a 20 mL glass scintillation vial, Na[Re(η^5-Cp)(BDI)] (50 mg, 0.072 mmol) was dissolved in 3 mL Et$_2$O, and the solution was added to a stirred solution of dibenzyl diselenide (Se$_2$(CH$_2$(C$_6$H$_5$))$_2$, 25 mg, 0.073 mmol) in 2 mL of Et$_2$O. The mixture was stirred for 20 minutes at room temperature, during which time white-grey solids precipitated out of solution. Volatiles were removed *in vacuo*, and the residue was extracted with toluene (11 mL) and filtered through Celite. The extracts were then concentrated under reduced pressure and stored at –40 ºC overnight. Upon removal of the supernatant and drying *in vacuo*, dark red crystals of **3-SeBn** (29 mg) were isolated. Concentration of the supernatant and storage at –40 ºC gave a second crop of **3-SeBn** (9 mg). Total yield: 38 mg, 63 %. X-ray quality crystals of **3-SeBn** were obtained from toluene at –40 ºC. ^{1}H NMR (600 MHz, 298 K, C$_6$D$_6$) δ 9.64 (s, 2H, SeCH_2Ph), 8.14 (s, 5H, Cp), 7.57 (d, J = 7.2 Hz, 2H, Benzyl Ar), 7.16 (d, 2H, Benzyl Ar), 7.05 (t, J = 7.4 Hz, 1H, Benzyl Ar), 7.01 (dd, J = 7.6, 1.7 Hz, 2H, BDI Ar), 6.91 (dd, J = 7.7, 1.7 Hz, 2H, BDI Ar), 6.86 (t, J = 7.6 Hz, 2H, BDI Ar), 4.41 (s, 6H, HC[MeC(NAr)]$_2$), 3.84 (hept, J = 6.7 Hz, 2H, BDI CH(Me)$_2$), 3.51 (hept, J = 6.8 Hz, 2H, BDI CH(Me)$_2$), 2.32 (s, 1H, HC[MeC(NAr)]$_2$), 1.67 (d, J = 6.7 Hz, 6H, BDI CH(Me)$_2$), 1.28 (d, J = 6.6 Hz, 6H, BDI CH(Me)$_2$), 1.14 (d, J = 6.8 Hz, 6H, BDI CH(Me)$_2$), 0.86 (d, J = 6.9 Hz, 6H, BDI CH(Me)$_2$). ^{13}C NMR (151 MHz, 298 K, C$_6$D$_6$) δ 180.83, 158.30, 150.51, 147.02, 146.35, 136.90 (HC[MeC(NAr)]$_2$), 129.79 (Benzyl Ar), 128.81 (Benzyl Ar), 126.24 (Ar), 125.97 (Ar), 125.20 (Ar), 92.33 (Cp), 50.24 (SeCH$_2$Ph), 31.34 (BDI CH(Me)$_2$), 28.26 (BDI CH(Me)$_2$), 27.41 (BDI CH(Me)$_2$), 26.71 (BDI CH(Me)$_2$), 25.08 (BDI CH(Me)$_2$), 24.91 (BDI CH(Me)$_2$), 22.48 (HC[MeC(NAr)]$_2$). IR: 1542 (m), 1491 (m), 1316 (m), 1275 (w), 1244 (m), 1158 (m), 1098 (m), 1055 (w), 1040 (w), 1032 (w), 994 (w), 981 (w), 932 (w), 901 (w), 854 (w), 815 (s), 794 (s), 759 (s), 693 (s), 614 (w). Anal. calcd. for C$_{41}$H$_{53}$N$_2$ReSe (**3-SeBn**): C, 58.69; H, 6.37; N, 3.34 %. Found: C, 58.73; H, 6.33; N, 3.19 %. M.p.: 175–181 ºC.

Re(Te(C₆H₅))(η⁵-Cp)(BDI) (3-TePh)

In a 20 mL glass scintillation vial, Na[Re(η⁵-Cp)(BDI)] (50 mg, 0.072 mmol) was dissolved in 3 mL Et₂O, and the solution was added to a stirred solution of (C₆H₅)₂Te₂ (31 mg, 0.076 mmol) in 2 mL of Et₂O. The mixture was stirred for 20 minutes at room temperature before volatiles were removed *in vacuo*. The residue was triturated with hexane (2 mL), extracted with hexane (15 mL), and the resulting solution was filtered through Celite, concentrated under reduced pressure, and stored at –40 ºC overnight. Upon removal of the supernatant and drying *in vacuo*, dark green crystals of **3-TePh** (52 mg) were isolated. Total yield: 52 mg, 83 %. X-ray quality crystals of **3-TePh** were obtained from hexane at –40 ºC. ¹H NMR (600 MHz, 298 K, C₆D₆) δ 9.02 (s, 5H, Cp), 8.12 (d, J = 7.4 Hz, 2H, Phenyl Ar), 7.29 (t, J = 7.5 Hz, 2H, Phenyl Ar), 6.98 (t, J = 7.4 Hz, 1H, Phenyl Ar), 6.84–6.78 (m, 4H, BDI Ar), 6.75 (t, J = 7.6 Hz, 2H, BDI Ar), 4.68 (s, 6H, HC[*Me*C(NAr)]₂), 4.01 (s, 1H, *H*C[MeC(NAr)]₂), 3.44 (hept, J = 6.7 Hz, 2H, BDI C*H*(Me)₂), 3.38 (hept, J = 6.8 Hz, 2H, BDI C*H*(Me)₂), 1.72 (d, J = 6.7 Hz, 6H, BDI CH(*Me*)₂), 1.03 (d, J = 6.8 Hz, 6H, BDI CH(*Me*)₂), 1.00 (d, J = 6.6 Hz, 6H, BDI CH(*Me*)₂), 0.78 (d, J = 6.9 Hz, 6H, BDI CH(*Me*)₂). ¹³C NMR (151 MHz, 298 K, C₆D₆) δ 187.46, 159.51, 152.87 (Phenyl Ar), 145.90, 145.81, 136.60, 136.00 (H*C*[MeC(NAr)]₂), 130.10 (Phenyl Ar), 127.61 (Phenyl Ar), 126.31 (BDI Ar), 126.03 (BDI Ar), 124.98 (BDI Ar), 94.40 (Cp), 31.20 (BDI *C*H(Me)₂), 28.85 (BDI *C*H(Me)₂), 26.59 (BDI CH(*Me*)₂), 26.50 (BDI CH(*Me*)₂), 25.03 (BDI CH(*Me*)₂), 23.69 (HC[*Me*C(NAr)]₂). ¹²⁵Te NMR (189 MHz, 298 K, C₆D₆) δ 513. IR: 1566 (w), 1533 (m), 1354 (m), 1311 (m), 1273 (w), 1241 (w), 1216 (w), 1172 (w), 1156 (w), 1099 (m), 1058 (w), 1040 (w), 1013 (w), 996 (w), 984 (w), 932 (w), 840 (w), 822 (w), 812 (w), 794 (s), 757 (m), 731 (s), 696 (m), 637 (w). Anal. calcd. for C₄₀H₅₁N₂ReTe (**3-TePh**): C, 54.99; H, 5.88; N, 3.21 %. Found: C, 54.99; H, 5.96; N, 3.15 %. M.p.: 188–190 ºC.

NMR Spectroscopy
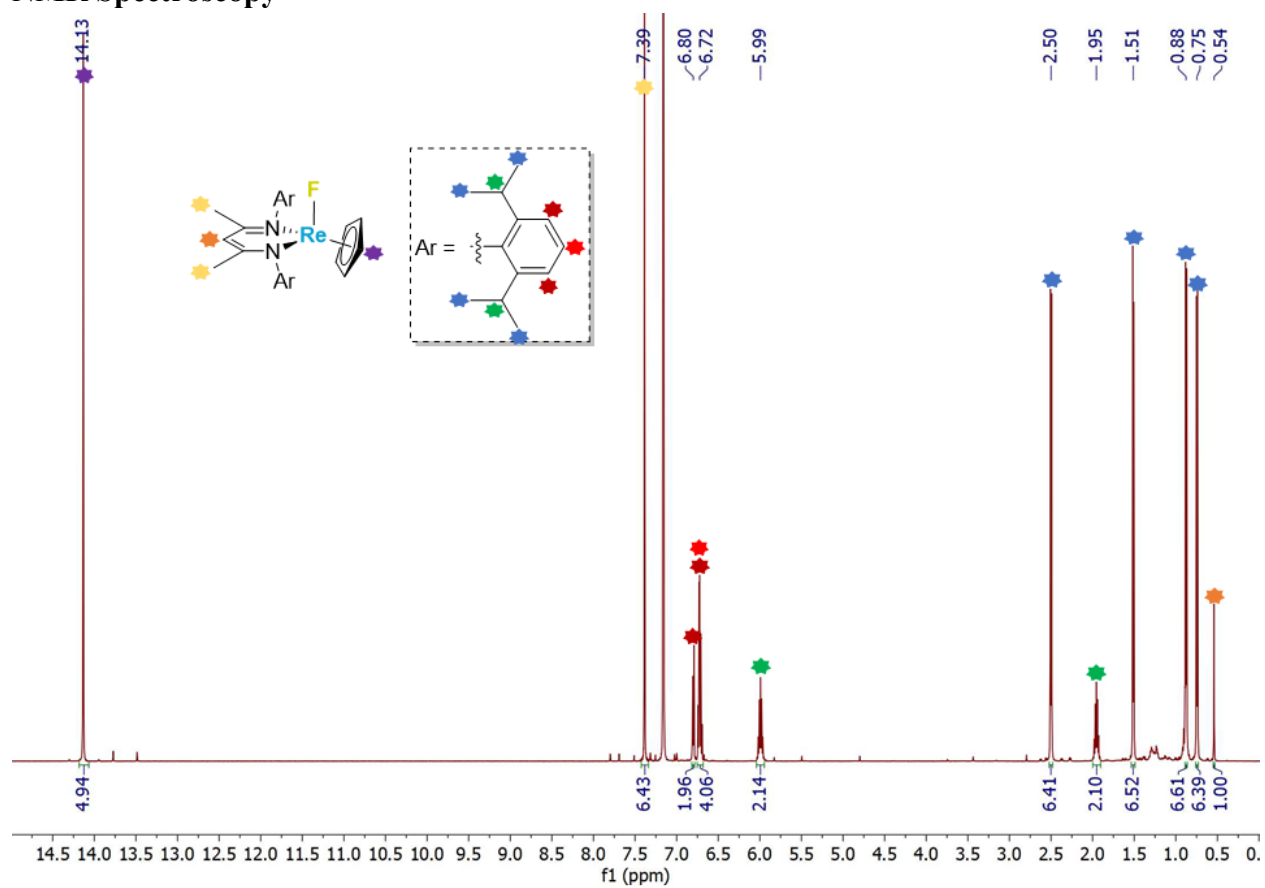
Figure S1. ^{1}H NMR spectrum of Re(F)(η^5-Cp)(BDI) (**1-F**) in C_6D_6 (500 MHz, 293 K).
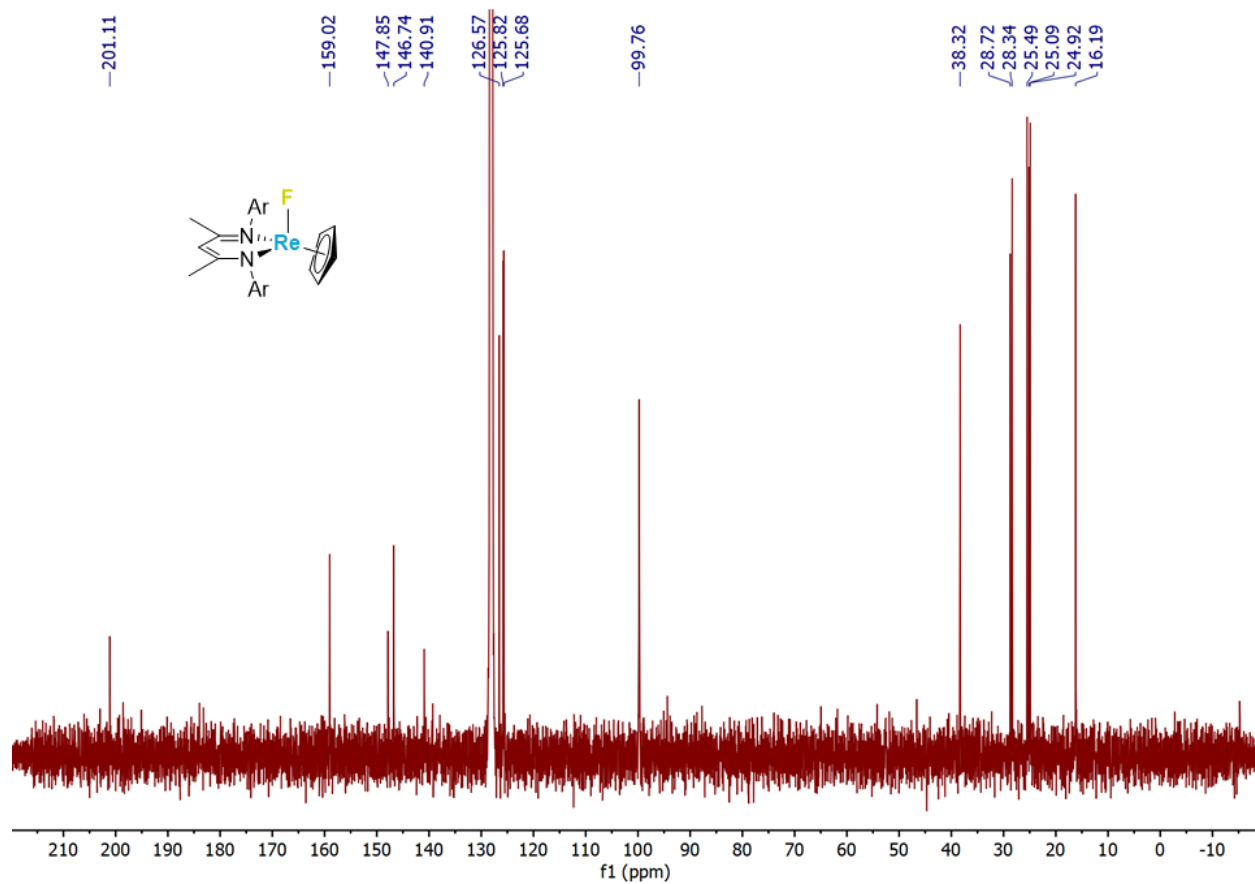
Figure S2. ^{13}C NMR spectrum of Re(F)(η^5-Cp)(BDI) (**1-F**) in C$_6$D$_6$ (151 MHz, 298 K).
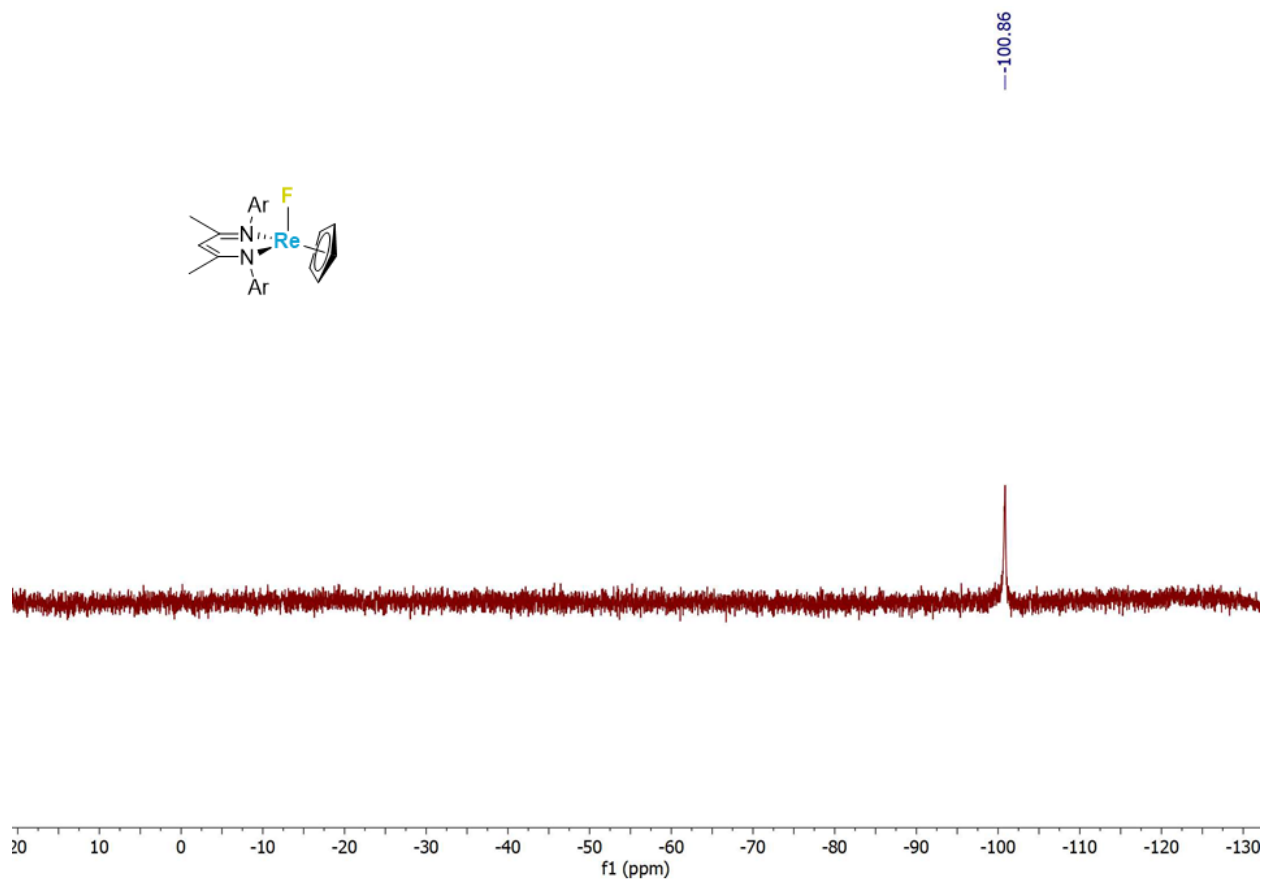
Figure S3. ^{19}F NMR spectrum of Re(F)(η^5-Cp)(BDI) (**1-F**) in C$_6$D$_6$ (376 MHz, 298 K).
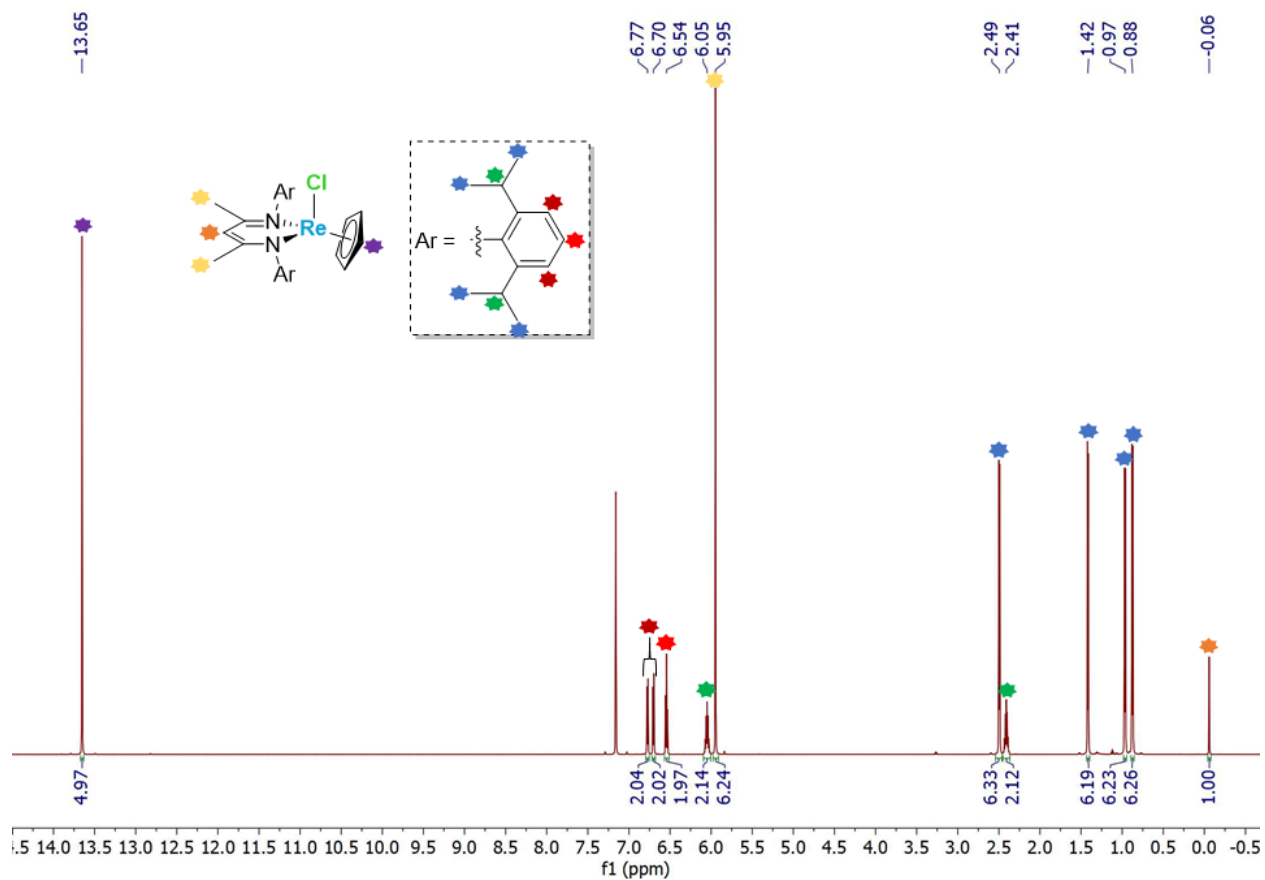
Figure S4. ^{1}H NMR spectrum of Re(Cl)(η^5-Cp)(BDI) (**1-Cl**) in C_6D_6 (600 MHz, 298 K).
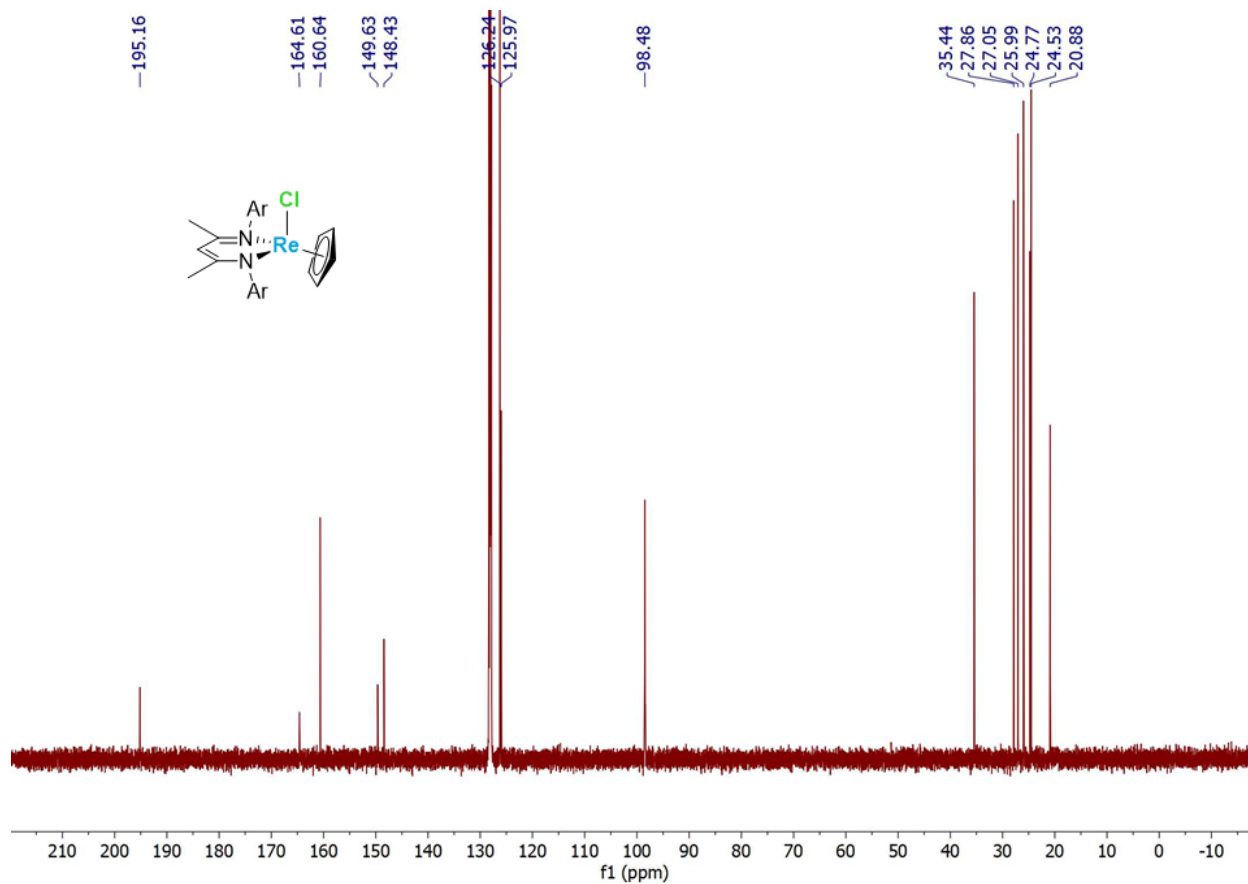
Figure S5. ^{13}C NMR spectrum of $Re(Cl)(\eta^5\text{-}Cp)(BDI)$ (**1-Cl**) in C_6D_6 (151 MHz, 298 K).
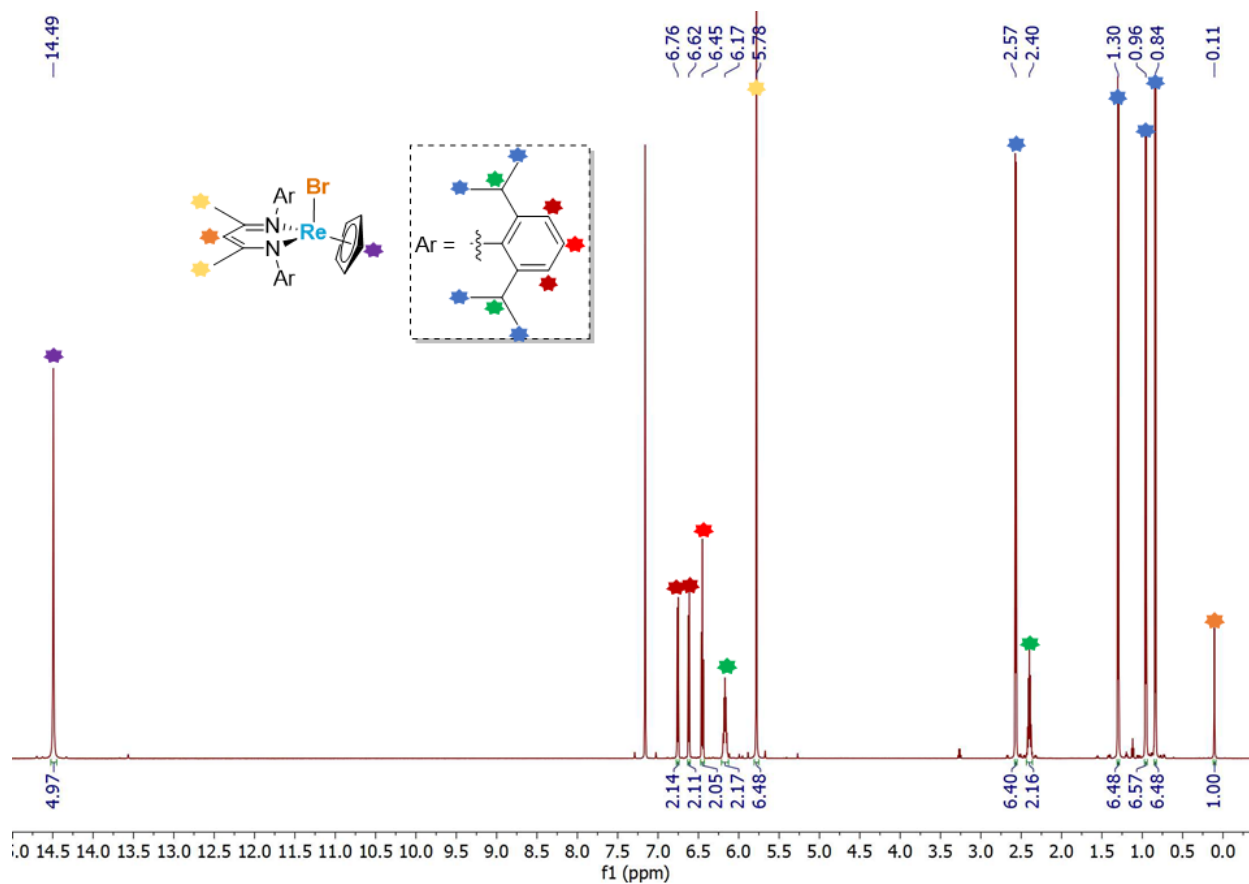
Figure S6. ^{1}H NMR spectrum of Re(Br)(η^5-Cp)(BDI) (**1-Br**) in C_6D_6 (600 MHz, 298 K).
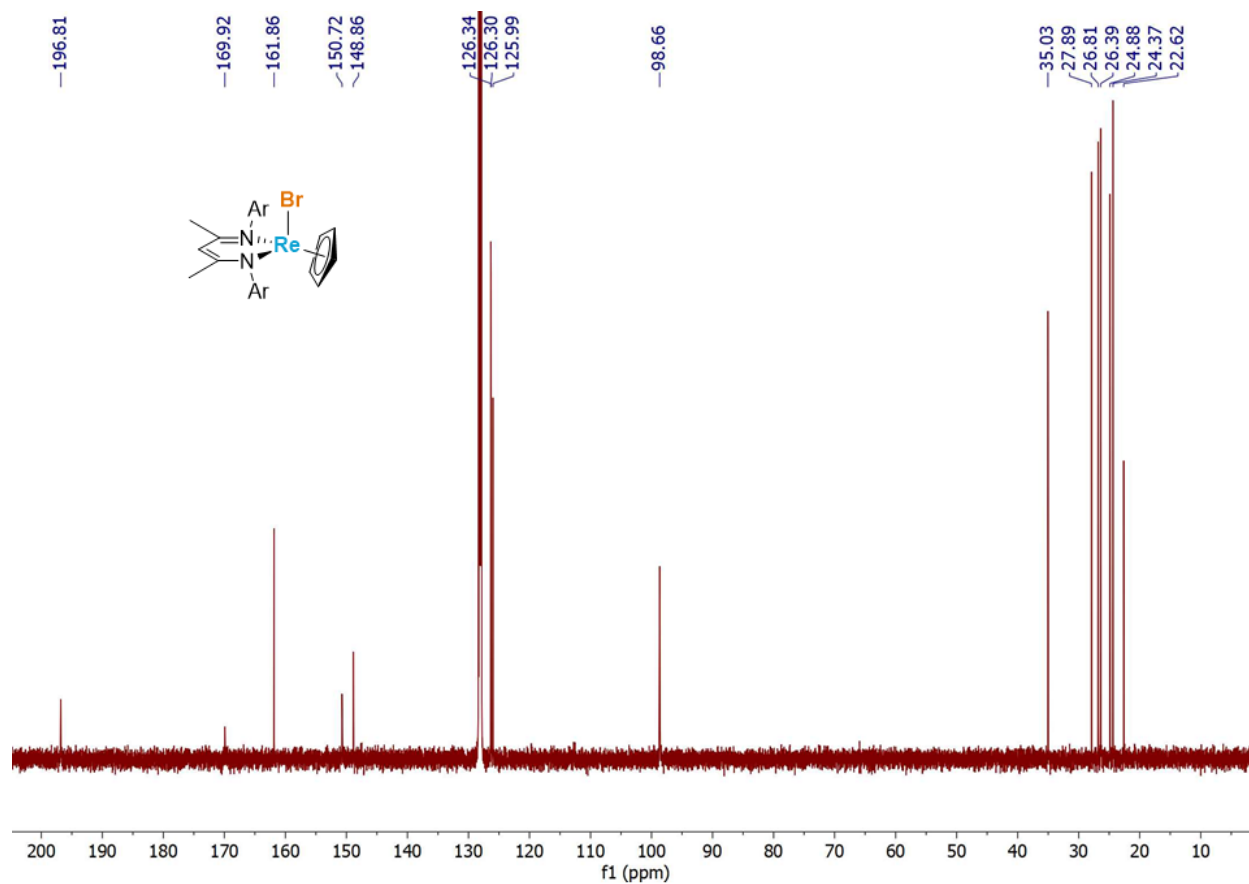
Figure S7. ^{13}C NMR spectrum of Re(Br)(η^5-Cp)(BDI) (**1-Br**) in C_6D_6 (151 MHz, 298 K).
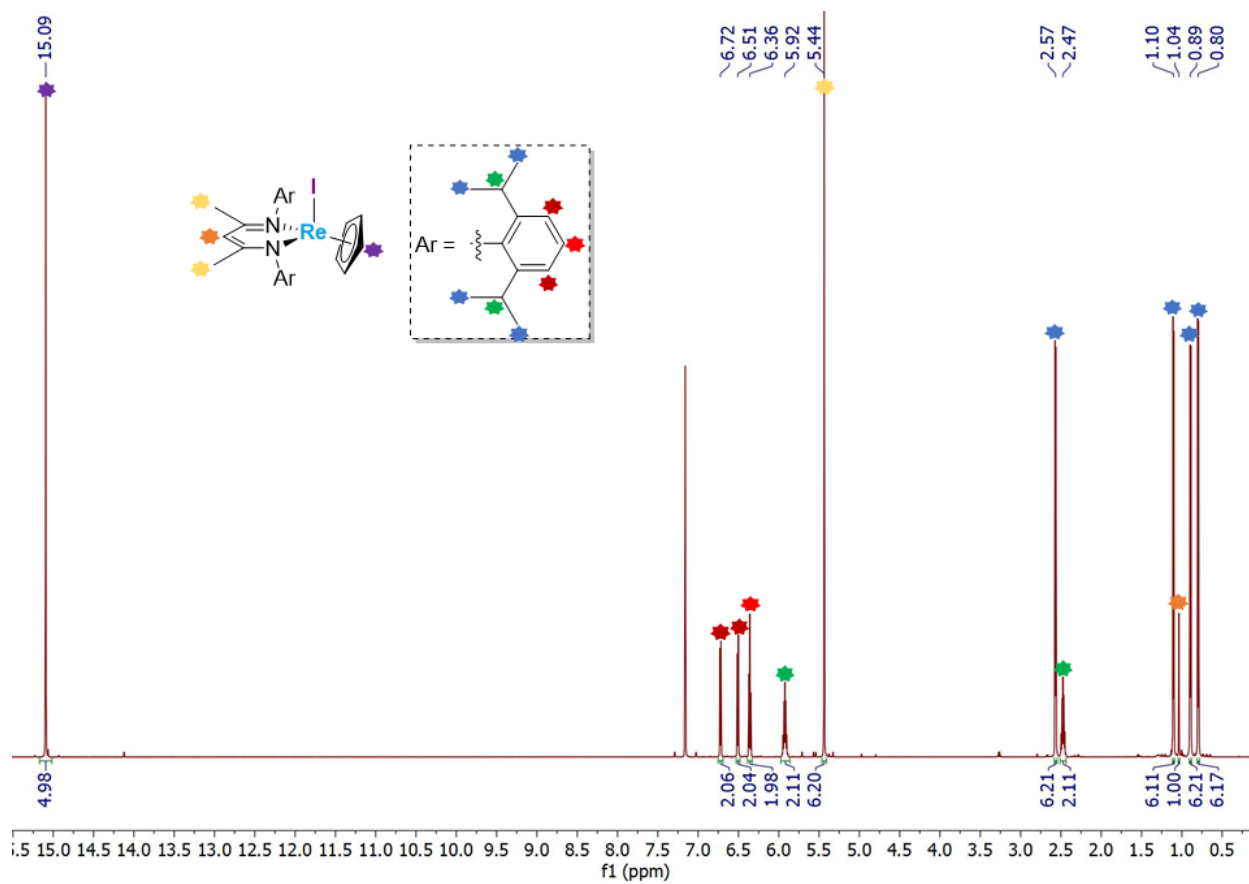
Figure S8. ^{1}H NMR spectrum of Re(I)(η^5-Cp)(BDI) (**1-I**) in C$_6$D$_6$ (600 MHz, 298 K).
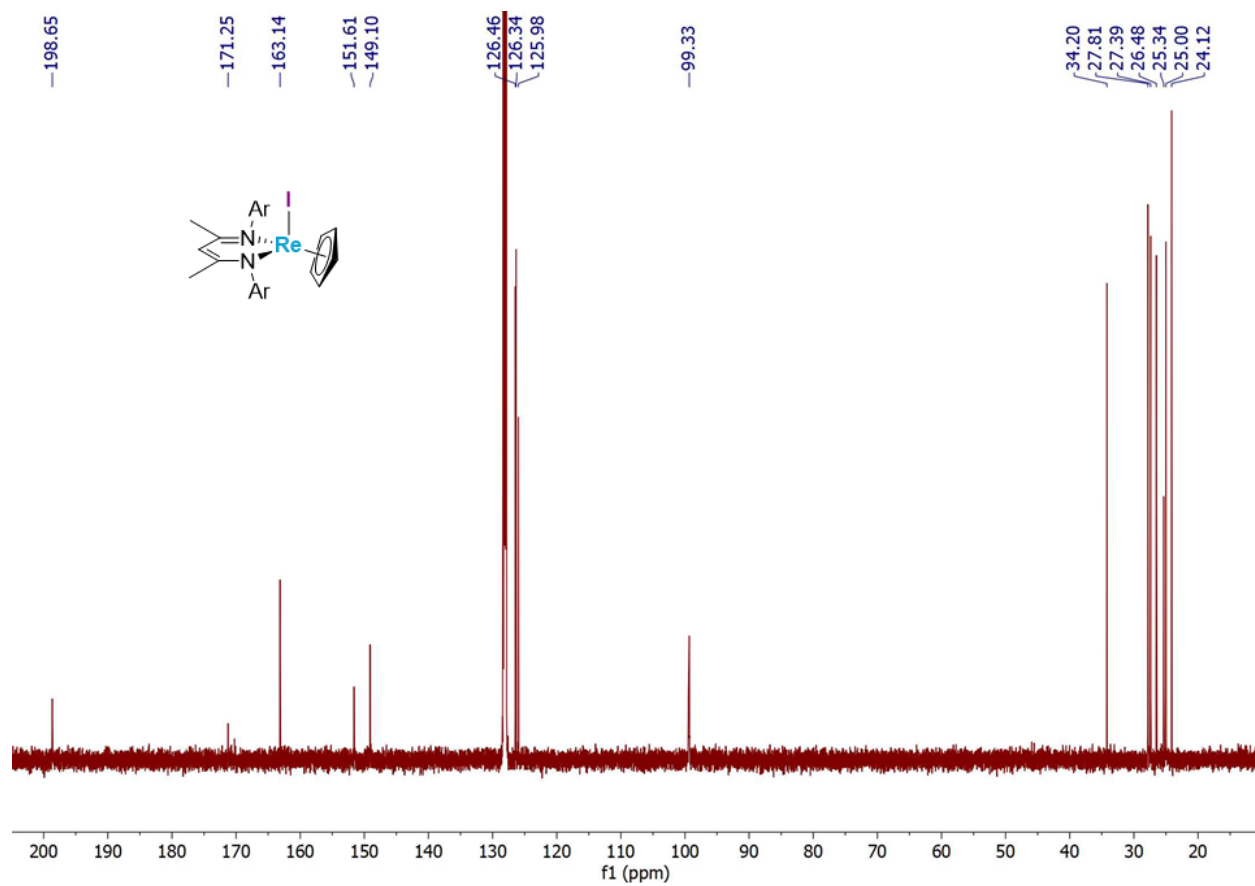
Figure S9. ^{13}C NMR spectrum of $\text{Re(I)}(\eta^5\text{-Cp})(\text{BDI})$ (**1-I**) in C_6D_6 (151 MHz, 298 K).
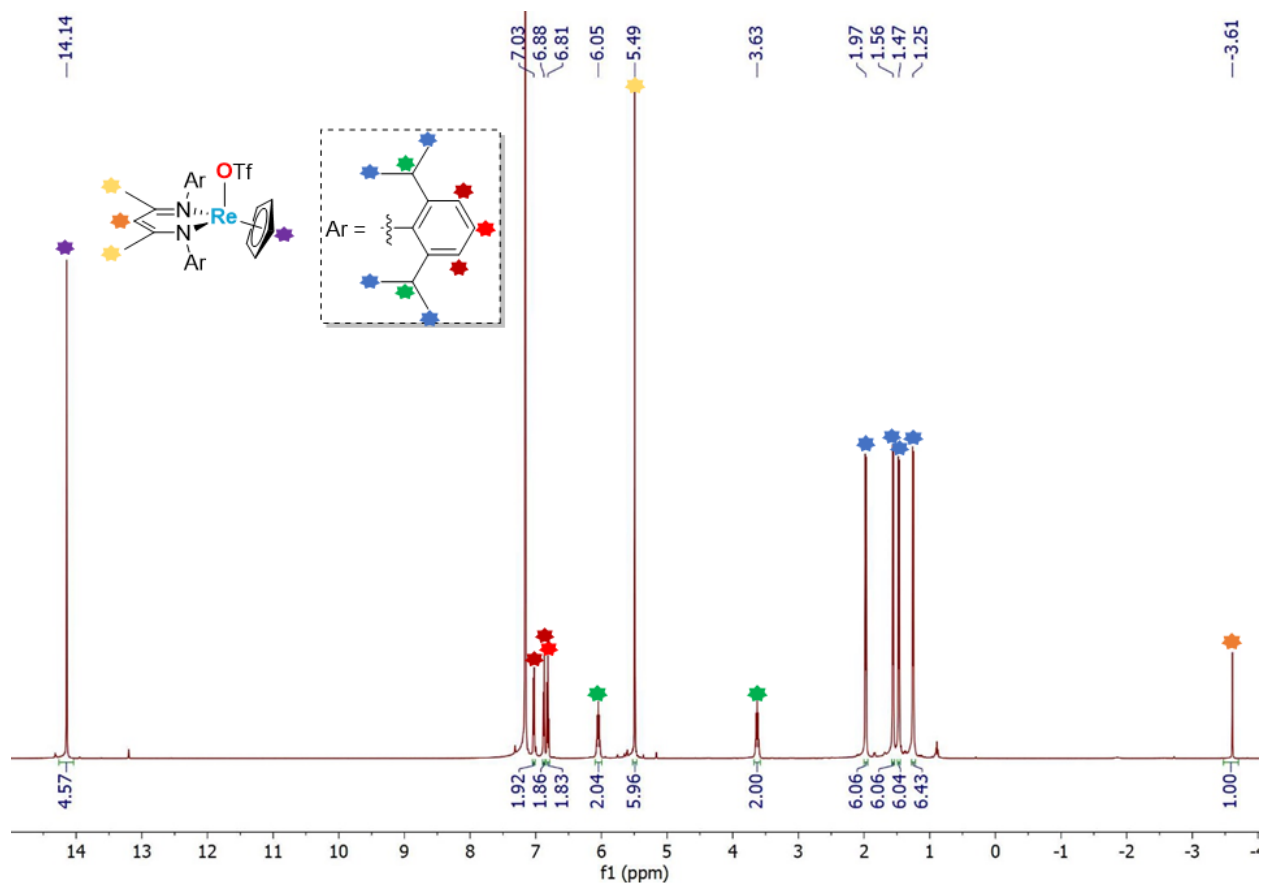
Figure S10. ^{1}H NMR spectrum of Re(OTf)(η^5-Cp)(BDI) (**2**) in C$_6$D$_6$ (500 MHz, 293 K).
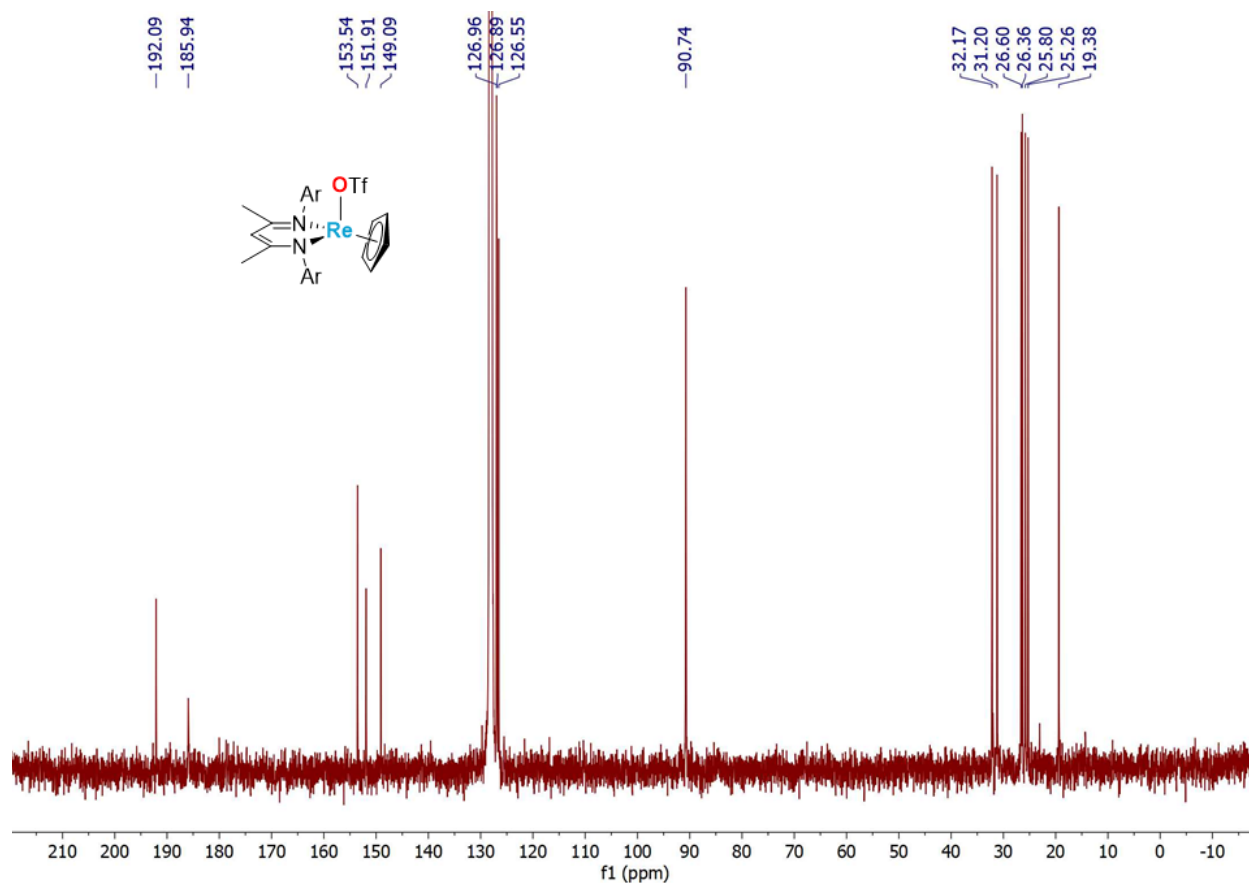
Figure S11. ^{13}C NMR spectrum of Re(OTf)(η^5-Cp)(BDI) (**2**) in C_6D_6 (151 MHz, 298 K).
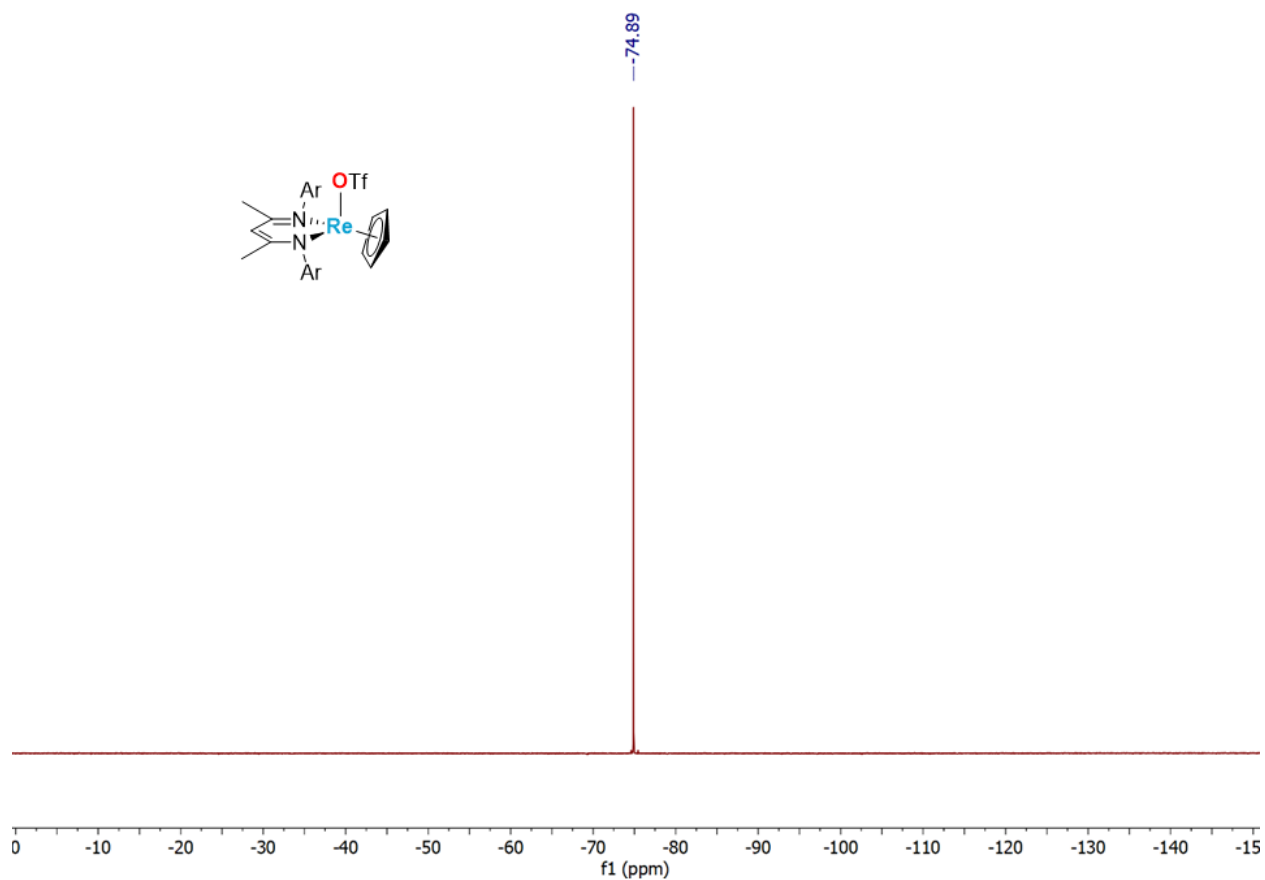
Figure S12. ^{19}F NMR spectrum of Re(OTf)(η^5-Cp)(BDI) (**2**) in C$_6$D$_6$ (376 MHz, 298 K).
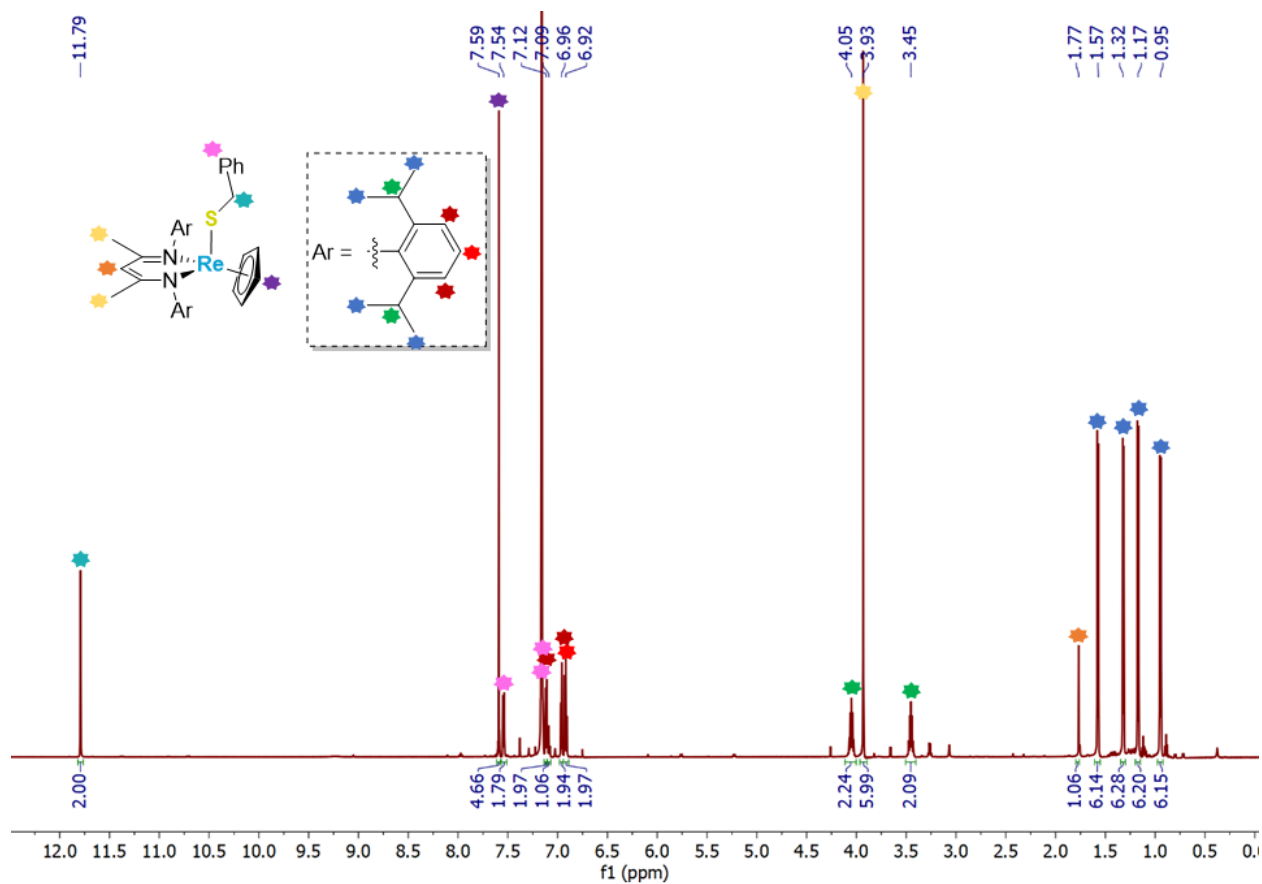
Figure S13. ^{1}H NMR spectrum of Re(SBn)(η^5-Cp)(BDI) (**3-SBn**) in C_6D_6 (600 MHz, 298 K).
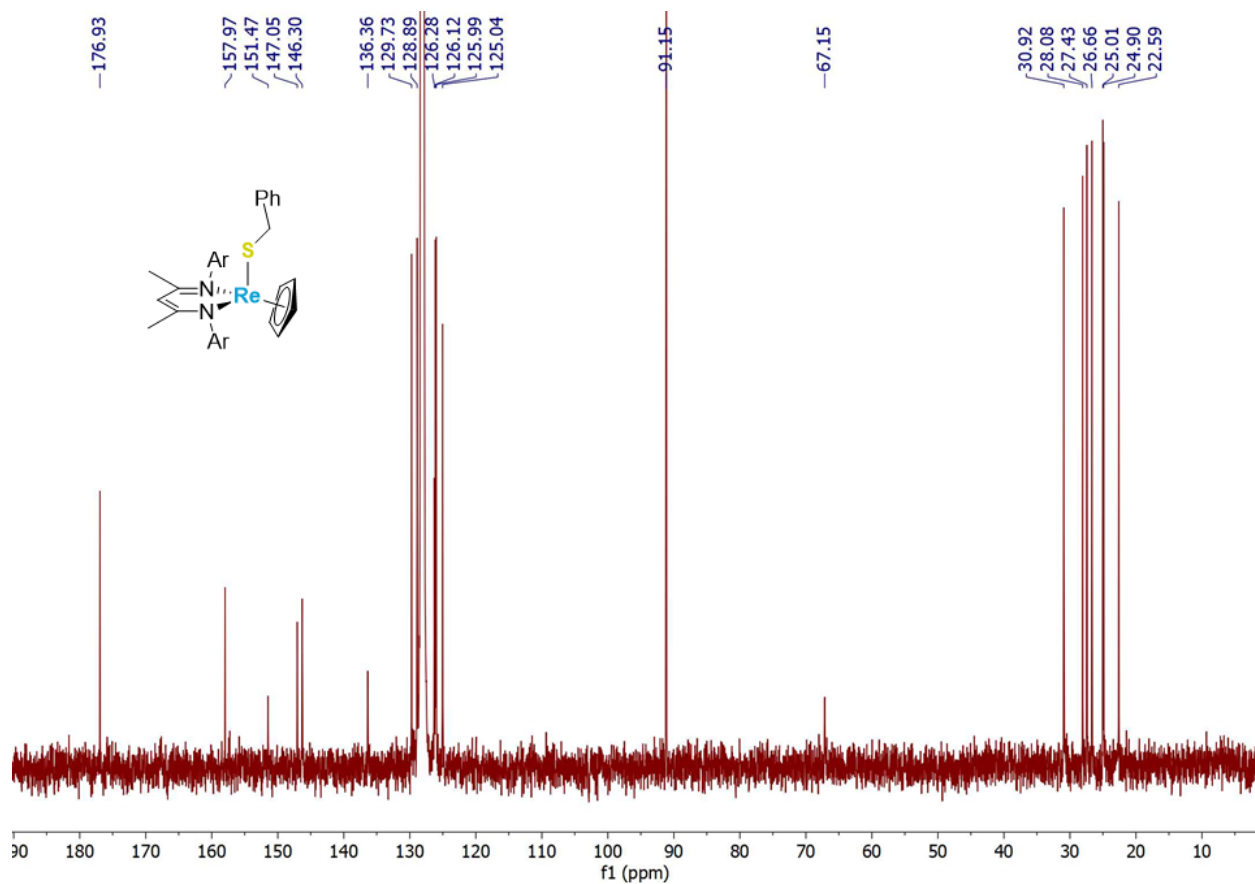
Figure S14. ^{13}C NMR spectrum of Re(SBn)(η^5-Cp)(BDI) (**3-SBn**) in C_6D_6 (151 MHz, 298 K).
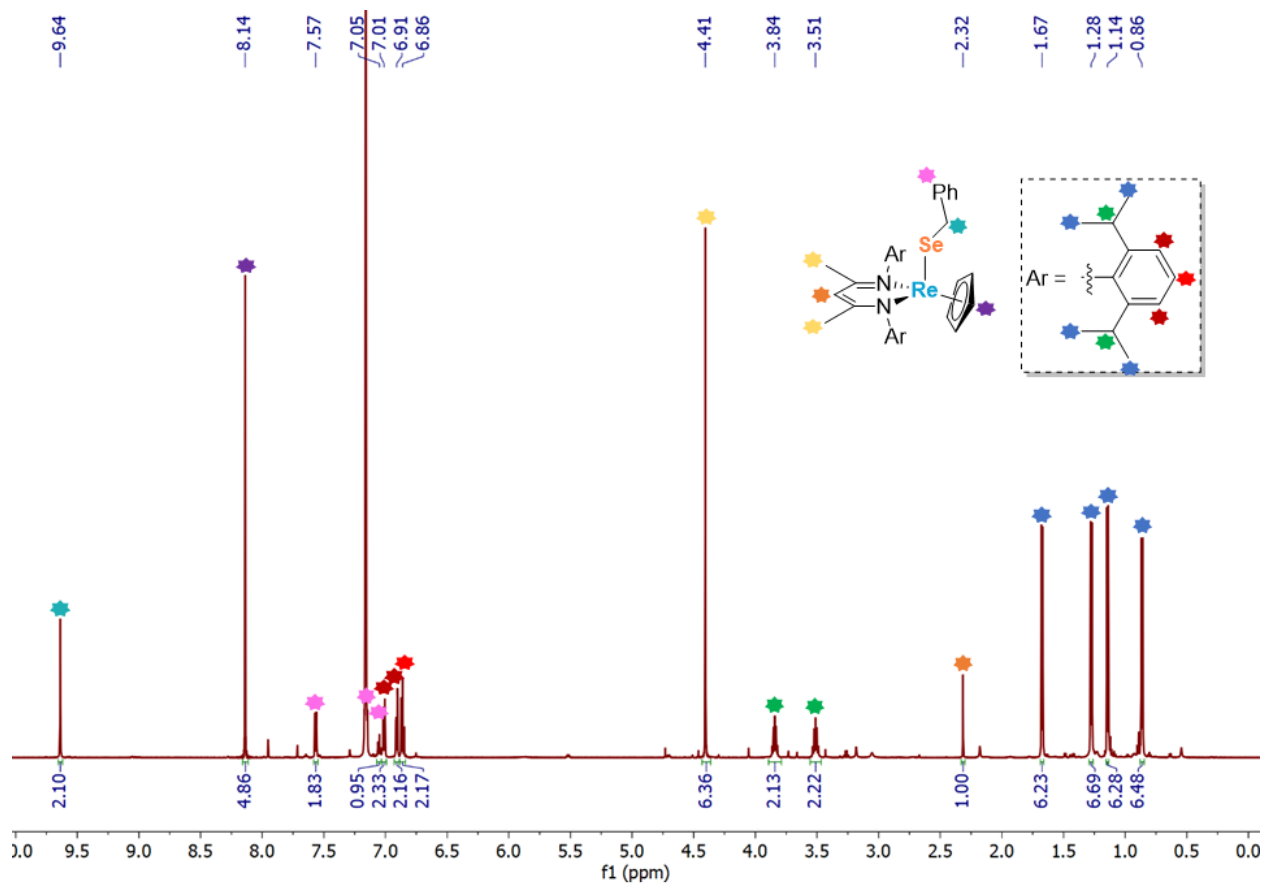
Figure S15. ^{1}H NMR spectrum of Re(SeBn)(η^5-Cp)(BDI) (**3-SeBn**) in C$_6$D$_6$ (600 MHz, 298 K).
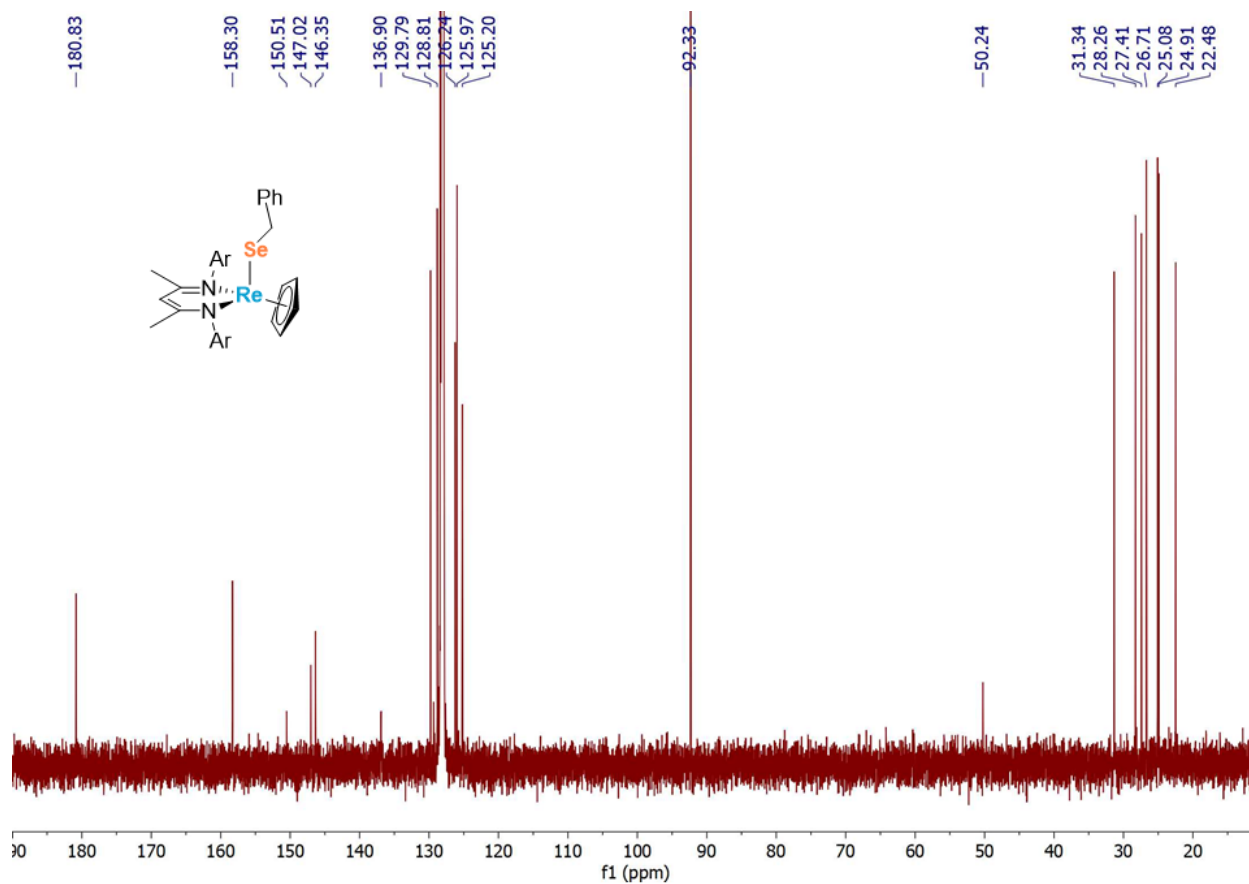
Figure S16. ^{13}C NMR spectrum of Re(SeBn)(η^5-Cp)(BDI) (**3-SeBn**) in C$_6$D$_6$ (151 MHz, 298 K).
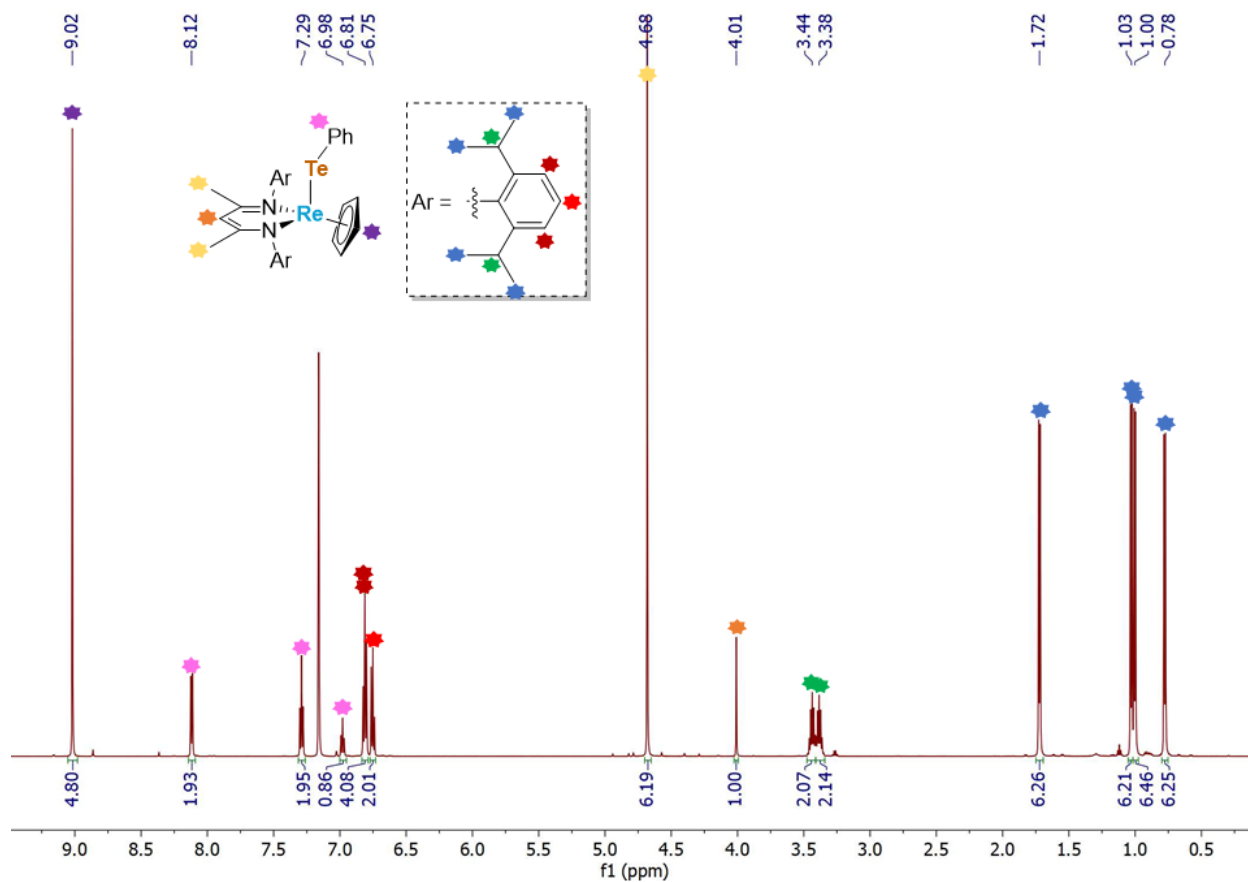
Figure S17. ^{1}H NMR spectrum of Re(TePh)(η^5-Cp)(BDI) (**3-TePh**) in C_6D_6 (600 MHz, 298 K).
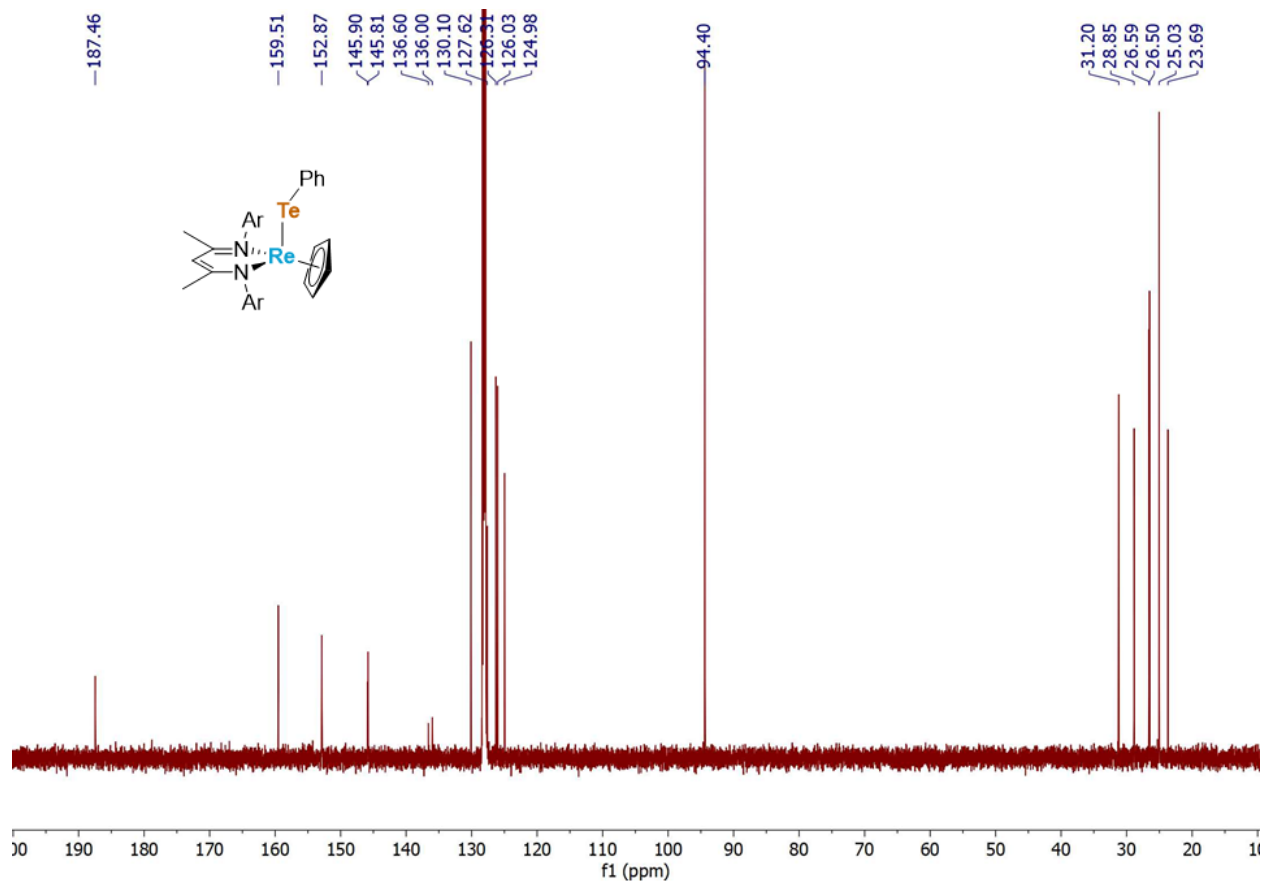
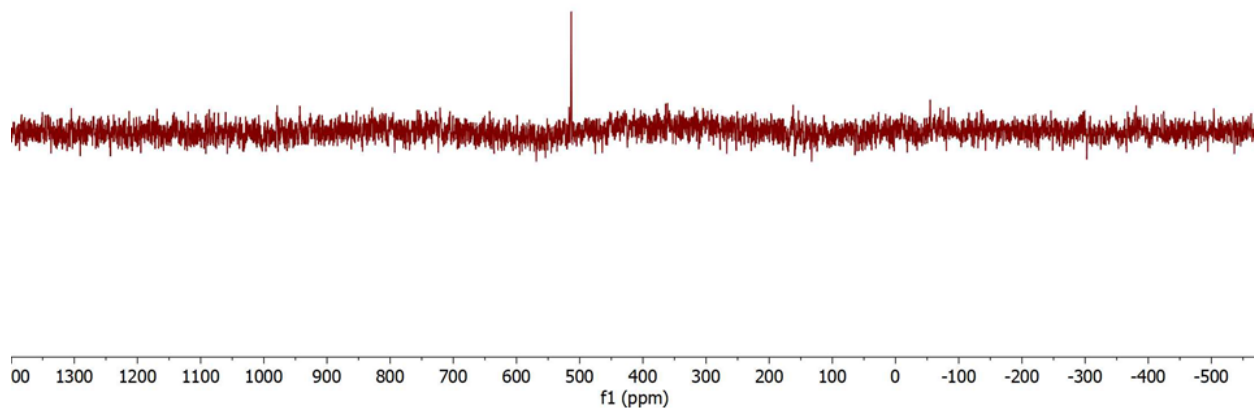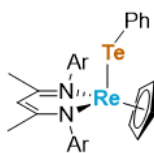**Figure S18.** ^{13}C NMR spectrum of Re(TePh)(η^5-Cp)(BDI) (**3-TePh**) in C_6D_6 (151 MHz, 298 K).

Figure S19. ^{125}Te NMR spectrum of Re(TePh)(η^5-Cp)(BDI) (**3-TePh**) in C_6D_6 (189 MHz, 293 K).
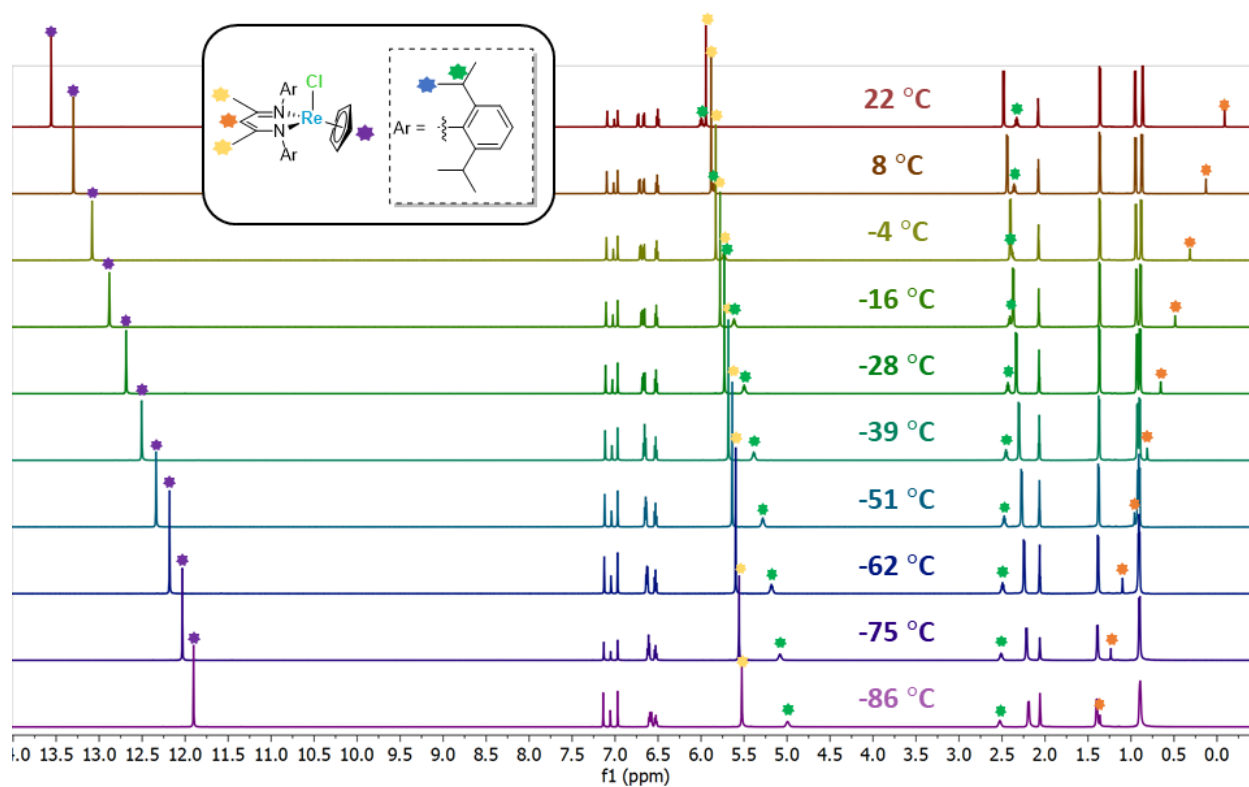
Figure S20. Variable temperature ^{1}H NMR spectra of Re(Cl)(η^5-Cp)(BDI) (**1-Cl**) in toluene-d_8 (188-295 K, 600 MHz). Cyclopentadienyl (moving upfield) and BDI backbone protons (moving downfield) show the most significant trends in chemical shift upon lowering temperature.
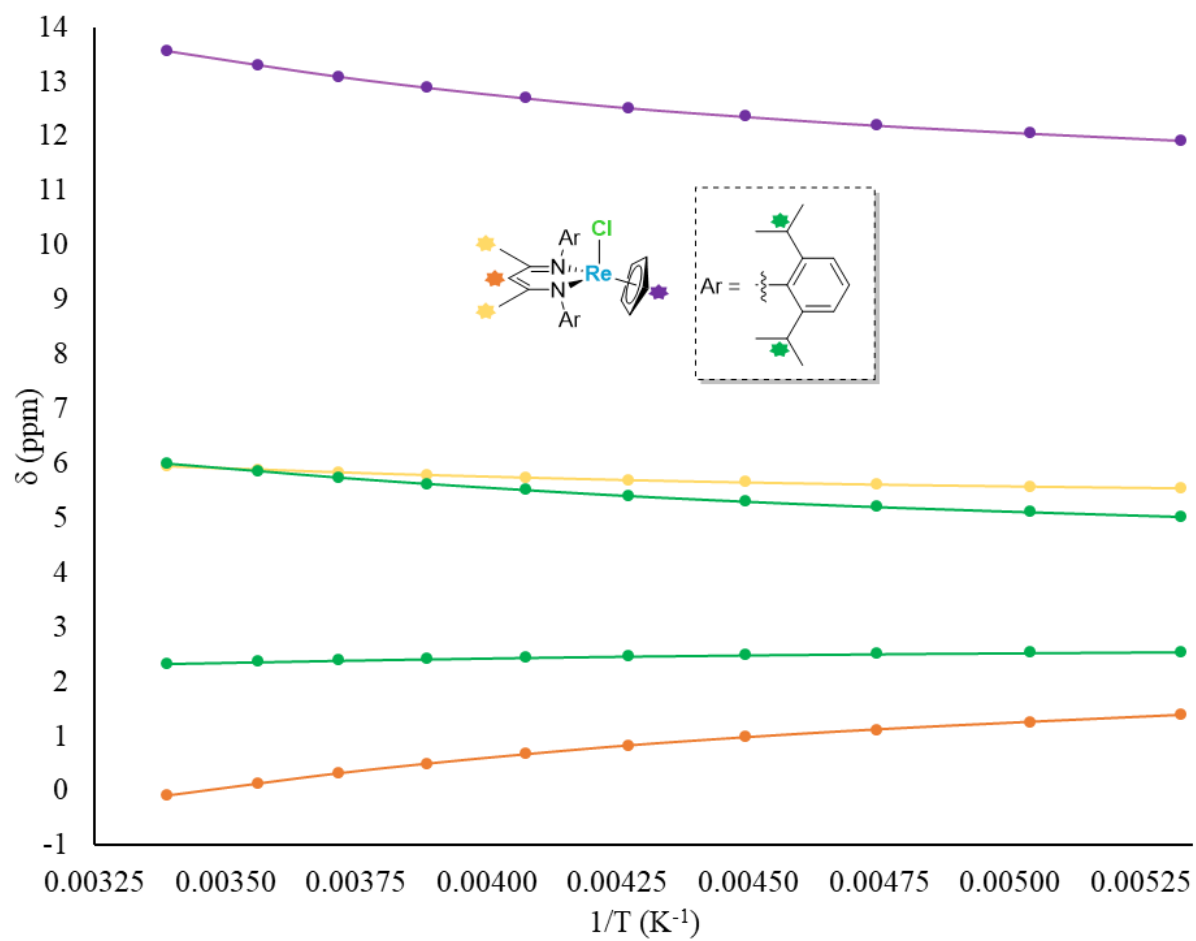
Figure S21. Plot of ^{1}H NMR chemical shifts of Re(Cl)(η^5-Cp)(BDI) (**1-Cl**) in toluene-d_8 (188-295 K, 600 MHz) versus inverse temperature. Chemical shifts do not appear to follow a strict $(1/T)^n$ dependence.

Figure S22. Stacked ^{1}H NMR spectra of **3-ER** (E = SBn, SeBn, TePh) in C$_6$D$_6$ showing a trend in which the Cp, BDI backbone proton, and BDI methyl group peaks shift downfield while the benzyl methylene peaks shift upfield with increasing atomic number of bound chalcogenolate.

X-ray Crystallography

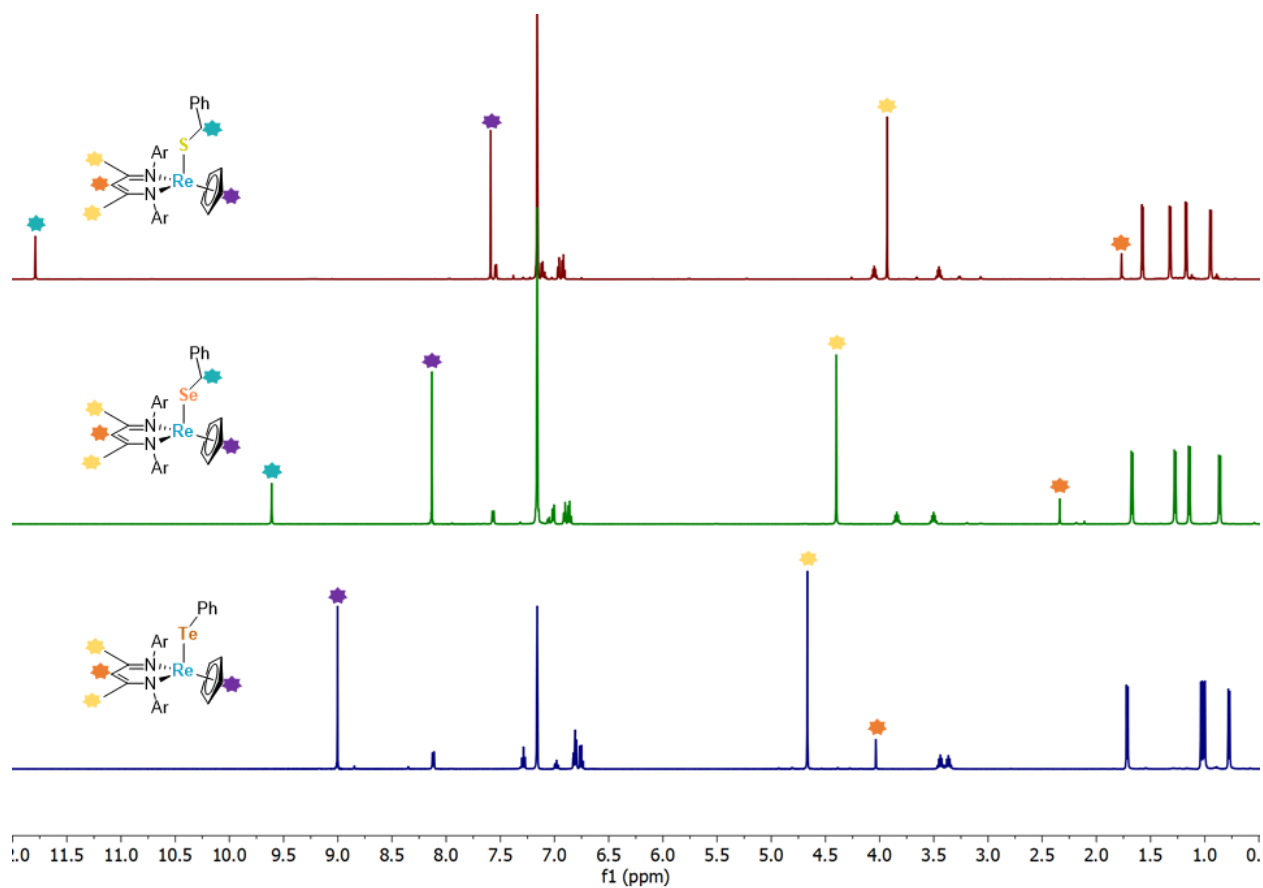In a dry nitrogen glovebox, samples of single crystals of **1-X** (X = F, Cl, Br, I), **2**, and **3-ER** (ER = SBn, SeBn, TePh) were coated in Paratone-N oil for transport to diffraction facilities. Crystals were mounted on either a MiTeGen 10 μm aperture Dual-Thickness MicroMount (for **1-X**) or on a Kaptan loop (for **2** and **3-ER**). X-ray diffraction data for **1-X** were collected at the Advanced Light Source (ALS), Lawrence Berkeley National Lab, Berkeley, CA, station 12.2.1 using a silicon monochromated beam of 17 keV (λ = 0.7288 Å) synchrotron radiation. X-ray diffraction data for **2** and **3-ER** were collected at CheXray, Berkeley, CA, using a Rigaku XtaLAB P200 instrument equipped with a MicroMax-007 HF microfocus rotating anode and a Pilatus 200K hybrid pixel array detector using monochromated Mo Kα radiation (λ = 0.71073 Å). All data collections were conducted at 100 K, with the crystals cooled by a stream of dry nitrogen. For **1-X**, Bruker APEX 2 or APEX3 software was used for the data collections, Bruker SAINT V8.37A or V8.38A software was used to conduct the cell refinement and data reduction procedures,[3] and absorption corrections were carried out by a multi-scan method utilizing either the SADABS (for **1-F**, **1-Br**, and **1-I**) or TWINABS (for **1-Cl**) programs.[3] For **2** and **3-ER**, CrysAlisPro was used for the data collections and data processing, including a multi-scan absorption correction applied using the SCALE3 ABSPACK scaling algorithm within CrysAlisPro.[4] Initial structure solutions were found using direct methods (SHELXT),[5] and refinements were carried out using SHELXL-2014,[6] as implemented by WinGX (for **1-X**)[7] or Olex2(for **2** and **3-ER**).[8] Thermal parameters for all non-hydrogen atoms were refined anisotropically. Hydrogen atoms were placed in calculated positions and refined isotropically. Thermal ellipsoid plots were made using Mercury.[9] The crystal of **1-Cl** displayed non-merohedral twinning, requiring the use of a TWINABS absorption correction and preparation of an HKLF 5 file for structure solution, resulting in a final twin scale factor of 0.333(2). All structures were deposited to the Cambridge Crystallographic Data Centre (CCDC), with deposition numbers 2015396 (**1-F**), 2015397 (**1-Cl**), 2015398 (**1-Br**), 2015399 (**1-I**), 2015400 (**2**), 2015401 (**3-SBn**), 2015402 (**3-SeBn**), and 2015403 (**3-TePh**).

Table S1. Crystallographic details and refinement metrics for compounds **1-X** (X = F, Cl, Br, I).

	1-F	1-Cl	1-Br	1-I
Empirical formula	$C_{34}H_{46}FN_2Re$	$C_{34}H_{46}ClN_2Re$	$C_{34}H_{46}BrN_2Re$	$C_{34}H_{46}IN_2Re$
Formula weight	687.93	704.38	748.84	795.83
Color, habit	Red, prism	Red, prism	Red, block	Red, block
Temperature/K	100(2)	100(2)	100(2)	100(2)
Crystal system	monoclinic	monoclinic	monoclinic	monoclinic
Space group	$P2_1/c$	$P2_1/m$	$P2_1/n$	$P2_1/n$
a/Å	10.4270(6)	9.8838(5)	10.0963(4)	10.1905(4)
b/Å	12.8141(7)	21.1140(11)	25.7569(11)	25.8668(11)
c/Å	22.7453(13)	14.6728(7)	12.1893(5)	12.2240(5)
α/°	90	90	90	90
β/°	95.925(2)	92.032(2)	106.380(2)	106.590(2)
γ/°	90	90	90	90
Volume/Å^3	3022.8(3)	3060.1(3)	3041.2(2)	3088.1(2)
Z	4	4	4	4
ρ_{calc}g/cm^3	1.512	1.529	1.636	1.712
μ/mm^{-1}	4.288	4.323	5.651	5.248
F(000)	1392.0	1424.0	1496.0	1568.0
Crystal size/mm^3	0.150 × 0.130 × 0.060	0.090 × 0.085 × 0.025	0.060 × 0.030 × 0.025	0.050 × 0.035 × 0.025
Radiation	synchrotron (λ = 0.7288)	synchrotron (λ = 0.7288)	synchrotron (λ = 0.7288)	synchrotron (λ = 0.7288)
2Θ range for data collection/°	3.692 to 56.598	2.848 to 56.588	3.242 to 56.616	3.23 to 56.584
Index ranges	-13 ≤ h ≤ 13, -16 ≤ k ≤ 16, -29 ≤ l ≤ 29	-12 ≤ h ≤ 12, 0 ≤ k ≤ 27, 0 ≤ l ≤ 19	-13 ≤ h ≤ 13, -33 ≤ k ≤ 33, -15 ≤ l ≤ 15	-13 ≤ h ≤ 13, -33 ≤ k ≤ 33, -15 ≤ l ≤ 15
Reflections collected	43594	52646	47165	42673
Independent reflections	6903	7236	7003	7098
R_{int}	0.0562	0.1623	0.0529	0.0796
Completeness to Θ = 25.93°	98.90	100.0	99.90	99.80
Data/restraints/parameters	6903/0/353	7236/18/336	7003/0/353	7098/0/353
Goodness-of-fit	1.082	1.243	1.055	1.059
R_1 / wR_2 [I≥2σ(I)]	0.0224 / 0.0551	0.0606 / 0.1560	0.0190 / 0.0447	0.0355 / 0.0886
R_1 / wR_2 [all data]	0.0236 / 0.0560	0.0628 / 0.1570	0.0208 / 0.0457	0.0374 / 0.0910
Largest diff. peak/hole / e Å^{-3}	0.82/ −1.08	3.24/−2.25	0.49/−0.73	1.08/−2.04
CCDC	2015396	2015397	2015398	2015399

Table S2. Crystallographic details and refinement metrics for compounds **2** and **3-ER** (ER = SBn, SeBn, TePh).

|	2	3-SBn	3-SeBn	3-TePh
Empirical formula	$C_{35}H_{46}F_3N_2O_3ReS$	$C_{41}H_{53}N_2ReS$	$C_{41}H_{53}N_2ReSe$	$C_{40}H_{51}N_2ReTe$
Formula weight	818.00	792.11	839.01	873.62
Color, habit	Red, prism	Red, prism	Red, prism	Green, prism
Temperature/K	100(2)	100(2)	100(2)	100(2)
Crystal system	monoclinic	monoclinic	monoclinic	triclinic
Space group	$P2_1/n$	$P2_1/n$	$P2_1/n$	P-1
a/Å	12.1952(3)	13.1341(5)	13.1521(4)	11.2958(4)
b/Å	13.3754(4)	13.0813(4)	13.1148(3)	12.7208(5)
c/Å	21.2609(6)	21.3759(7)	21.5967(5)	14.0557(4)
α/°	90	90	90	67.751(3)
β/°	94.783(3)	105.666(4)	106.290(3)	86.624(2)
γ/°	90	90	90	68.934(3)
Volume/Å^3	3455.91(17)	3536.2(2)	3575.60(17)	1737.40(11)
Z	4	4	4	2
ρ_{calc}g/cm^3	1.572	1.488	1.559	1.670
μ/mm^{-1}	3.629	3.526	4.447	4.350
F(000)	1648.0	1616.0	1688.0	864.0
Crystal size/mm^3	0.21 × 0.11 × 0.11	0.22 × 0.12 × 0.08	0.4 × 0.27 × 0.15	0.26 × 0.1 × 0.07
Radiation	MoKα (λ = 0.71073)	MoKα (λ = 0.71073)	MoKα (λ = 0.71073)	MoKα (λ = 0.71073)
2Θ range for data collection/°	6.092 to 52.746	5.942 to 50.696	5.874 to 52.742	5.716 to 52.726
Index ranges	-15 ≤ h ≤ 15, -16 ≤ k ≤ 16, -22 ≤ l ≤ 26	-15 ≤ h ≤ 15, -15 ≤ k ≤ 15, -25 ≤ l ≤ 25	-16 ≤ h ≤ 16, -16 ≤ k ≤ 16, -26 ≤ l ≤ 26	-14 ≤ h ≤ 14, -15 ≤ k ≤ 15, -17 ≤ l ≤ 17
Reflections collected	37414	42434	45707	36574
Independent reflections	7071	6463	7312	7080
R_{int}	0.0616	0.0718	0.0714	0.0667
Completeness to Θ = 25.93°	99.80	99.80	99.80	99.89
Data/restraints/parameters	7071/0/416	6463/0/416	7312/0/416	7080/0/407
Goodness-of-fit	1.043	1.045	1.025	1.084
R_1 / wR_2 [I≥2σ(I)]	0.0246 / 0.0517	0.0240 / 0.0516	0.0288 / 0.0721	0.0239 / 0.0680
R_1 / wR_2 [all data]	0.0323 / 0.0537	0.0306 / 0.0533	0.0338 / 0.0741	0.0255 / 0.0687
Largest diff. peak/hole / e Å^{-3}	1.02/–0.66	0.48/–0.58	2.76/–1.18	0.67/–0.79
CCDC	2015400	2015401	2015402	2015403
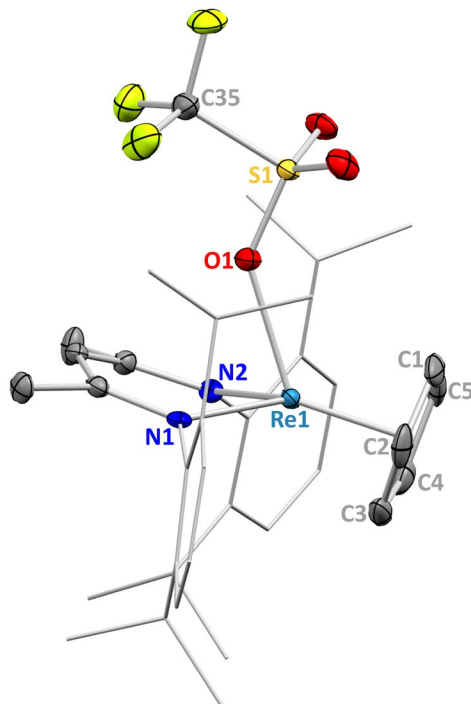
Figure S23. X-ray crystal structure of **2** shown with 50% probability ellipsoids. The BDI aryl groups are shown in wireframe, and hydrogen atoms are omitted for clarity.

Table S3. Selected distances (Å) for **1-X** (X = F, Cl, Br, I), **2**, and **3-ER** (ER = SBn, SeBn, TePh).

complex	Re–C1	Re–C2	Re–C3	Re–C4	Re–C5
1-F	2.332(3)	2.278(3)	2.170(3)	2.178(3)	2.298(3)
1-Cl[a]	2.34(2), 2.34(2)	2.236(8), 2.310(9)	2.202(9), 2.191(8)	–	–
1-Br	2.330(3)	2.287(3)	2.179(3)	2.183(3)	2.298(3)
1-I	2.331(4)	2.288(4)	2.180(4)	2.183(4)	2.298(4)
2	2.314(4)	2.310(4)	2.196(4)	2.173(4)	2.257(4)
3-SBn	2.340(4)	2.245(4)	2.164(3)	2.199(3)	2.325(3)
3-SeBn	2.332(4)	2.333(4)	2.197(4)	2.164(4)	2.239(3)
3-TePh	2.350(3)	2.317(3)	2.184(3)	2.186(3)	2.282(3)

[a]The asymmetric unit consists of two independent halves of the molecule (**1-Cl** and **1-Cl-a**), leading to two reported values for some measurements.

Magnetic Measurements

Microcrystalline samples of **1-Cl**, **1-Br**, and **1-I** were prepared by loading finely ground powders (29.1 mg, 20.1 mg, and 25.1 mg, respectively) into 7mm quartz tubes, which were then subsequently packed with glass wool (30.9 mg, 9.0 mg, and 6.2 mg, respectively) to prevent crystallite torqueing. The quartz tubes were then fitted with Teflon sealable adapters, evacuated on a Schlenk line or by using a glove box vacuum pump, and then flame-sealed under static vacuum using an H_2/O_2 torch to prevent exposure to air. Magnetic measurements were performed using a Quantum Design MPMS2 SQUID magnetometer. All dc susceptibility data were corrected for diamagnetic contributions from the compounds ($\chi_d = -2.627 \times 10^{-4}$ cm^3/mol for **1-Cl**, -2.700×10^{-4} cm^3/mol for **1-Br**, and -2.890×10^{-4} cm^3/mol for **1-I**), which were stimated using Pascal's constants,[11] as well as from glass wool ($\chi_d = -4.07 \times 10^{-7}$ cm^3/g)[10].
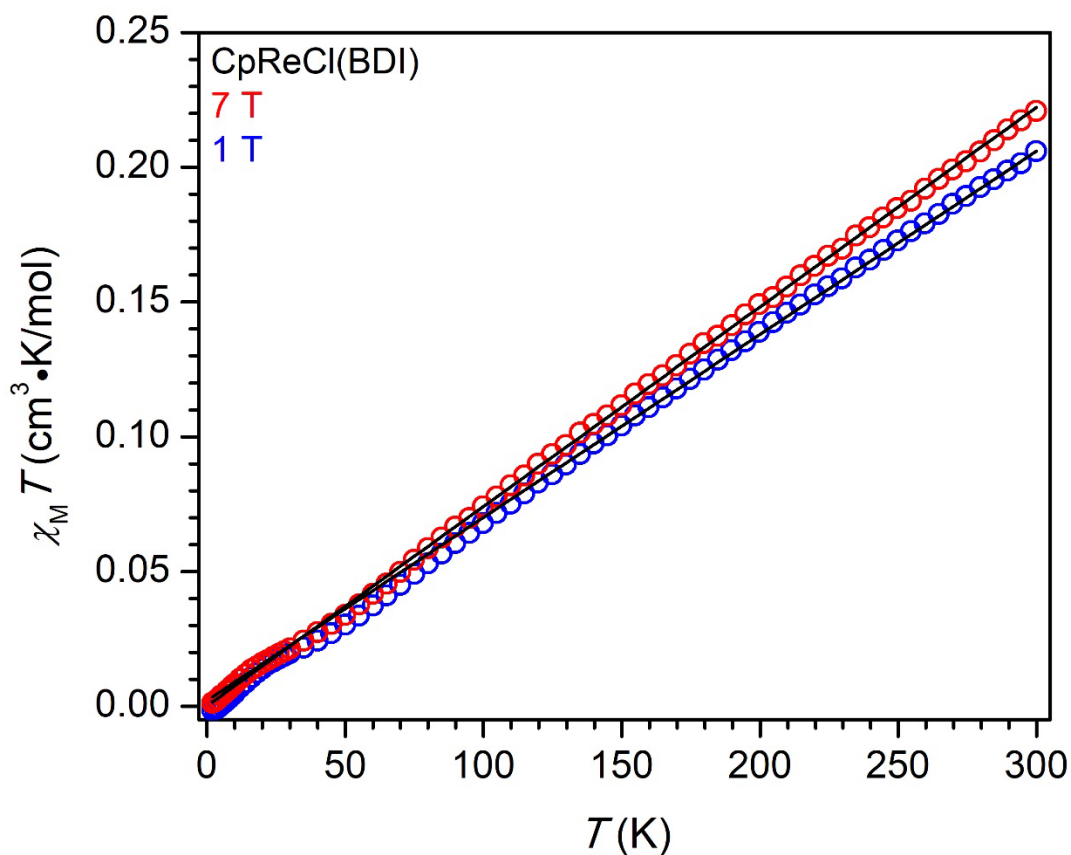

Figure S24. Plots of the molar magnetic susceptibility times temperature ($\chi_M T$) versus temperature for **1-Cl** under applied fields of 1 T (blue circles) and 7 T (red circles).
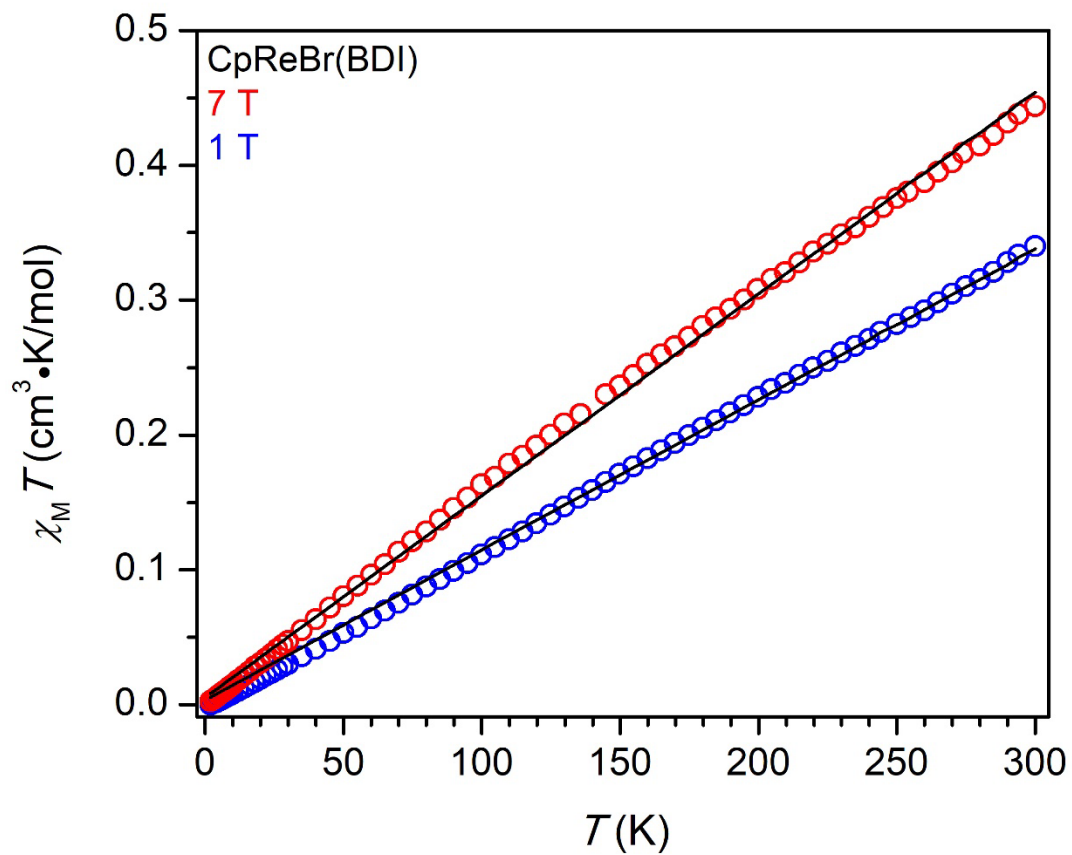
Figure S25. Plots of the molar magnetic susceptibility times temperature ($\chi_M T$) versus temperature for **1-Br** under applied fields of 1 T (blue circles) and 7 T (red circles).
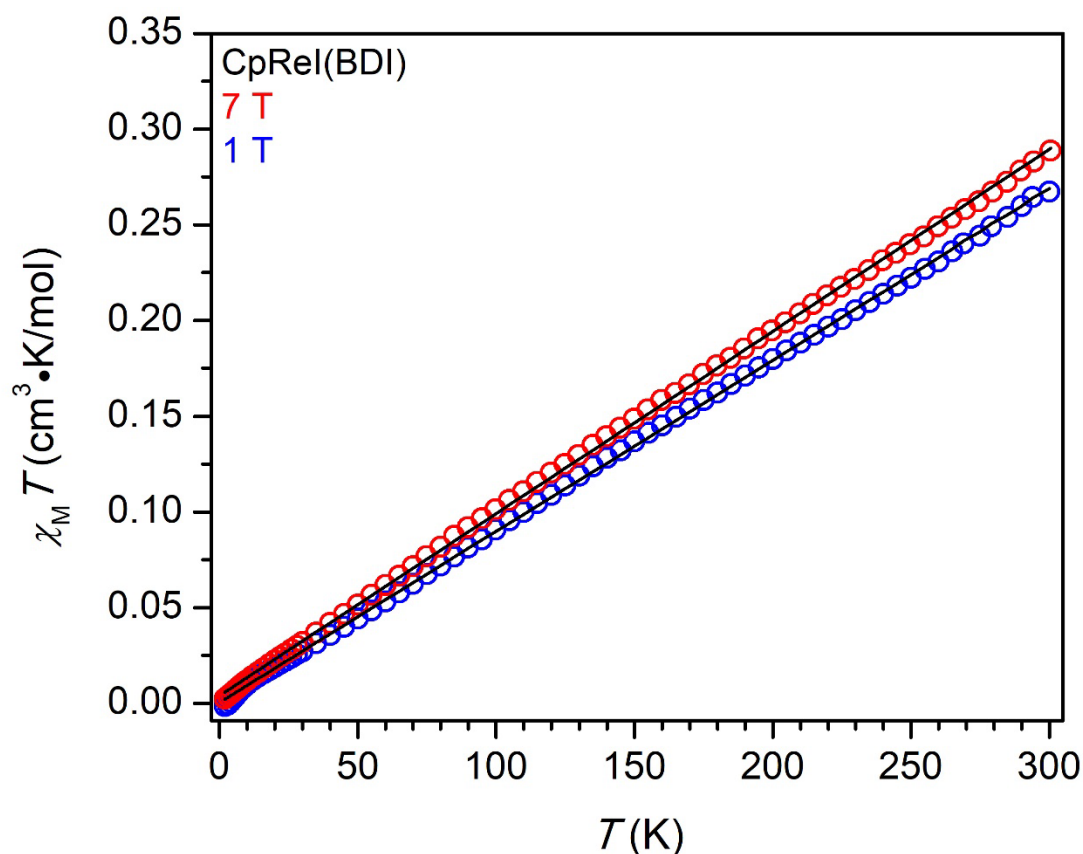
Figure S26. Plots of the molar magnetic susceptibility times temperature ($\chi_M T$) versus temperature for **1-I** under applied fields of 1 T (blue circles) and 7 T (red circles).

Table S4. Tabulated values of χ_{TIP} (cm^{-1}/mol) for complexes **1-X** (**X** = Cl, Br, I) obtained from least-squares fits of the measured variable-temperature DC magnetic susceptibilities of each complex, taken between 2 and 300 K, and under applied fields of 1 and 7 T.

complex	H_{dc} (T)	χ_{TIP} (cm^{-1}/mol)
1-Cl	1	7(5) x 10^{-4}
	7	7.41(44) x 10^{-4}
1-Br	1	1.12(52) x 10^{-3}
	7	1.50(51) x 10^{-3}
1-I	1	9(5) x 10^{-4}
	7	9(3) x 10^{-4}

UV-Visible Spectroscopy

The UV–visible absorption spectra of **1-X** were obtained in THF (Figure S27). The salient features include strong absorption peaks at ~290 nm (ε = 13000–18800 M^{-1} cm^{-1}) and ~370 nm (ε = 6600–12800 M^{-1} cm^{-1}) for all four complexes, which, given their intensities, are attributable to ligand-to-metal charge transfer

(LMCT) transitions (Table S4). The energies of these transitions do not vary greatly between the halide complexes. Additionally, there appear to be weaker absorption peaks at lower energies for **1-F** (480 nm, ε = 1866 M^{-1} cm^{-1}) and **1-I** (438 nm, ε = 2660 M^{-1} cm^{-1}). Absorption traces of complexes **1-Cl** and **1-Br** do not contain distinguishable peaks at lower energy, but rather display peak shoulders at ~465 nm (ε = 1205–1295 M^{-1} cm^{-1}). These collective peaks/shoulders at lower energy may be attributable to weaker LMCT transitions due to their relative intensities.
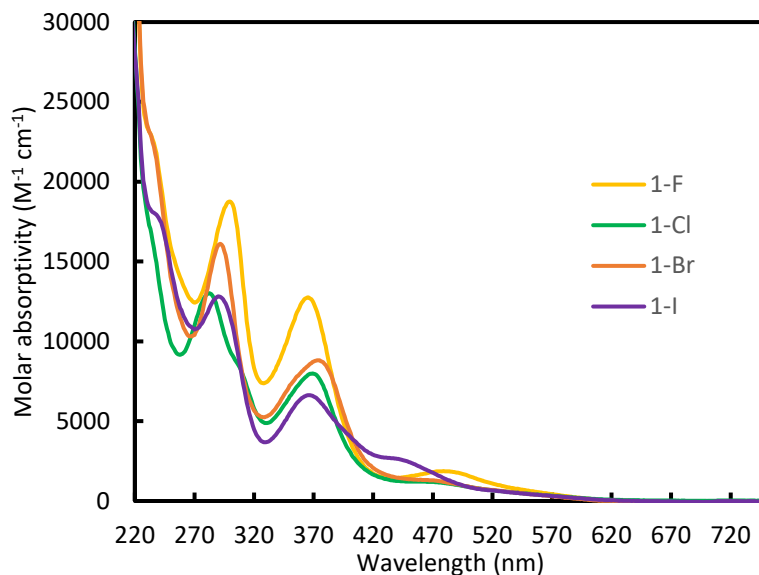

Figure S27. UV-visible absorption spectra of **1-X** (X = F, Cl, Br, I) in THF.

Table S5. Experimental maximum absorption energies and intensities of **1-X** dissolved in THF.

complex	1st peak		2nd peak		3rd peak/shoulder	
	λ_{max} (nm)	ε (M^{-1} cm^{-1})	λ_{max} (nm)	ε (M^{-1} cm^{-1})	λ_{max} (nm)	ε (M^{-1} cm^{-1})
1-F	299	18759	365	12759	480	1866
1-Cl	282	13011	369	7992	465	1205
1-Br	292	16104	373	8813	470	1295
1-I	290	12815	367	6628	438	2660

Computational Details

We carried out a series of systematic Complete Active Space Self Consistent Field (CASSCF) calculations on Re(X)(η^5-Cp)(BDI) (**1-X**) (X = F, Cl, Br, I). Geometry optimizations without any symmetry restrictions have been performed at the B3PW91/6-31G(d,p) level. The inner shells of heavy atoms were described by employing relativistic effective core potentials (RECPs).[12] The geometry optimizations were followed by Restricted Open Shell (ROHF) calculations for different spin values (S = 0, 1 and 2). The electronic states of this series of four rhenium halides were analyzed through CASSCF(6,5) calculations, in which six electrons were accommodated in five orbitals. Note that the optimal sets of molecular orbitals for each rhenium halide obtained at ROHF level were employed as an initial guess in the CASSCF(6,5) calculations. In figures S28-31 we show the orbital sets used to construct the complete active space or CAS for each rhenium halide. For **1-F**, the CAS was built by distributing six electrons in the HOMO-6, HOMO-5, SOMO-3, SOMO-2 and SOMO orbitals obtained from the quintet state. In the case of the **1-Cl** and **1-Br**, the CAS(6,5) was generated using the HOMO-5, HOMO-3, HOMO-2, SOMO-1 and SOMO orbitals obtained from the triplet state. For **1-I**, six electrons were allocated in the triplet HOMO-4, HOMO-3, HOMO-2, SOMO-1 and SOMO orbitals. Note that we have used this methodology previously to study the ground-state and electronic excited states of other complexes.[13] The DFT, ROHF and CASSCF calculations were carried out with version 09 of Gaussian software.[14] Spin-orbit calculations were carried out with the CIPSO program.[15,16] Cartesian coordinates of optimized structures of **1-F**, **1-Cl**, and **1-Br** are included as a separate .xyz document.

[Quintet]

HOMO-6   **HOMO-5**

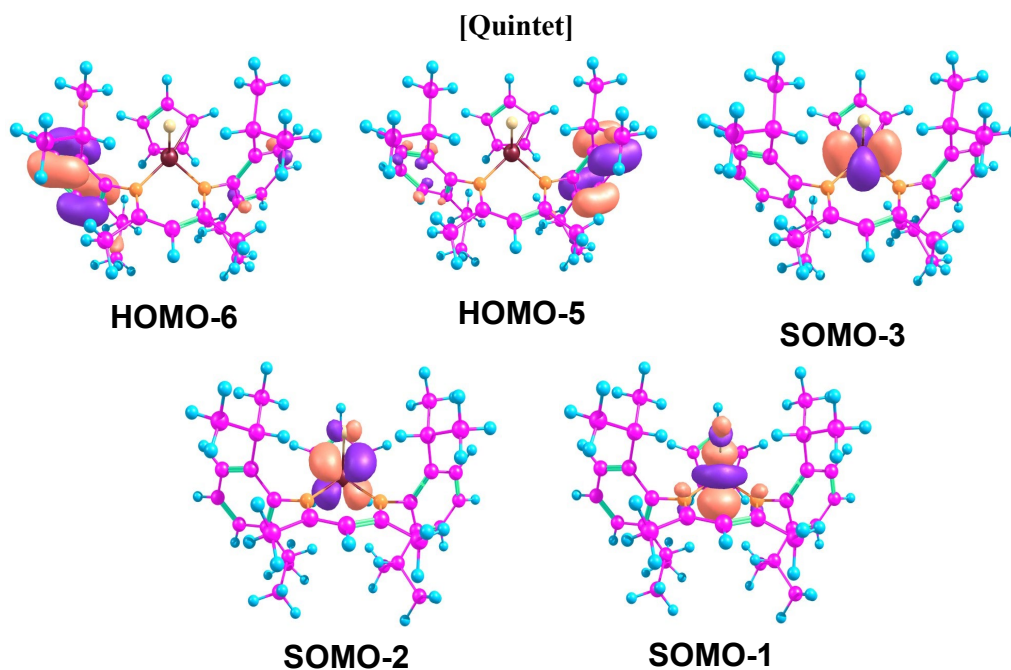**SOMO-3**

SOMO-2   **SOMO-1**

Figure S28. Molecular orbital set (obtained at the ROHF level) used to build the Complete Active Space (CAS) for **1-F**. Spin-multiplicity shown in brackets.
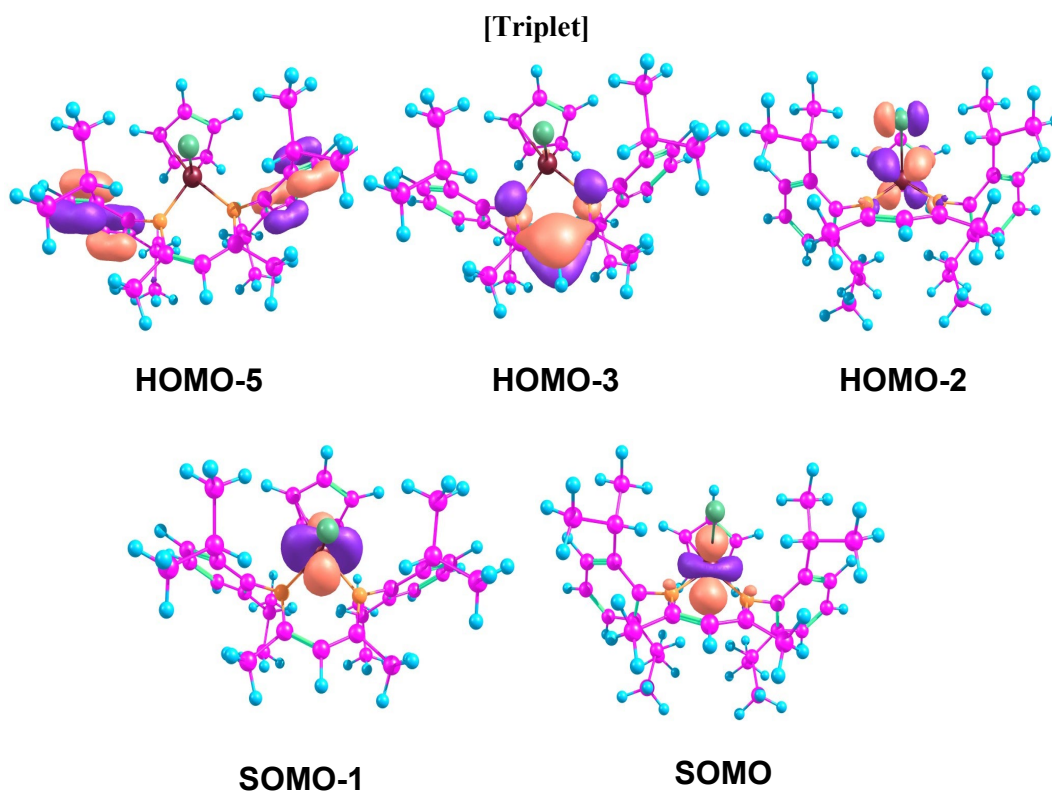
[Triplet]

HOMO-5   **HOMO-3**   **HOMO-2**

SOMO-1   **SOMO**

Figure S29. Molecular orbital set (obtained at the ROHF level) used to build the Complete Active Space (CAS) for **1-Cl**. Spin-multiplicity shown in brackets.

[Triplet]

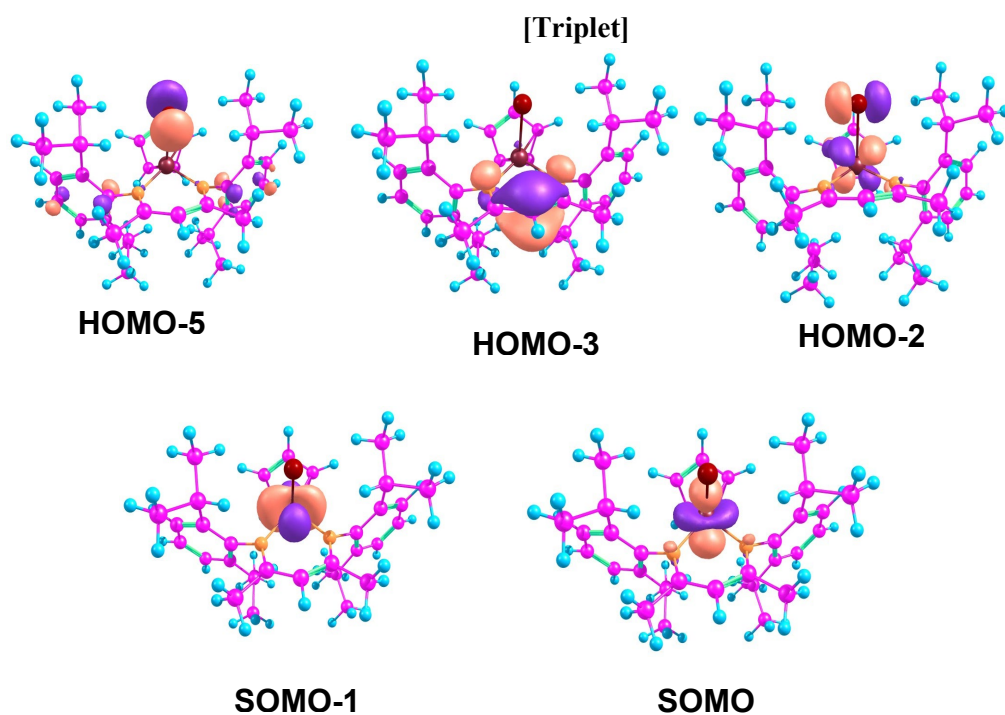**HOMO-5**

HOMO-3

HOMO-2

SOMO-1

SOMO

Figure S30. Molecular orbital set (obtained at the ROHF level) used to build the Complete Active Space (CAS) for **1-Br**. Spin-multiplicity shown in brackets.

[Triplet]

HOMO-4
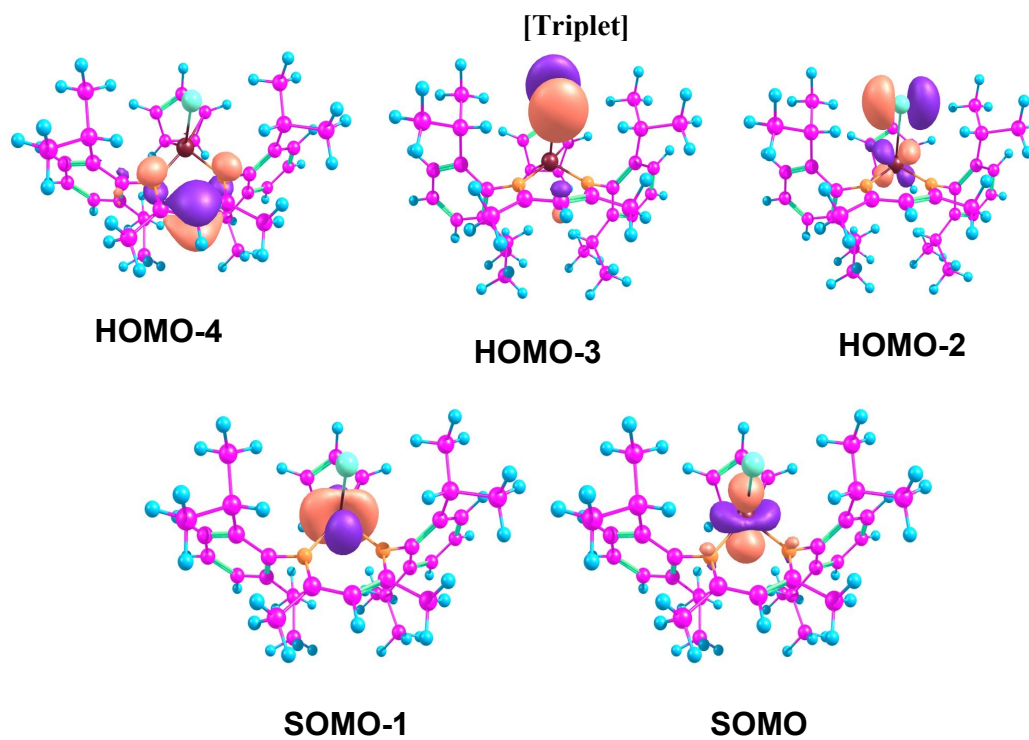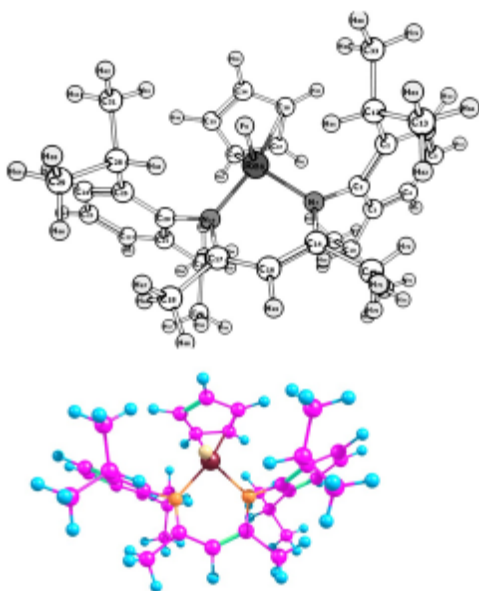
HOMO-3

HOMO-2

SOMO-1

SOMO

Figure S31. Molecular orbital set (obtained at the ROHF level) used to build the Complete Active Space (CAS) for **1-I**. Spin-multiplicity shown in brackets.

Re(F)(Cp)(BDI)

	Exp	Singlet	Triplet
Re-N7	2.03	2.04	2.13
Re-N19	2.03	2.04	2.10
Re-F	1.97	1.97	1.96
Re-C34	2.33	2.38	2.28
Re-C35	2.29	2.33	2.24
Re-C36	2.17	2.18	2.26
Re-C37	2.16	2.18	2.26
Re-C38	2.27	2.32	2.32
N7-Re-F	89.86	90.18	87.99
N19-Re-F	88.38	89.12	86.56
N7-Re-N19	87.74	88.88	87.17
C34-Re-F	80.53	77.42	94.14

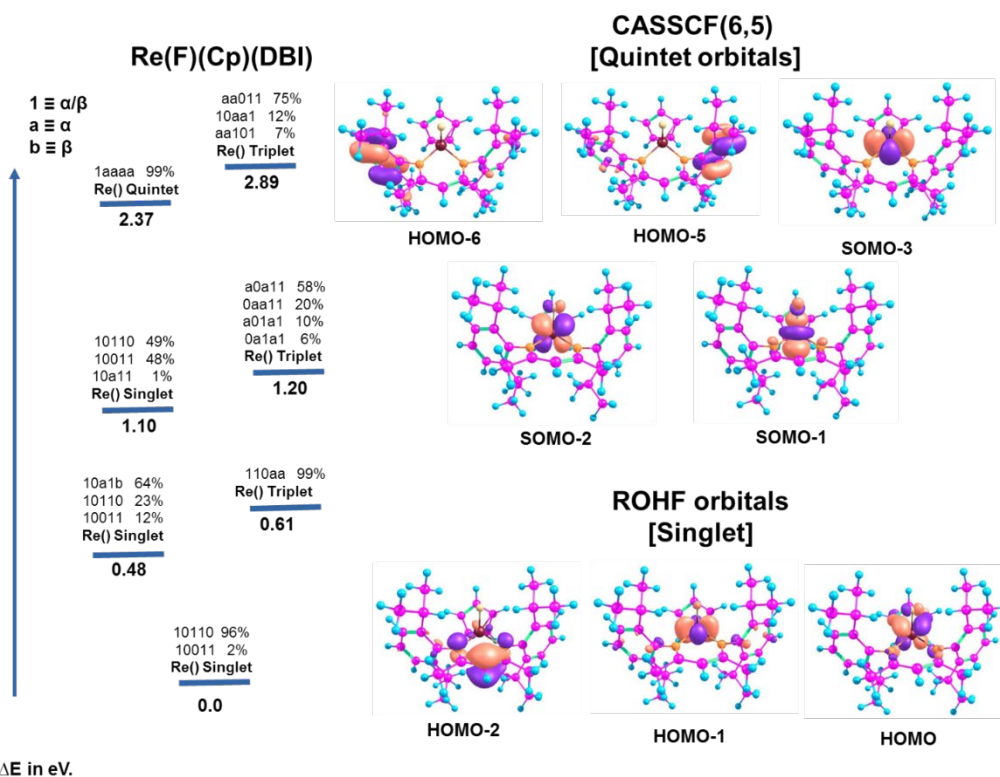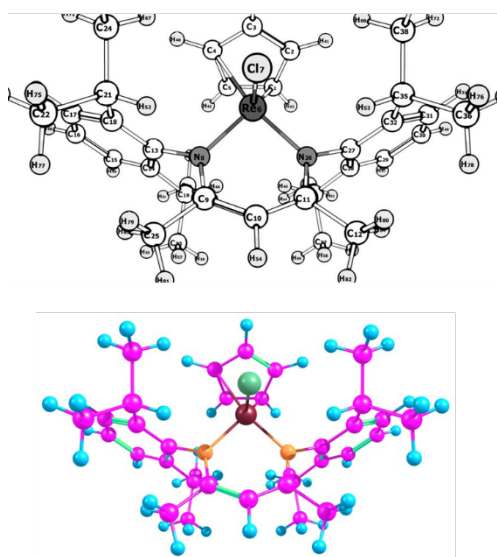$\Delta E(E_{singlet} - E_{triplet}) = -0.787$ kcal/mol

Figure S32. Optimized structure of **1-F** (top left), comparison of structural metrics between experimental and calculated singlet or triplet geometries (top right), energy diagram of ground and excited states (bottom left), and molecular orbital set used to build the Complete Active Space (CAS) (bottom right).

Re(Cl)(Cp)(BDI)

	Exp	Singlet	Triplet
Re-N8	2.05	2.04	2.09
Re-N26	2.05	2.04	2.09
Re-Cl	2.20	2.47	2.52
Re-C1	2.20	2.17	2.19
Re-C2	2.31	2.32	2.31
Re-C3	2.34	2.37	2.34
Re-C4	2.31	2.32	2.31
Re-C5	2.20	2.17	2.19
N8-Re-Cl	88.56	87.40	86.41
N26-Re-Cl	88.56	87.40	86.40
N8-Re-N26	87.80	89.80	89.84
C3-Re-Cl	82.39	81.49	85.56

$\Delta E(E_{singlet} - E_{triplet}) = -1.92$ kcal/mol

Re(Cl)(Cp)(DBI)

CASSCF(6,5) [Triplet orbitals]

ΔE in eV.

Figure S33. Optimized structure of **1-Cl** (top left), comparison of structural metrics between experimental and calculated singlet or triplet geometries (top right), energy diagram of ground and excited states (bottom left), and molecular orbital set used to build the Complete Active Space (CAS) (bottom right).
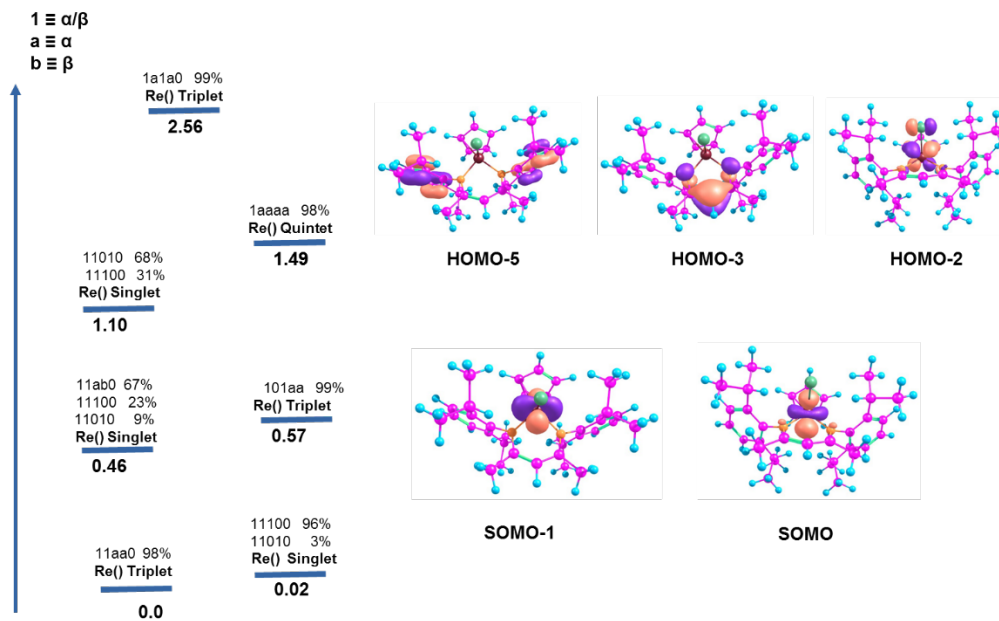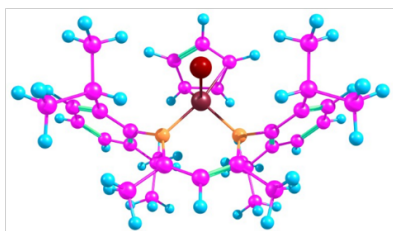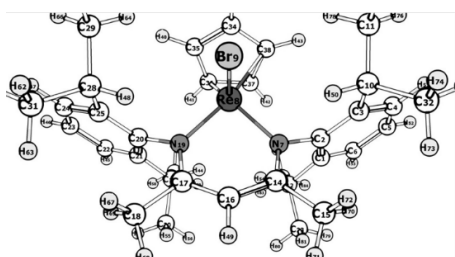
Re(Br)(Cp)(DBI)

	Exp	Singlet	Triplet
Re-N7	2.03	2.04	2.12
Re-N19	2.03	2.03	2.08
Re-Br	2.54	2.61	2.63
Re-C34	2.32	2.37	2.36
Re-C35	2.29	2.31	2.27
Re-C36	2.18	2.18	2.20
Re-C37	2.17	2.18	2.20
Re-C38	2.28	2.33	2.34
N7-Re-Br	87.72	87.45	90.19
N19-Re-Br	89.17	88.26	88.40
N7-Re-N19	88.07	89.92	88.85
C34-Re-Br	83.08	81.49	87.30

$$\Delta E(E_{singlet} - E_{triplet}) = -1.16 \text{ kcal/mol}$$

Re(Br)(Cp)(DBI)

CASSCF(6,5)
[Triplet orbitals]

$1 \equiv \alpha/\beta$
$a \equiv \alpha$
$b \equiv \beta$

0aa11 99%
Re() Triplet
2.50

1aaaa 99%
Re() Quintet
1.44

aa011 99%
Re() Triplet
1.18

11010 50%
11100 49%
Re() Singlet
0.85

11ab0 65%
11010 17%
11100 17%
Re() Singlet
0.31

11aa0 99%
Re() Triplet
0.0

11100 96%
Re() Singlet
0.02

HOMO-5

HOMO-3

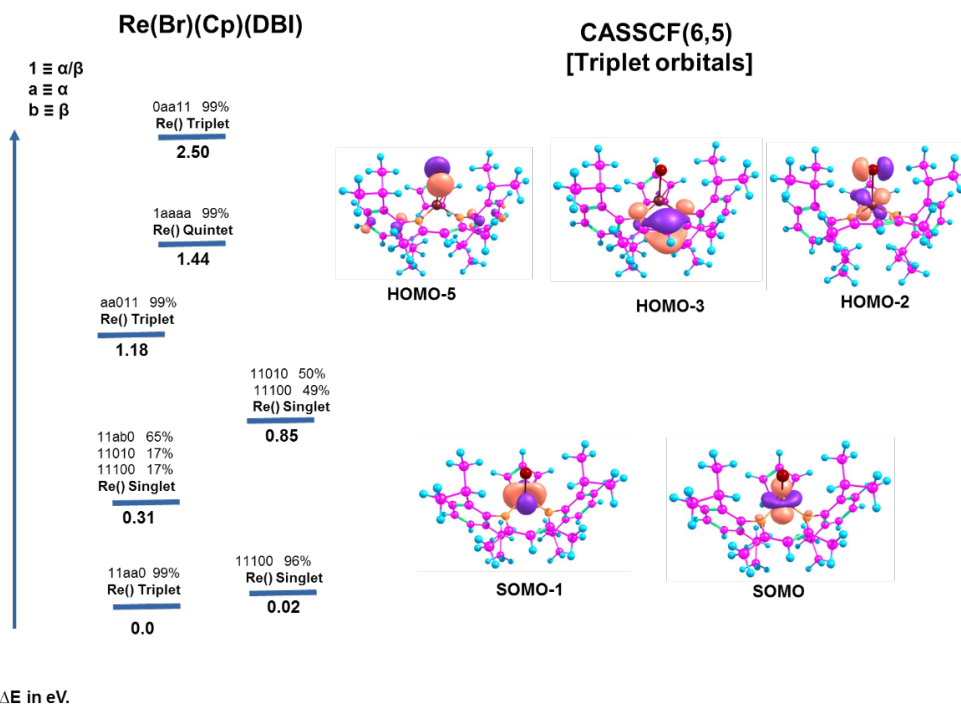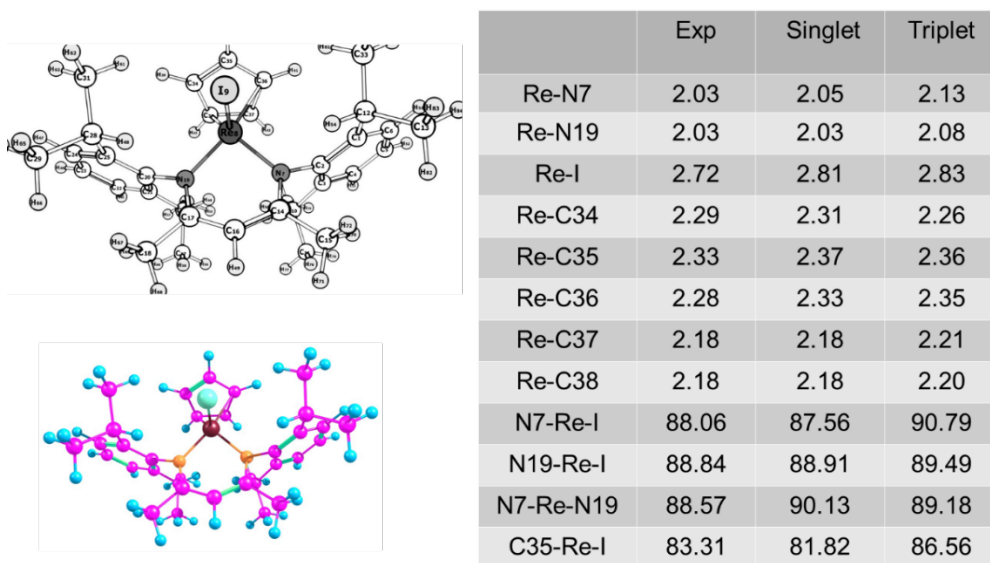HOMO-2

SOMO-1

SOMO

ΔE in eV.

Figure S34. Optimized structure of **1-Br** (top left), comparison of structural metrics between experimental and calculated singlet or triplet geometries (top right), energy diagram of ground and excited states (bottom left), and molecular orbital set used to build the Complete Active Space (CAS) (bottom right).

Re(I)(Cp)(DBI)

	Exp	Singlet	Triplet
Re-N7	2.03	2.05	2.13
Re-N19	2.03	2.03	2.08
Re-I	2.72	2.81	2.83
Re-C34	2.29	2.31	2.26
Re-C35	2.33	2.37	2.36
Re-C36	2.28	2.33	2.35
Re-C37	2.18	2.18	2.21
Re-C38	2.18	2.18	2.20
N7-Re-I	88.06	87.56	90.79
N19-Re-I	88.84	88.91	89.49
N7-Re-N19	88.57	90.13	89.18
C35-Re-I	83.31	81.82	86.56

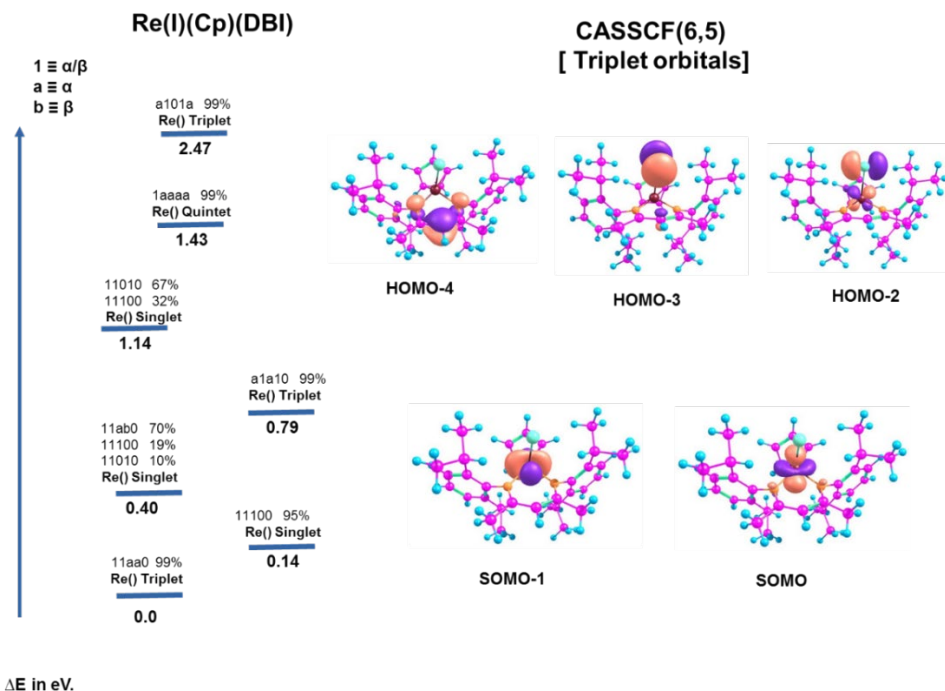$$\Delta E(E_{singlet} - E_{triplet}) = -1.32 \text{ kcal/mol}$$

Figure S35. Optimized structure of **1-I** (top left), comparison of structural metrics between experimental and calculated singlet or triplet geometries (top right), energy diagram of ground and excited states (bottom left), and molecular orbital set used to build the Complete Active Space (CAS) (bottom right).

References

(1) Hermann, W. A.; Zybill, C. E. Vol. 4: Sulfur, Selenium, and Tellurium. In *Synthetic Methods of Organometallic and Inorganic Chemistry*; Thieme, 1997.

(2) Lohrey, T. D.; Maron, L.; Bergman, R. G.; Arnold, J. Heterotetrametallic Re-Zn-Zn-Re Complex Generated by an Anionic Rhenium(I) β-Diketiminate. *J. Am. Chem. Soc.* **2019**, *141* (2), 800–804. https://doi.org/10.1021/jacs.8b12494.

(3) APEX2, APEX3, SADABS, TWINABS and SAINT. Bruker AXS. Madison, WI, USA.

(4) CrysAlisPro 1.171.39.45f (Rigaku Oxford Diffraction, 2018).

(5) Sheldrick, G. M. SHELXT - Integrated Space-Group and Crystal-Structure Determination. *Acta Crystallogr. Sect. A Found. Crystallogr.* **2015**, *71* (1), 3–8. https://doi.org/10.1107/S2053273314026370.

(6) Sheldrick, G. M. Crystal Structure Refinement with SHELXL. *Acta Crystallogr. Sect. C Struct. Chem.* **2015**, *71* (1), 3–8. https://doi.org/10.1107/S2053229614024218.

(7) Farrugia, L. J. WinGX and ORTEP for Windows: An Update. *J. Appl. Crystallogr.* **2012**, *45* (4), 849–854. https://doi.org/10.1107/S0021889812029111.

(8) Dolomanov, O. V.; Bourhis, L. J.; Gildea, R. J.; Howard, J. A. K.; Puschmann, H. OLEX2: A Complete Structure Solution, Refinement and Analysis Program. *J. Appl. Crystallogr.* **2009**, *42* (2), 339–341. https://doi.org/10.1107/S0021889808042726.

(9) Macrae, C. F.; Bruno, I. J.; Chisholm, J. A.; Edgington, P. R.; McCabe, P.; Pidcock, E.; Rodriguez-Monge, L.; Taylor, R.; Van De Streek, J.; Wood, P. A. Mercury CSD 2.0 - New Features for the Visualization and Investigation of Crystal Structures. *J. Appl. Crystallogr.* **2008**, *41* (2), 466–470. https://doi.org/10.1107/S0021889807067908.

(10) Wapler, M. C.; Leupold, J.; Dragonu, I.; Von Elverfeld, D.; Zaitsev, M.; Wallrabe, U. Magnetic Properties of Materials for MR Engineering, Micro-MR and Beyond. *J. Magn. Reson.* **2014**, *242*, 233–242. https://doi.org/10.1016/j.jmr.2014.02.005.

(11) Bain, G. A.; Berry, J. F. Diamagnetic Corrections and Pascal's Constants. *J. Chem. Educ.* **2008**, *85* (4), 532–536. https://doi.org/10.1021/ed085p532.

(12) Pritchard, B. P.; Altarawy, D.; Didier, B.; Gibson, T. D.; Windus, T. L. New Basis Set Exchange: An Open, Up-to-Date Resource for the Molecular Sciences Community. *J. Chem. Inf. Model.* **2019**, *59* (11), 4814–4820. https://doi.org/10.1021/acs.jcim.9b00725.

(13) Halbach, R. L.; Nocton, G.; Amaro-Estrada, J. I.; Maron, L.; Booth, C. H.; Andersen, R. A. Understanding the Multiconfigurational Ground and Excited States in Lanthanide Tetrakis Bipyridine Complexes from Experimental and CASSCF Computational Studies. *Inorg. Chem.* **2019**, *58* (18), 12083–12098. https://doi.org/10.1021/acs.inorgchem.9b01393.

(14) Frisch, M. J.; Trucks, G. W.; Schlegel, H. B.; Scuseria, G. E. .; Robb, M. A.; Cheeseman, J. R.; Scalmani, G.; Barone, V.; Mennucci, B.; Petersson, G. A. .; Nakatsuji, H.; Caricato, M.; Li, X.; Hratchian, H. P.; Izmaylov, A. F.; Bloino, J.; Zheng, G. .; Sonnenberg, J. L.; Hada, M.; Ehara, M.; Toyota, K.; Fukuda, R.; Hasegawa, J.; Ishida, M. .; Nakajima, T.; Honda, Y.; Kitao, O.; Nakai, H.; Vreven, T.; Montgomery, J. A., Jr.; Peralta, J. E. .; S84; Ogliaro, F.; Bearpark, M.; Heyd, J. J.; Brothers, E.; Kudin, K. N.; Staroverov, V. N. . K.; R.; Normand, J.; Raghavachari, K.; Rendell, A.; Burant, J. C.; Iyengar, S. S.; Tomasi, J. . C.; M.; Rega, N.; Millam, J. M.; Klene, M.; Knox, J. E.; Cross, J. B.; Bakken, V.; Adamo, C. .; Jaramillo, J.; Gomperts, R.; Stratmann, R. E.; Yazyev, O.; Austin, A. J.; Cammi, R.; Pomelli, C. .; et al. Gaussian 09, Revision A.01. Gaussian, Inc.: Wallingford, CT 2009.

(15)   Teichteil, C.; Pelissier, M.; Spiegelmann, F. Ab Initio Molecular Calculations Including Spin-Orbit Coupling. I. Method and Atomic Tests. *Chem. Phys.* **1983**, *81* (3), 273–282. https://doi.org/10.1016/0301-0104(83)85321-X.

(16)   Teichteil, C.; Spiegelmann, F. Ab Initio Molecular Calculations Including Spin-Orbit Coupling. II. Molecular Test on the InH Molecule and Application to the g States of the Ar2* Excimer. *Chem. Phys.* **1983**, *81* (3), 283–296. https://doi.org/10.1016/0301-0104(83)85322-1.